Influence of humic acid on colloidal illite stability and attachment and transport of $nTiO_2$ in water saturated sand columns

By

©AKM Fayazul Kabir

A Thesis submitted to the School of Graduate Studies

In the partial fulfillment of the requirements for the degree of

Master of Science
Department of Earth Science

Memorial University of Newfoundland

October 2016

St. John's Newfoundland

Abstract

Effects of pH and humic acid on the attachment of illite particles to sand, and effects of surfactant and grain size of the porous media on the transport of $nTiO_2$ in sand columns were investigated. Results showed that illite colloids were stable in 1 mM NaCl solutions at pH 5 and 9 at HA concentrations of 0-20 mg/L. The attachment of illite colloids to quartz sand was not influenced by HA or pH, but illite attachment to Fe coated sand at pH 5 decreased with increasing HA concentration. Stability of TiO_2 particles were influenced by pH, ionic strength and surfactant. Transport of $nTiO_2$ was influenced by pH, xanthan gum, and higher in coarse-grained sand columns compared to that in fine-grained sand columns under certain conditions. Interaction energies between particles and between particles and sand calculated based on Derjaguin-Landau-Verwey-Overbeek theory agreed with the experimentally observed particle stability, attachment, and transport.

Acknowledgements

I would like to express my sincere gratitude to my supervisor Dr. Tao Cheng for the continuous support and the mentorship during my research, for his patience, motivation and immense knowledge. I could not have imagined having a better supervisor and mentor for my M.Sc. research.

I would like to thank Dr. Penny Morrill for her precious support and valuable advices time to time during my research as my master committee. With her support it would not be possible to finish my research.

I would also like to show my gratitude to Dr. Valerie Booth for using the Zetasizer, Wanda Aylward for her help in SEM measurements, Jamie Warren for DOC measurements.

Furthermore, I would like to evolve my special appreciation and thanks to the Natural Science and Engineering Research Council of Canada (NSERC) for the research financial support and Memorial University of Newfoundland to provide School of Graduate Studies (SGS) fellowship.

A special thanks to my wife and words can't express how grateful I am to my Father, mother, my one and only elder brother for all of the sacrifices that you have made on my behalf. Your prayer for me was what sustained me thus far.

Table of Contents

List of Tables

List of Figures

Fig. A4. Zeta potential reports (Graphs) measured using Zetasizer Nano S (Malvern Instrument Inc.).

List of Abbreviations and symbols

DOC – Dissolve organic carbon

DLVO – Derjaguin-Landau-Verwey-Overbeek

EDX – Energy dispersive X ray

Fe – Iron

g – gram

HDD – Hydrodynamic diameter

HA – Humic acid

IS – Ionic strength

K_BT – Thermal energy scale at absolute temperature T.

L – Liter

mg – milligram

mol/L – moles/liter

nm – nanometer

mg/kg – milligrams per kilograms

mg/L – milligram per liter

NOM – Natural organic matter

SEM – Scanning electron microscope

XG – Xanthan Gum

ZP – Zeta potential

List of Appendices

Chapter 1: Introduction and Overview

1.1 Illite colloidal particles and their role in the subsurface environment

Illite colloid is one of the major clay particles in the environment and it has important implications to the fate and transport of contaminant (e.g., arsenic, $nTiO_2$ and various isotopes) in soil and groundwater (Polubesova and Nir, 1999). For example, salicylic acid, ethanol, and humic substances are found to be absorbed by illite in the subsurface environment (Kubicki et al, 1997). Adsorption of $^{60}Co(II)$ to illite is strongly affected by pH and dominated by ion exchange (Zhang et al., 2013). Clay minerals especially illite scavenge arsenic (As) from groundwater in high pH and low redox environments (Guo et al., 2003), but at low pH it was also found that illite, kaolinite, montmorillonite and Fe oxyhydroxides promote the mobilization and transport of arsenic in groundwater (Guo et al., 2003). Fe rich clays (such as illite and biotite) and Fe coated grains adsorb arsenic and may cause groundwater contamination (Pal et al., 2002). The presence of suspended clay colloids such as illite and kaolinite can facilitate the transport of titanium dioxide nanoparticles ($nTiO_2$) through quartz sand porous media (Cai et al., 2014). Bayat et al. (2015) showed that illite particles are very effective in retaining $nTiO_2$ in porous media. Arsenic adsorption to illite particles occurs up to pH 7 and larger surface area of the illite particles leads to higher As sorption capacity. So it is very important to know the factors that may influence illite particle transport in the subsurface environment.

1.2 Engineered titanium dioxide nanoparticles ($nTiO_2$) in the subsurface environment

Nanoparticles are important components in the environment. Millions of tons of titanium dioxide nanoparticles are produced per year globally and most of them are produced in order to use as a pigment in paints, glazes, enamels, plastics, paper, fibers, foods, pharmaceuticals, cosmetics, and toothpaste (Weir et al., 2012). Engineered nanoparticles like titanium dioxide nanoparticles may be released to the environment from point sources such as manufacturing, landfills and waste water effluent and nonpoint sources such as wear or attrition of tires, sunscreen, brake pads, storm water runoff and wet deposition (Wiesner et al., 2006). Many household and industrial commodities that contains nanoparticles are disposed as waste into the wastewater treatment facilities (Brar et al., 2010). Waste water treatment plants remove most of the nanoscale and larger-sized TiO_2 from the influent waste water but titanium dioxide nanoparticles size ranging between 4 and 30 nm are still found in the treated water and these nanomaterials remained in the surface water (Kiser et al., 2009).

Nanoparticles potentially pose a risk to aquatic ecosystems as well as human health (Sharma, 2009). They have the potential to cause adverse effects to the immune system, oxidative stress related disorders, lung disease, and inflammation etc. (Gottschalk and Nowack, 2011). Among them titanium dioxide nanoparticles with a particle sizes between 10 nm to 20 nm are found toxic to human cells, aquatic organisms, and mice (Hund-Rinke and Simon, 2006; Wiesner et al., 2006; Grassian et al., 2007; Warheit et al., 2008; Battin et al., 2009; Brunet et al., 2009). Nano-titanium dioxide particles can induce

oxidative DNA damage to human bronchial epithelial cells. $nTiO_2$ can also increase hydrogen peroxide and nitric oxide production in human cells (Gurr et al., 2005).

In order to understand the fate and distribution of nanoparticles after they are released to the environment, it is important to understand the factors that influence nanoparticle stability, transport and mobilization in vadose zone and groundwater (Jovanović et al., 2011). Titanium dioxide nanoparticles were found stable after 24 hour in water with the presence of dissolve organic matter and clay particles extracted from the soil, but the $nTiO_2$was found to be unstable at low pH and high ionic strength (Fang et al., 2009). Xanthan gum, which is produced from a kind of bacterium known as *Xanthomonas Campestris,* can be used as a surfactant to suspend titanium dioxide in subsurface environment (García et al., 2000). Xanthan gum and humic acid, commonly found in nature, can stabilize suspended nanoparticles and facilitate their transport in water saturated porous media (Dalla et al., 2009). It was found that, xanthan gum also stabilizes highly concentrated suspensions of iron nanoparticles (Comba and Sethi, 2009).

In recent years, progress has been made in understanding the transport of nanoparticles in groundwater (Chen et al., 2009). Most of the studies on nanoparticle transport emphasized on water saturated media, and the major focus was the effects of solution chemistry such as pH, ionic strength, and natural organic matter (NOM). It was found that the mobility of nano-ZnO and iron nanoparticles changed with pH and ionic strength (Wang et al., 2012). It was observed that the NOM enhanced the mobility of nanoparticles in saturated porous media (Wang et al., 2012). It was also observed by Chen et al. (2008) that the transport and retention of nanoparticles in saturated porous media are very sensitive to ionic strength and ion valence. It was found that in the

absence of NOM, suspended nanoparticles remained stable when they migrated through porous media (Chen et al., 2009). DLVO (Derjaguin-Landau-Verwey-Overbeek) theory was used to calculate the nanoparticle-nanoparticle and nanoparticle-sand interaction energies and it helped to understand the transport and retention of nano-sized particle aggregates in saturated porous media (Chen et al., 2009).

Wang et al.(2012) observed that most of the nanoparticles have more negative surface charge at higher pH, making nanoparticles suspension more stable. An experiment was conducted to investigate the effects of pH on nanoparticle aggregation and transport in porous media in two dimensional porous structures (Dunphy et al., 2006). It was found that 80% of suspended nanoparticles and nanoparticle aggregates (crystalline diameter of 5-12 nm) were mobile over the pH range of 1-12 (Dunphy et al., 2006). It was found that the transport of nanoparticles was higher at higher pH (Godinez and Darnault, 2011).

He et al.(2008) found that aggregation rates are higher for smaller particles at the same ionic strength. Cox (2012) studied the transport of $nTiO_2$ nanoparticles through sandy porous medium at a range of pore water velocities and different ionic strengths and found that ionic strength was most influential at low pore water velocities but had minimal effects at high pore water velocity. Cox (2012) reported that natural porous media had higher retention capability of nanoparticles compared to quartz sand due to heterogeneities.

1.3 Gaps in knowledge

The attachment of colloidal and nano-scale particles to transport medium grains removes the particles from groundwater and reduces particle transport. Wu and Cheng (2016) reported that the effects of HA on $nTiO_2$ attachment to sand depend on pH and HA concentration. At pH 9, HA does not adsorb to $nTiO_2$ and does not have a big impact on $nTiO_2$ attachment. At pH 5, however, HA adsorption to $nTiO_2$ and Fe oxide can change the surface charge of these metal oxides from positive to negative. As a result, $nTiO_2$ adsorption to quartz sand or Fe oxide coated quartz sand (Quartz sand is a major component in many natural aquifers, and quartz sands are often covered by Fe oxide coating, therefore, quartz sand and Fe coated sand are frequently used to mimick natural sediment grains in laboratory studies of contaminant transport.) can be either very low (e.g., zero) or very high (e.g., 100%) or something in between, depending on HA concentration. HA, phosphate, xanthan gum all of them could be present in the groundwater, and can be worked as surfactant which may influence the attachment and transport of nanoparticles. Freake (2016) examined the influence of phosphate on the attachment of illite and $nTiO_2$ colloidal particles to quartz sand and found that the influence of phosphate on illite and $nTiO_2$ are different. While the effects of phosphate on $nTiO_2$ attachment to quartz sand are similar to those of HA at pH 5 and 9 respectively, it was shown that phosphate does not substantially influence illite attachment at either pH. The distinct roles of phosphate on illite and $nTiO_2$ was attributed to the difference in the surface charge ofillite and $nTiO_2$, i.e., at pH 5, the negatively charged phosphate adsorbs to the positively charged $nTiO_2$ and changes the surface charge of $nTiO_2$. Yet, phosphate adsorption to negatively-charged illite is weak and therefore does not influence the surface charge of illite. Both illite colloidal particles and HA are commonly found in

groundwater. A hypothesis can be defined as, HA may strongly influence illite particle attachment to sand, like it does for $nTiO_2$. Or HA could besimilar to phosphate and does not influence illite particle attachment to the sand. In order to answer these important questions, detail experimental studies are needed to elucidate the effects of pH and HA on illite particle adsorption to representing medium such as pure quartz sand and Fe coated sand.

A number of studies have been carried out on the affects of surfactant in the attachment and transport of $nTiO_2$ in water-saturated porous media. In most of the studies HA behaves as a surfactant, e.g., Wu and Cheng (2016) studied the influence of HA on the stability of $nTiO_2$ and the attachment of $nTiO_2$ to sand. Xanthan gum is one of the common surfactant which is very available in groundwater. Comba and Sethi (2009) studied xanthan gum and iron nanoparticle and found that xanthan gum can stabilize iron nanoparticle. So it would be interesting to identify the effects of xanthan gum in the transport of $nTiO_2$ in porous media.

Additionally, the transport of nanoparticles in porous media depends on the grain size of the porous media and the size of the particles. Straining is one of the mechanism of colloid retention in porous media, Xu et al. (2006) found that when the ratio of colloid diameter tograin diameter exceeds 0.008 straining occured. Transport of Ag nanoparticle was enhanced with increasing gain size of the porous media (Liang et al., 2013). Mattison et al., (2011) and Kasel et al., (2013) showed that transport of multi-walled carbon nanotubes depends on the grain size of the porous media. These studies suggested that grain size of the porous media may play an important role in the transport of engineered nanoparticles. As $nTiO_2$ is one of the common nanoparticles that may found in the

groundwater, therefore, more experimental studies are needed to clarify the effects of grain size of the porous media in the transport of titanium dioxide particles.

1.4 Thesis objectives

The main objectives of my research were to achieve a better understanding of: (1) the effects of HA on the stability of the illite particles in water and on illite particle attachment to pure quartz sand and Fe coated sand, and (2) the effects of surfactant (xanthan gum) and grain size of the porous media on the transport of $nTiO_2$ in water-saturated quartz sand columns.

Wu and Cheng (2016) and Freake (2015) showed that HA can substantially influence $nTiO_2$ stability and its attachment to sand. Illite, which is an important type of particle in the subsurface environment, has very different properties compared to $nTiO_2$. Therefore, it would be interesting to observe how HA influence illite stability and attachment. Additionally, Wu and Cheng (2016), Freake (2015) or other researchers did not study $nTiO_2$ transport with column experiments, therefore, it is important to investigate how $nTiO_2$ behaves in sand columns.

1.5 Approaches

A number of batch experiments were performed in order to determine: (1) the stability of illite particles in water at different concentration of HA, (2) influence of HA on illite particle attachment to quartz sand and Fe coated sand, and (3) the stability of $nTiO_2$ particles in water at different ionic strength, and in the absence and presence of a surfactant (xanthan gum). Furthermore, several column experiments were performed to investigate the effects of pH, xanthan gum, and grain size of the sand on $nTiO_2$ transport in water-saturated sand columns. Interaction energies between colloidal particles, and

between colloidal particle and sand were calculated based on Derjaguin-Landau-Verwey-Overbeek (DLVO) theory in order to explain the stability of particle suspensions and the degree of particle attachment to sand.

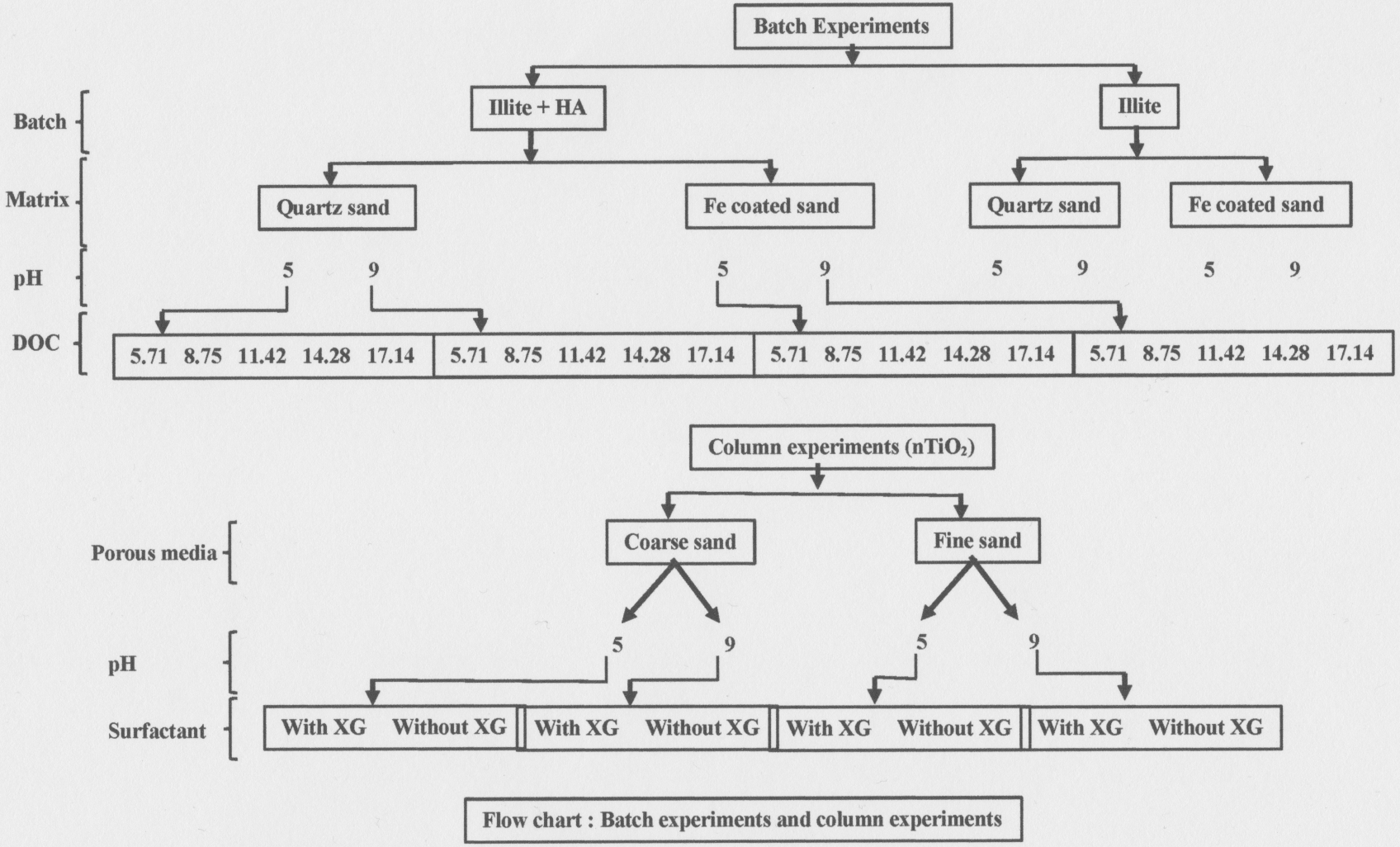

Flow chart : Batch experiments and column experiments

Chapter 2: Materials and Methods

2.1 Attachment behavior of illite colloid particles to clean quartz sand and Fe coated sand at different pH and the affects of humic acid

2.1.1 Porous media

2.1.1.1 Pure quartz sand

Clean quartz sand and Fe coated sand was used for the experiments. Clean quartz sand (Ottawa 20/40, US sieve no. 16-50, US Silica) was purchased and sieved into different fractions. Sieved fractions of 0.250-0.355 mm and 0.600-0.710 mm (referred as "fine sand" and "coarse sand" respectively in this thesis) were used for my experiments. The quartz sand was washed 15 times with nano-pure water to remove the turbidity until the supernatant had an absorbance less than 0.004 at a wavelength of 368 nm.

2.1.1.2 Fe coated sand

For Fe coated sand, The procedure of Scheidegger et al.(1993) and Mills et al., (1994) was followed. $FeCl_3$ (Iron (III) chloride hexahydrate, 99+%, extra pure) from Fisher Scientific was used for coating the quartz sand. 1 M NaOH was used to control the pH. This coated sand was prepared by mixing 200 g of quartz sand and 20 g $FeCl_3$ in 400 ml nanopure water in high-density poly-ethylene (HDPE) bottle. $FeCl_3$ is an acid salt because $Fe(OH)_3$ is weak base and HCl is a strong acid, therefore, the initial pH was measured and found acidic (pH approximately 1.5). The mixture was shaken at 25◦C and gradually added 1 M NaOH to increase the pH to around 4.5-5.0. Approximately 225-250 ml 1 M NaOH was required to buffer the pH around 4.5-5.0. This mixture was shaken for

45-48 hours on a shaker table in order to coat the sand with Fe. This coated sand was rinsed with nano pure water 20 times. Thereafter, in order to remove all the small particles, this coated sand was soaked in 0.01 M NaOH solution for 24 hours. Eventually this coated sand was rinsed multiple times again with nano pure water and oven dried at 120◦C. Then the iron coated sand from each HDPE bottle was put together and mixed for future experiments.

Scanning electron microscopy (SEM) was used to visualize the surface morphology of the quartz sand and Fe coated sand. To quantify the percentage of Fe coated surface area of the quartz sand, backscatter SEM images of the Fe coated sand and energy dispersive X-ray (EDX) was used (Fig. 2.1).

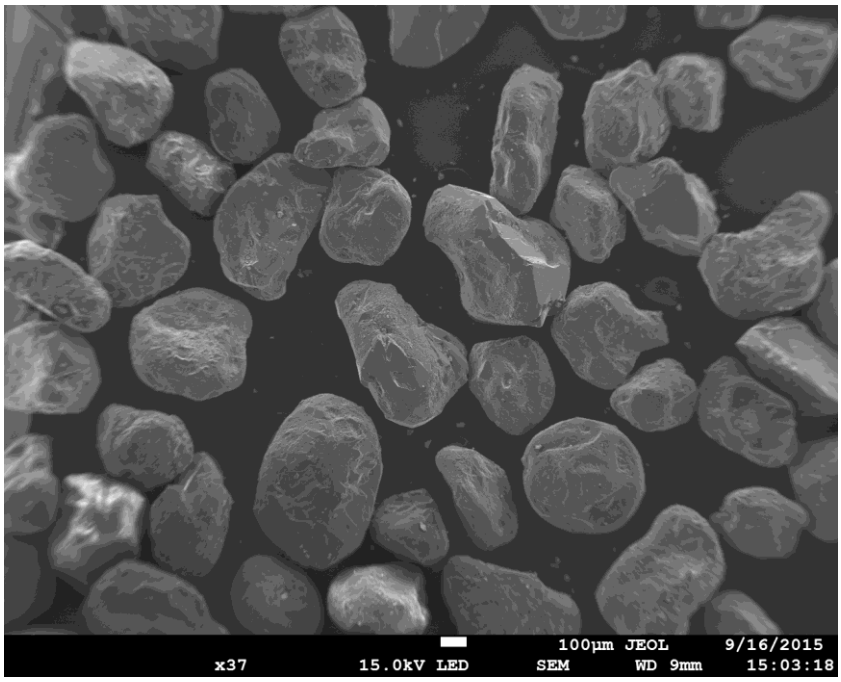

Fig.2.1. Backscatter SEM image of sand grains

2.1.2 Fe coating powder

Similar procedure was used to prepare Fe oxyhydroxide powder. I dissolved 2 g of $FeCl_3$ in 40 ml nano pure water. 1 M NaOH was used to control pH. Approximately 6-8 ml of 1 M NaOH was gradually added to the solution until the pH of the solution reached 5. Then this solution was shaken on a shaker table for 36 hours. After mixing, this solution was centrifuged for 60 minutes at 5000 rpm. Then all of the supernatant from different centrifuge tubes were decanted and suspended in nano pure water and then centrifuged again. This procedure was followed three times before the residuals were dried in the oven at 120◦C.

In order to determine the Fe concentration in Fe coated sand and Fe oxyhydroxide powder Citrate-Bicarbonate-Dithionate (CBD) extraction method (Mehra and Jackson, 1958) was used. One gram of Fe coated sand was mixed with 22.5 ml of 0.3 M sodium citrate and 2.5 ml of 1 M sodium bicarbonate in a 50 ml HDPE falcon tube. Then the tube was placed in a water bath at 80ºC. 0.5 g of sodium dithionite was added to the mixture and vigorously shaken for 1 minute every 5 minutes. After 15 minutes of heating at 80ºC in the water bath, another 0.5 g sodium dithionite was added to the mixture and the mixture was shaken for 1 minute every 5 minutes. After 10 minutes, the tube was taken off from the water bath and kept for cooling. After that the sample was centrifuged and the supernatant was pipetted into another HDPE falcon tube and sent to be analyzed for Fe concentration by ICP-OES. Experimental result showed that, 1.48 ± 0.005 g Fe was present per kg of the Fe coated sand and 15.50 ± 0.03 mg of Fe was present per 100 mg of Fe oxyhydroxide powder.

2.1.3 Preparation of illite suspension

For my experiments I used ACS grade certified chemicals and nano pure water. Illite (IMt-2) from the clay mineral society which contains SiO_2 (49.3%), Al_2O_3 (24.25%), Fe_2O_3 (7.32%), K_2O (7.83%), LOI (8.02%), TiO_2 (0.55%), FeO (0.55%), MnO (0.03%), MgO (2.56%), CaO (0.43%), P_2O_5 (0.08%) (Van Olphena and Fripiat, 1979) was used to prepare the illite suspension. Illite suspension was prepared according to the method described by Saiers and Hornberger (1999). In a high-density-poly-ethylene (HDPE) bottle, 4 grams of illite powder was mixed with 1000 mL of nano pure water and suspended in a Branson Ultrasonic bath (Branson Ultrasonic) for 30 minutes. After that the suspension was shaken on a shaker table and then transferred into an Erlenmeyer flask and kept for 24 hours. Then the supernatant was transferred again into a clean HDPE bottle. The illite concentration in the supernatant was measured gravimetrically using a 0.1 µm polyethersulfone membrane filter (Pall Life Sciences). 100 mL of the suspension was filtered through a filter each time. Before and after the filtration the filter was dried in the oven at 60 ºC and then weighed using an analytical balance. The mass of the illite colloid was calculated as the difference between the two weights.

2.1.4 Humicacid (HA) stock solution

Humic acid stock solution was prepared using humic acid powder from Alfa Aesar. 0.050 g of HA powder was dissolved in 500 mL of nano pure water. This solution was then filtered repeatedly three times through a 0.1 µm polyethersulfone membrane filter (Pall Life Sciences). Each time a new filter membrane was used. The HA concentration of the HA stock solution was determined as by a Shimadzu TOC-V analyzer. The stock solution was stored in a refrigerator at 4 ºC for subsequent use.

2.1.5 Preparation of samples for Zeta potential (ZP) and hydrodynamic diameter (HDD) measurement

To measure the zeta potential (ZP) and hydrodynamic diameter (HDD) of the quartz sand, Fe coating, illite, and humic acid (HA), Zetasizer Nano ZS (Malvern) was used. Quartz sand samples were prepared by sonicating quartz sand grains in 1 mM NaCl solution using a Branson digital sonifier. After 60 minutes of sonication, suspensions with small quartz particles were taken to measure the ZP at pH 5 and pH 9. HA stock solution was used to measure the ZP of HA at pH 5 and pH 9. 50 mg/L of illite suspension was prepared in 1mM NaCl solution at pH 5 and 9 for measuring the ZP and HDD of illite in the absence of HA. For measuring the ZP of illite in the presence of HA, 50 mg/L of illite suspensions were prepared in 1 mM of NaCl solution with appropriate amount of HA stock solution being added. Fe oxyhydroxide suspensions were prepared by suspending 25 mg of Fe oxyhydroxide powder in 200 ml nano pure water with a Branson digital sonifier for 80 minutes with a power level of 50 W. Concentration of HA in groundwater is around 10 mg/L (Crittenden et al., 2012). Therefore, five different concentrations (0-20 mg/L) (17.14 mg DOC/L, 14.28 mg DOC/L, 11.42 mg DOC/L, 8.75 mg DOC/L, 5.7 mg DOC/L) of HA were mixed with Fe oxyhydroxide suspension at pH 5 and 9 to measure the ZP of Fe oxyhydroxide in the presence of HA.

2.1.6 Stability of the illite suspension

To investigate the stability of illite suspension at pH 5 and 9 (average pH of groundwater is 6.5 to 8.5), illite suspensions were prepared (described in Section 2.1.3)

with and without HA. For the HA mixed suspension, the concentrations of spiked HA were 20 mg DOC/L, 1.25 mg DOC/L, and 0.625 mg DOC/L. 1 M NaOH and 1 M HCl were used to adjust the pH. A small quantity of 1 M NaCl was added to adjust the ionic strength of the solution to 1 mM. These suspensions were stirred using a magnetic stirring plate. At pre-determined time intervals, light absorbance of the suspensions was measured using a spectrophotometer at a wavelength of 368 nm.

2.1.7 Adsorption isotherms

2.1.7.1 HA attachment to illite

A number of batch experiments were done in order to investigate the attachment of HA to the illite particles. Five different concentrations (17.14 mg DOC/L, 14.28 mg DOC/L, 11.42 mg DOC/L, 8.75 mg DOC/L, 5.71 mg DOC/L) of HA were added to illite suspension. The illite concentration in all the experiments was 100 mg/L. 15 mL of HDPE falcon centrifuge tubes were used to perform these experiments. 1 M NaCl solution was added to each prepared sample to adjust the ionic strength of 0.001 M. 1 M HCl and 1 M NaOH solutions were added to adjust the pH. The experiments were at both pH 5 and pH 9. After preparing the samples the tubes were capped and gently mixed with a Fisher Scientific Nutating Mixer at 24 rpm. After mixing of HA with illite for 3 hours, these suspensions were filtered through 0.1 µm polyethersulfone membrane filter. HA free controls were also performed at both pH 5 and pH 9. It was found that all the illite particles were retained by the filter in the HA free controls. On the other hand, all the HA could pass through the filter. The light absorbance of the filtered samples was measured using a spectrophotometer at a wavelength of 368 nm. The concentration of HA remaining in water was calculated using the HA calibration curve (Appendix 1). The

amount of HA adsorbed to illite was calculated as the difference between the initial HA concentration and the concentration remaining in water after mixing.

2.1.7.2 Illite attachment to sand in the absence of HA

To determine the attachment of illite particles to quartz sand and Fe coated sand, several batch experiments were performed at pH 5 and 9. These experiments were performed by mixing 25 g quartz sand or Fe coated sand with different illite particle concentrations (20 mg/L, 25 mg/L, 35 mg/L, 50 mg/L, 70 mg/L, and 100 mg/L) in 50 ml HDPE falcon centrifuge tubes at room temperature (25 ºC). The total volume of the solution in each tube was 35 mL. Ionic strength of the solution was adjusted to 1 mM by adding NaCl and the pH of the solutions were controlled with 0.1 M HCl and 0.1M NaOH solutions. Tubes were capped and gently mixed at 24 rpm on a Fisher Scientific Nutating Mixer for 3 hours. After 3 hours of mixing the tubes were removed from the mixer and uncapped and kept for 60 seconds to let the sand grains to settle down. The light absorbance of the supernatant was measured with a spectrophotometer at a wavelength of 368 nm. Concentrations of the suspended illite particles after mixing were calculated using the illite calibration curves (Appendix 1). The quantities of the illite particles attached to sand were calculated as the difference between initial illite concentration and the concentration of illite particles remaining in water after mixing.

2.1.7.4 HA attachment to sand

Batch experiments were performed to understand the HA attachment to quartz sand and Fe coated sand at both pH 5 and pH 9. 25g of quartz sand or Fe coated sand was mixed with six different concentrations of HA (17.14 mg DOC/L, 14.28 mg DOC/L,

11.42 mg DOC/L, 8.75 mg DOC/L, 5.71 mg DOC/L, and a HA free sample) in HDPE falcon centrifuge tubes. The total volume of the solution was 35 ml. 35 µL of 1 M NaCl solution was added to each of the tubes to adjust the ionic strength of the solution to 0.001 M. Very small volumes of 1 M NaOH and 1 M HCl solutions were used to adjust the pH of the solution. The tubes were capped and gently mixed with a Fisher Scientific Nutating Mixer at 24 rpm. After 3 hours of mixing the tubes were removed from the mixer table, uncapped and kept for 60 seconds to let the sand grains settle down. Then a supernatant sample was collected from the tubes using a pipette and the light absorbance was measured using a spectrophotometer at a wavelength of 368 nm. Absorbance of the solution of the HA free controls was also measured and found to be 0.015 Au at pH 5 and 0.018 Au at pH 9. The concentration of HA remaining in water was calculated using the HA calibration curve (Appendix 1), and the amount of HA adsorbed to the sand was calculated as the difference between the initial HA concentration and the concentration remaining in water after mixing.

2.1.7.5 Influence of HA concentration on illite attachment to sand

To investigate the influence of HA concentration on illite attachment to quartz and Fe coated sand, batch experiments were performed at pH 5 and pH 9. In each experiment, 25g of quartz sand or Fe coated sand was mixed in 100 mg/L illite suspension with six different concentrations of HA (17.14 mg DOC/L, 14.28 mg DOC/L, 11.42 mg DOC/L, 8.75 mg DOC/L, 5.71 mg DOC/L, and a HA free sample) in HDPE falcon centrifuge tubes. The total volume of the solution was 35 ml. 35 µL of 1 M NaCl solution was added to each of the tubes to adjust the ionic strength of the solution to 0.001 M. Very small volumes of 1 M NaOH and 1 M HCl solutions were used to adjust the pH of the solution.

The tubes were capped and gently mixed with a Fisher Scientific Nutating Mixer at 24 rpm. After 3 hours of mixing the tubes were removed from the mixer table, uncapped and kept for 60 seconds to settle down the sand grains. Supernatant was collected from the tubes using a pipette and the light absorbance of the supernatant was measured using a spectrophotometer at a wavelength of 368 nm. The concentration of illite particle in the supernatant was calculated based on the measured light absorbance and the illite calibration curves (Appendix 1). The amount of illite particles attached to sand was calculatedas the difference between the spiked illite concentration and the illite concentration in the supernatant after 3 hours mixing.

2.2 Effects of pH, surfactant (xanthan gum), and grain size of the porous media on the transport of $nTiO_2$ in water saturated sand column

2.2.1 Porous media

Sieved Ottawa sand (US Silica) with the grain size range of 0.250-0.355 mm (fine sand) and 0.600-0.710 mm (coarse sand) were used as the porous media in my experiments. Before used in column experiments, the quartz sand samples were washed 15 times with nano pure water to remove the turbidity (i.e., small particles) until the supernatant has a light absorbance less than 0.01 Au (measured at a wavelength of 368 nm). The washed sand samples were oven dried at 120 ºC and stored in plastic buckets.

2.2.2 Preparation of nanoparticle suspension and xanthan gum

Titanium (IV) oxide nanoparticle ($nTiO_2$) powder (Acros Organics BVBA, Belgium) was used to prepare the suspensions for the column experiments. $nTiO_2$ consists

89.6% anatase and 10.4% rutaile, confirmed by X-ray Diffraction (Langford and Louër, 1999). $nTiO_2$ powder (20mg/L) was added tonano pure water (Nanopure® Water Purification Systems, Thermo Scientific) and suspended with an ultrasonic probe (Digital sonifier, Branson Ultrasonics).For some of the $nTiO_2$ suspension samples, 10 mg/L xanthan gum was also added. 1 M NaOH and 1 M HClwere used to adjust the pHat 5 and 9 and NaCl was used to adjust the ionic strength (IS)of the suspensionsto 0.1 mM.

2.2.3 Preparation of samples for Zeta potential (ZP) and hydrodynamic diameter (HDD) measurement

To measure the zeta potential (ZP) and hydrodynamic diameter (HDD) of $nTiO_2$, xanthan gum, $nTiO_2$ with xanthan gum presence, Zetasizer Nano ZS (Malvern) was used. For all the measurements, 20 mg/L of $nTiO_2$ and 10 mg/L of xanthan gum were used. 0.1 mM of NaCl was used as background solution, and 1 M NaOH and 1 M HCl solutions were used to adjust the pH of the samples to 5 and 9. Calibration curbes were prepared with different concentration of $nTiO_2$ for both pH 5 and pH 9 (Appendix 3).

2.2.4 Stability of the $nTiO_2$ suspension

To investigate the stability of $nTiO_2$ suspension at pH 5 and 9, 20 mg/L of $nTiO_2$ suspensions were prepared (described in Section 2.2.2). 10 mg/L of xanthan gum was added to the suspension to prepare the suspensions with xanthan gum. NaCl was added to the suspension to adjust theionic strength to 1, 2, 10, 50, and 100 mM. 1 M NaOH and 1 M HCl were used to adjust the pH. Light absorbance of the suspension was monitored up to 4 hours using a spectrophotometer at a wavelength of 368 nm.

2.2.5 Column experiments

For the column experiments, KontesChromaFlex™ Chromatography Column (2.5 cm inner diameter, 15 cm length) was used. To pack my column, I followed the procedure by Wang et al., (2014). That is, the glass column was pre-filled with background solution at ~1 cm depth, and small amount of sand was slowly poured into the column. Then the column was tapped to pack the column uniformly and to remove any air bubbles. The above step was repeated until the column was fully filled with sand and water. A peristaltic pump (Masterflex, Cole-Parmer Instruments) was used to inject the solution through the column from bottom to top. I flushed the column overnight with the background solution so that the column became saturated and no air bubble remained in the column, then $nTiO_2$ suspensions were injected into the column. Upon completion of $nTiO_2$ injection, the influent solution was switched back to $nTiO_2$ free background solution. I maintained 0.2cm^3/min discharge rate for my column experiments all the time and the effluent samples were collected using a fraction collector (CF-2, Spectrum Chromatography) for analysis of $nTiO_2$ concentration. A UV-visible spectrophotometer was used to measure the light absorbance of the effluent samples and the concentration of $nTiO_2$ in the effluent was calculated based on the $nTiO_2$ calibration curves (Appendix 3).

2.3 Analytical Methods

2.3.1 Measurements of zeta potential and hydrodynamic diameter

Zetasizer Nano ZS was used for measuring zeta potential and hydrodynamic diameter of my samples (illite paricles, $nTiO_2$, HA, xanthan gum, sand and Fe coating). The analysis was done in the Biochemistry lab of Memorial University. Dynamic light

scattering was used to measure particle and molecule size, and laser doppler micro-electrophoresis was used to measure zeta potential. Sample analysis was performed following the procedure by Clogston and Patri (2011). For both ZP and HDD, triplicate measurements was performed on the same sample, and the mean and standard deviation were calculated.

2.3.2 Measurements of absorbance

Genesys 10 S UV-visible spectrophotometer was used to measure absorbance of my samples. Calibration curves were prepared using different concentration of the samples, And using the calibration curve concentration of the unknown samples were determined.

2.3.3 TOC measurements

Shimadzu TOC-V analyzer was used to measure TOC of my samples. Samples were analysis in the Biogeochemistry laboratory of Memorial University.

2.4Interaction energy calculation using DLVO theory

DLVO theory was used to understand the transport and retention of titanium dioxide nanoparticle in sand columns and the attachment of illite particles to the sands as well as the stability of titanium dioxide nanoparticles and illite colloidal particles. Total interaction energies $\phi_{DLVO}(h)$ between $nTiO_2$ particles, between $nTiO_2$ and sand, between illite particles, and between illite particle and sand grain (quartz sand and Fe coated sand) are the summation of the electrostatic energy $\phi_{dl}(h)$(Equation 1) due to electricstatic forces and the attractive interaction energy $\phi_{vdw}(h)$ due to van der Waals

forces. The electrostatic energy $\phi_{dl}(h)$ and the attractive interaction energy $\phi_{vdw}(h)$were calculated using the following equations (Elimelech et al., 1995).

$$\phi_{DLVO}(h) = \phi_{vdw}(h) + \phi_{dl}(h) \quad (1)$$

The attractive interaction energy $\phi_{vdw}(h)$ due to van der Waals interaction for the sphere-sphere geometry was calculated with Equation (2) (Ryan and Gschwend, 1994).

$$\phi_{vdw}(h) = -\frac{A_{123}}{12}\left\{\frac{y}{r^2 + ry + r} + \frac{y}{r^2 + ry + r + y} + 2\ln\left[\frac{r^2 + ry + r}{r^2 + ry + r + y}\right]\right\} \quad (2)$$

Where A = Hamaker constant, $y = r_2/r_1$and $r = h/2r_1$. r_1 is the radius of the smaller of the two particles, r_2 is the radius of the larger of the two particles (Hamaker, 1937).

The electrostatic interaction energy $\phi_{dl}(h)$ for the sphere-sphere geometry was calculated with Equation (3) (Hogg et al., 1966).

$$\phi_{dl}(h) = \pi\varepsilon\varepsilon_0 \frac{r_1 r_2}{(r_1 + r_2)}\left[2\Psi_1\Psi_2 \ln\left(\frac{1 + e^{-kh}}{1 - e^{-kh}}\right) + (\Psi_1^2 + \Psi_2^2)\ln\left(1 - e^{-2kh}\right)\right] \quad (3)$$

Where $\varepsilon =$ Di electric constant of water, $\varepsilon_0 =$ Permittivity of free space,

$\Psi_1 =$ Zeta potential of nanoparticle, $\Psi_2 =$ Zeta potential of the porous media,

$k =$ Debye length, $h =$ Separation distance

The attractive interaction energy $\phi_{vdw}(h)$ due to van der Waals interaction for the sphere-plate geometry was calculated with Equation (4) (Gregory, 1981).

$$\phi_{vdw}(h) = -\frac{A_{123} r_1}{6h}\left[1 + \left(\frac{14h}{\lambda}\right)\right]^{-1} (4)$$

Where A = hamaker constant, λ = Characteristic wavelength, h = Separation distance

The electrostatic interaction energy $\phi_{dl}(h)$ for the sphere-plate geometry was calculated with Equation (5) (Hogg et al., 1966).

$$\phi_{dl}(h) = \pi\varepsilon\varepsilon_0 r_1 \left[2\Psi_1\Psi_2 \ln\left(\frac{1+e^{-kh}}{1-e^{-kh}}\right) + (\Psi_1^2 + \Psi_2^2)\ln\left(1 - e^{-2kh}\right)\right] (5)$$

Where ε= Di electric constant of water,ε_0= Permittivity of free space, Ψ_1 = Zeta potential of nanoparticle,Ψ_2= Zeta potential of the porous media, k = Debye length, r_1 and $r_2$in Equation 1 refer to the radii of two interacting illite particles/titanium dioxide nanoparticles, his the distance between two interacting nanoparticles and A refers to the Hamaker constant (Hamaker, 1937). In Equation 2, K_B T, R, k refer to the Boltzman constant, absolute temperature, radiusof illite particle/titanium dioxide nanoparticle, surface potential, inverse Debye length respectively. In mycalculation, characteristics wavelength λ of interaction was 10^{-7}m, permittivity of free space (ϵ_0) was $8.85\times10^{-12}C^2J^{-1}m^{-1}$, dielectric constant of water (ϵ) was 80, Debye length was $1.04\times10^{8}m^{-1}$and zeta potential was used as approximate surface potential (Elimelech et al., 1995).

Hamaker constant of two dissimilar materials interaction in the presence of third media can be calculated by the following equation(Hiemenz and Rajagopalan, 1997):

$$A_{123} = \left(\sqrt{A_{11}} - \sqrt{A_{33}}\right)\left(\sqrt{A_{22}} - \sqrt{A_{33}}\right)(6)$$

Hamaker constant of illite ($A_{illite\text{-}H2O\text{-}illite}$) was $2.50x10^{-20}$J (Novich and Ring, 1985), Fe coating ($A_{FeOX\text{-}FeOX}$) was $68x10^{-20}$J (Faure et al., 2011), $A_{H2O\text{-}H2O}$ was $3.7x10^{-20}$J (Israelachvili, 2011).

The surface of the Fecoated sand was not chemically homogenous because of the incomplete coverage by Fe coating, therefore, a modified DLVO calculation was done to calculate interaction energy between illite and Fe coated sand. A linear equation was used by Bendersky and Davis (2011) and Bradford and Torkzaban (2013).

$$\Phi_{\mathrm{Total}} = \frac{\mathrm{N_1}}{\mathrm{N_t}}\Phi_1 + \frac{\mathrm{N_2}}{\mathrm{N_t}}\Phi_2(7)$$

Where, Φ_1 and Φ_1 are the total interaction energy between the two different type of surface. For my experiments 1 and 2 are quartz sand and Fe oxyhydroxide respectively. And N_t is the total surface area of the Fe coated sand where N_1 and N_2 are surface area covered by quartz and Fe oxyhydroxide respectively.

Chapter 3: Results and Discussions

3.1 Attachment behavior of illite colloid particles to clean quartz sand and Fe coated sand at different pH and the effects of humic acid

3.1.1 Characterization of illite colloid with and without the presence of HA, Fe coating

Hydrodynamic diameter (HDD) and zeta potential (ZP) of illite in the stock suspension (described in the Section 2.1.5) without the presence of humic acid were measured with Zetasizer at pH 5 and pH 9. At pH 5 and without the presence of HA, HDD of illite was 1378 nm and ZP was -19.4 mV (Fig. 3.1). At pH 9 and without the presence of HA, HDD and ZP of illite were 498 nm and -24.6 mV respectively (Fig. 3.1). These results indicate that the aggregation of illite particles are influenced by pH. Aggregations occurred when the repulsive electrostatic forces between illite particles were low. At pH 5 the absolute value of ZP of illite was low (-19.4 mV) compared to the absolute value of ZP of illite at pH 9 (24.6 mV). Therefore, larger HDD occurred at pH 5 compared to pH 9.

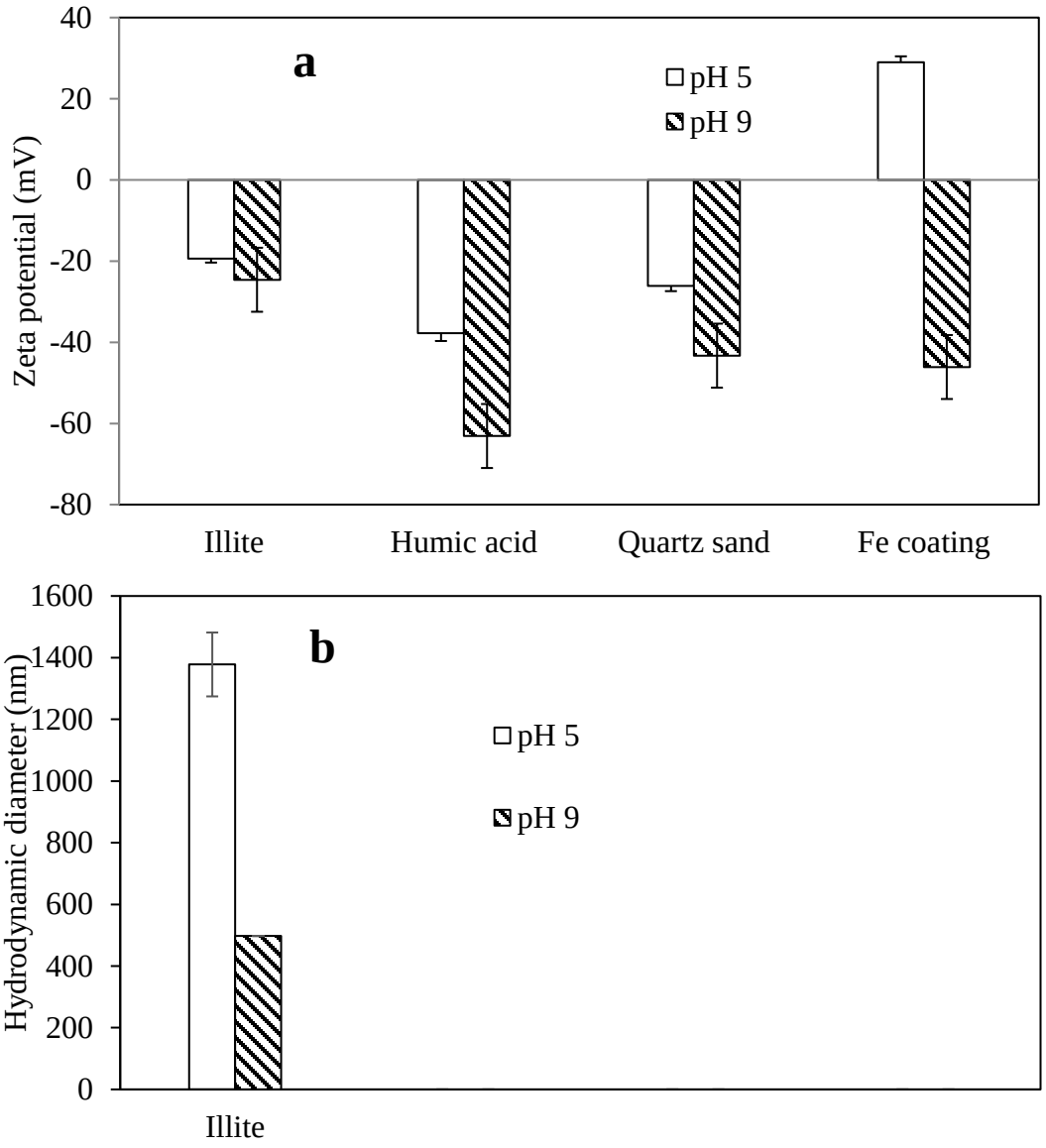

Fig.3.1. Zeta potential of illite, humic acid, quartz sand and Fe coating (Fe oxyhydroxide) (a), and hydrodynamic diameter of illite (b) at pH 5 and 9. Only HDD of the illite particle is needed for further calculations, therefore HDD of the HA and the sand were not measured. In all measurements the background solution was 1 mM NaCl solution. Hydrodynamic diameter was intensity weighted. Data is expressed as mean ± standard deviation of three measurements.

3.1.2 Stability of illite in water

At pH 5, light absorbance of the illite suspension was almost unchanged (A/A_0=1) when 0.625 to 20 mg DOC/L of humic acid was present in the suspension. When no humic acid was present, the light absorbance of the illite suspension decreased slightly (A/A_0=0.98) with time (Fig. 3.2). At pH 9, the light absorbance of illite suspensions was unchanged in presence of 0.625 to 1.25 mg DOC/L HA, and slightly decreased (A/A_0=0.98) in the absence of HA and in the presence of 20 mg DOC/L (Fig. 3.2). The decrease in light absorbance, if any, in all the experiments is negligibly small, indicating that illite suspensions were stable (A/A_0=1) under all these experimental conditions.

Stability of illite particles in water solution is controlled by DLVO forces between illite particles. I calculated the illite-illite interaction energy based on the classic DLVO theory by considering van der waals force and electrostatic force (described in the Section 2.3) for my experimental conditions. The calculated energy profile showed high energy barrier between particles for all the experiments (Fig. 3.2), indicating stable suspension, consistent with the results of the stability test. Illite particles were negatively charged under these conditions (Fig. 3.1), therefore, the high energy barrier was attributable to the repulsive electrostatic forces between negatively charged particles.

The results in the Fig. 3.3 are for the interactions between illite particles that were controlled by DLVO forces between illite particles. This interaction energy between illite particles were calculated by the Equation 1 (described in Section 1.4). This total interaction energies $\phi_{\mathrm{DLVO}}(\mathrm{h})$ between illite particles are the summation of the repulsive interaction energy $\phi_{\mathrm{dl}}(\mathrm{h})$ due to electric repulsion and the attractive interaction energy $\phi_{\mathrm{vdw}}(\mathrm{h})$ due to van der Waals interaction. At pH 5, when there is 20 mg DOC/L HA

present in the suspension, a high energy barrier (described in the Section 2.3) ϕ_{max} = +38.9 K_BT exist between illite particles (Fig. 3.3). Even, when there is no HA present in the illite suspension the energy barrier between the illite particles is ϕ_{max} = +38.5 K_BT (Fig. 3.3). This indicated the repulsive electrostatic forces between two negaively charged illite particles (ψ= - 19.4 mV, ψ= - 31.6 mV presence and absence of HA respectively) (Fig. 3.1). Suspension of the illite particles was stable at pH 5 due to this repulsive electrostatic forces between illite particles.

At pH 9, when there is 20 mg DOC/L HA presence in the suspension, a high energy barrier exists (ϕ_{max} =+66.2 K_BT) between the illite particles (Fig. 3.3). When there is no HA added to the suspension the energy barrier was ϕ_{max} =+22.4 K_BT (Fig. 3.3). This result indicated the repulsive electrostatic forces between two negatively charged illite particles (ψ= - 38.6 mV, ψ= - 24.6 mV presence and absence of HA respectively) (Fig. 3.1), therefore, suspension of the illite particle was stable at pH 9 due to this repulsive electrostatic forces between illite particles.

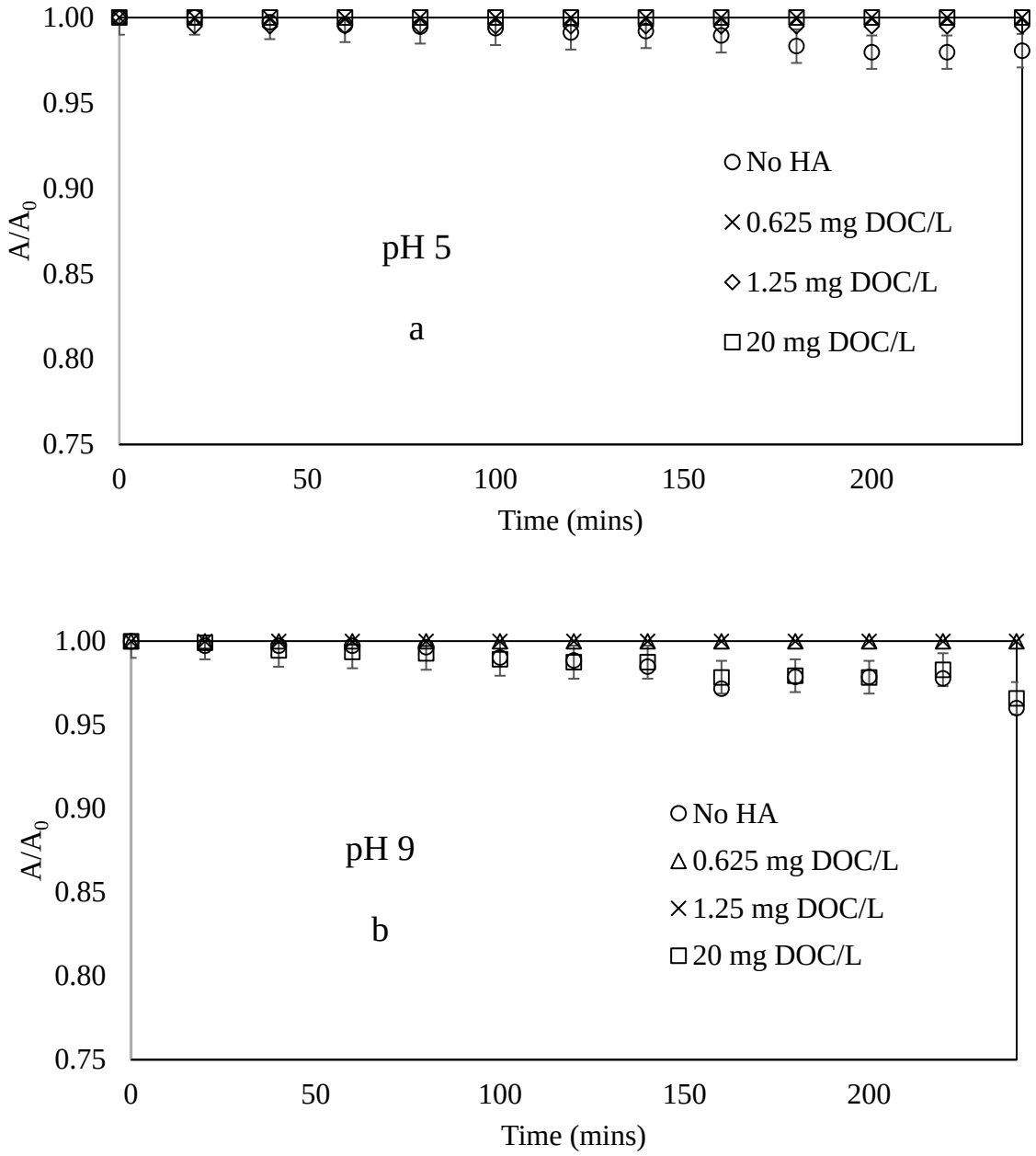

Fig.3.2. Stability tests for illite suspensions in 1 mM NaCl solutions with the presence of different concentrations of HA (no DOC added, 0.625 mg DOC/L, 1.25 mg DOC/L, 20 mg DOC/L) at pH 5 (a) and pH 9 (b). DOC was measured by Shimadzu TOC-V analyzer. A: light absorbance at time t. A_0:light absorbance at time t = 0. Error bars represent analytical errors.

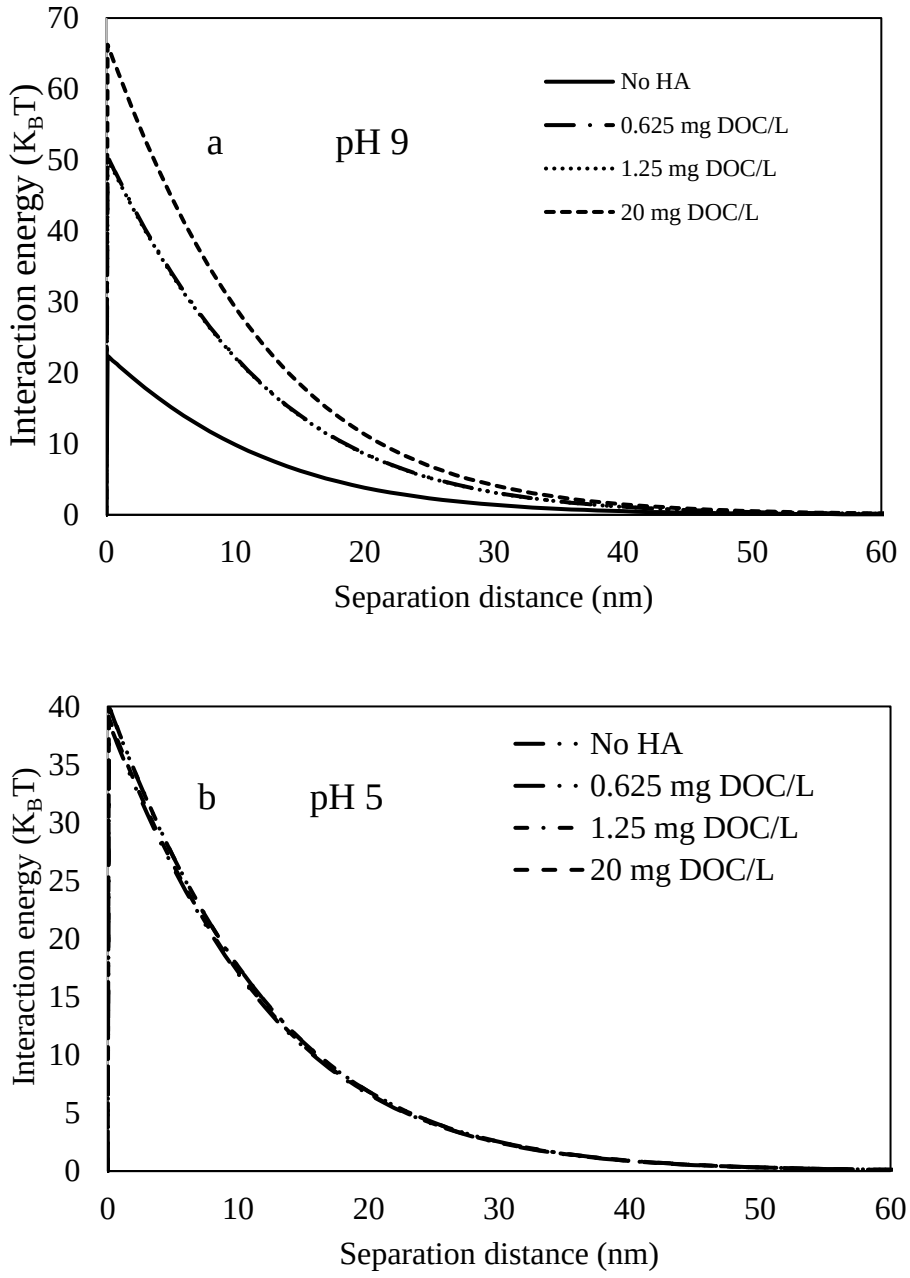

Fig.3.3. Illite-illite interaction energy (K_BT) profiles for illite particles with different concentration (no DOC, 0.625 mg DOC/L, 1.25 mg DOC/L and 20 mg DOC/L) of humic acid (HA) a (pH 9), b (pH 5).

3.1.3 HA attachment to illite at different concentration of HA and its influence on ZP and HDD of illite

Attachment of HA to illite is higher at pH 5 than at pH 9 (Fig. 3.4). Adsorption of HA to illite particles occurs due to hydrophobic interaction, surface complexation, and other nonelectrostatic mechanisms. Therefore, illite particles could adsorb HA even if both HA and illite are both negatively charged.Wu and Cheng (2016) conducted similar type of experiments with $nTiO_2$ and they found $nTiO_2$ adsorbed HA at pH 9, where both $nTiO_2$ and HA carried negative charge. Absolute value of ZP of HA and illite particles are lower at pH 5 than that at pH 9 (Fig. 3.1). Therefore, HA attachment to illite particles is lower at pH 9 due to lower repulsive forces between HA and illite particle. Attachment capacity of illite particles of HA was determined and modeled using Langmuir adsorption isotherm. My experiments showed that the attachment of HA to illite was q_{max}= 83.33 mg organic carbon/g illite at pH 5 and q_{max}= 38.0 mg organic carbon/g illite at pH 9 (Table 1). A very small quantity of HA was adsorbed by the illite particles. Therefore, the results of the calculations fluctuated. As result, a poor linear regression was found at pH 5. This suggests that Langmuir adsorption model may not be applicable under this condition and the q_{max} thus calculated may be inaccurate. For other similar experiments, the reason for the poor linear regression was the same.

At pH 5, ZP of the illite particles was -19.4 mV when there was no HA presence in the illite suspension (Fig. 3.5a). ZPs of the illite particles were approximately -43 mV when 5.7 mg DOC/L to 17.1 mg DOC/L of HA were present in the suspension (Fig. 3.5a and Fig. 3.5c). At pH 9, ZP of the illite particles is -24.6 mV when there is no HA presence (Fig. 3.5b). ZPs of illite particles were around -50 mV when 5.7 mg DOC/L to

17.1 mg DOC/L of HA were present (Fig. 3.5b and Fig. 3.5d). Both the HDD and ZP of the illite particles were influenced by the concentration of HA.

HDD of illite particles were maximum when there is no HA present in the suspension at both pH 5 and 9 (Fig. 3.6a and Fig. 3.6b). At pH 5, the range of HDD of the illite particles was 368.7 nm to 390.3 nm when 5.7 mg DOC/L to 17.1 mg DOC/L of HA were present in the suspension (Fig.3.6c). At pH 9, the range of HDD of the illite particles was 348.4 nm to 371.4 nm when 5.7 mg DOC/L to 17.1 mg DOC/L of HA were present in the suspension (Fig.3.6d).

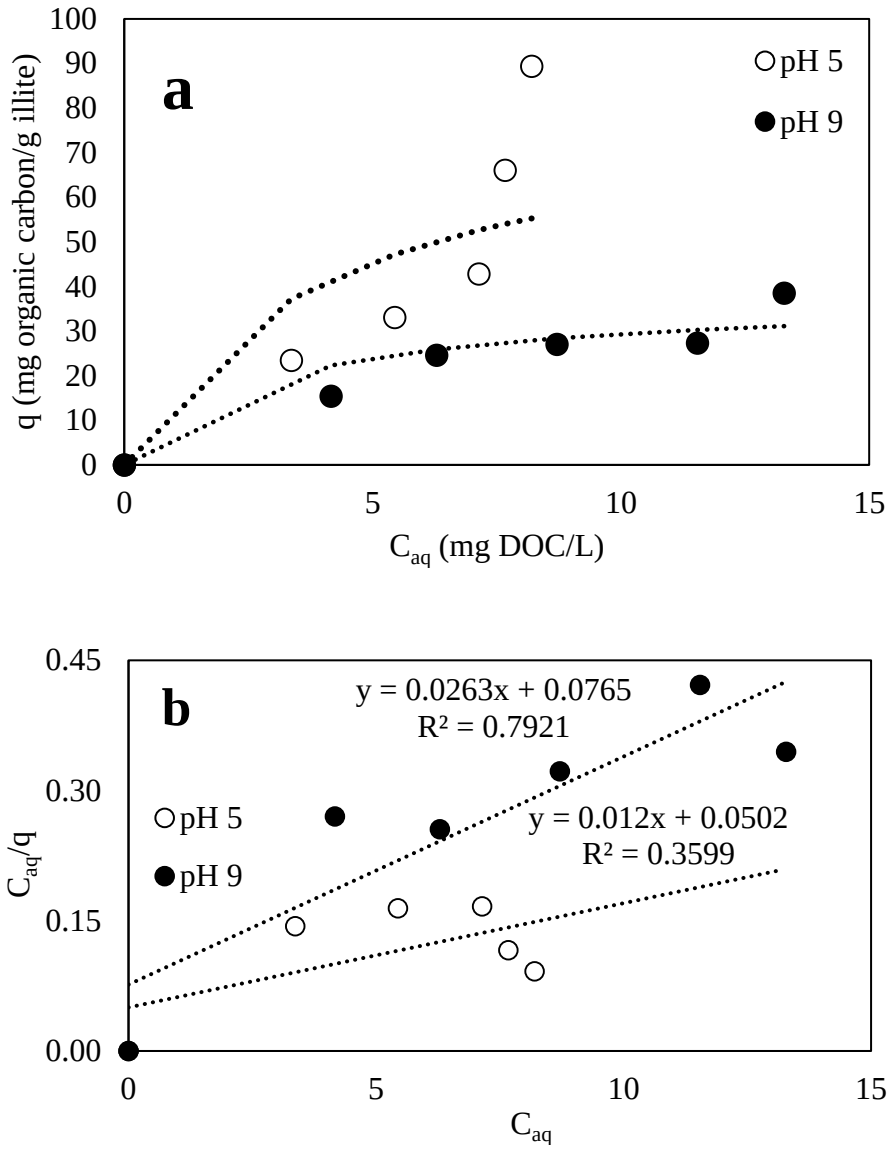

Fig.3.4. Panel (a) represents attachment of HA to 100 mg/L illitesuspension in 1 mM NaCl solution at pH 5 and pH 9. Symbols: experimental measurements; lines: simulated Langmuir adsorption isotherms. q= concentration of HA attached to illite; C_{aq}= concentration of aqueous HA. Panel (b) represents Langmuir adsorption isotherm ($q = \frac{q_{max} K C_{aq}}{1+KC_{aq}}$) parameters for HA attachment to illite at pH 5 and pH 9. K and q_{max} were determined from the slope and intercept of a linear plot of C_{aq}/q against C_{aq}. Dotted lines represent the linear regression. A very small quantity of HA was adsorbed by the illite particles. Therefore, the results of the calculations was fluctuated for a very small difference. As result, a poor linear regression was found at pH 5.

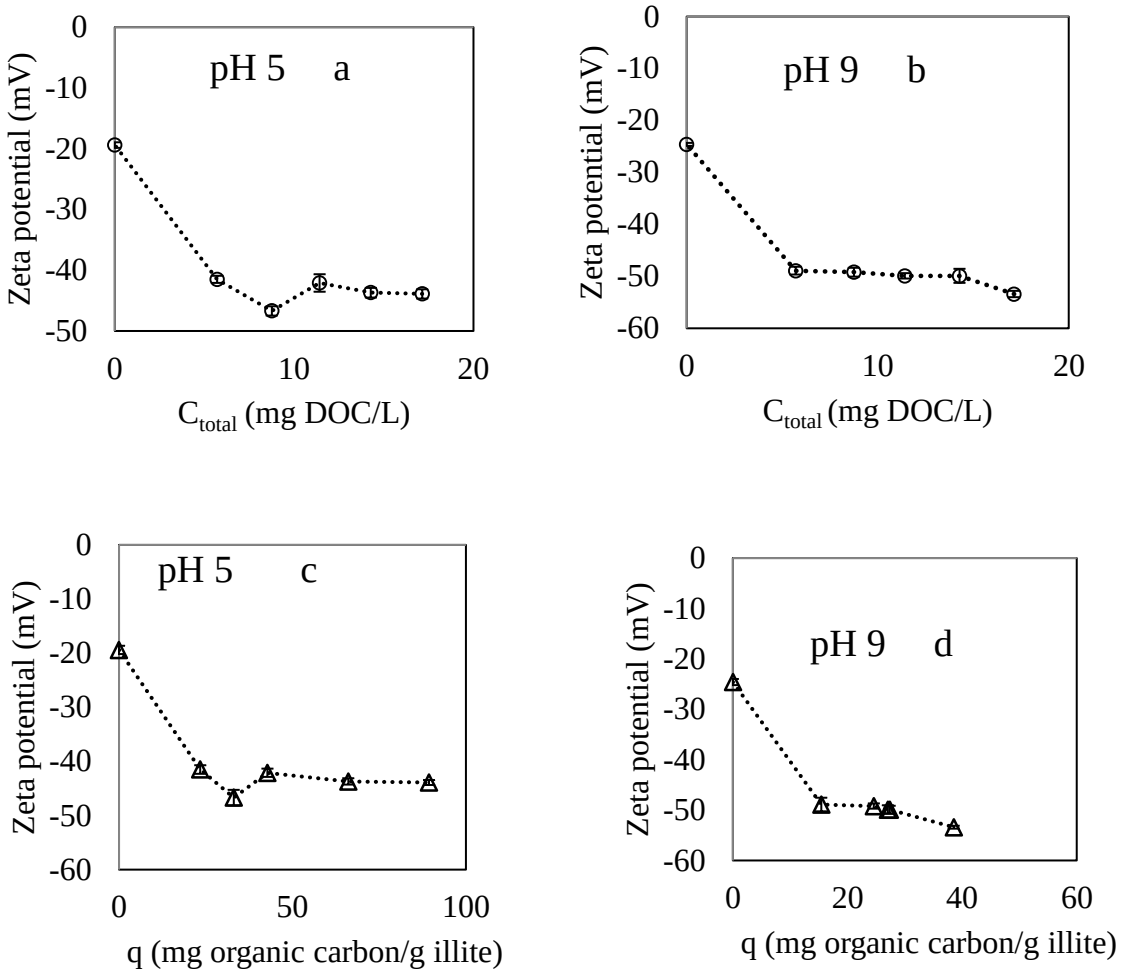

Fig.3.5. ZP of illite(100 mg/L)at different concentration of HA was measured by a Zetasizer at pH 5 and pH 9. Measured zeta potentials are expressed as mean of triplicate measurements. Trend lines are added to guide visual inspection. Panel (a) and (b) represent zeta potential of illite as a function of total HA concentration (C_{total}), Panel (c) and (d) represent zeta potential of illite as a function of adsorbed HA concentration on illite (q). q was calculated using Langmuir adsorption isotherm and mass balance equation (Wu and Cheng, 2016). Data is expressed as mean ± standard deviation of three measurements.

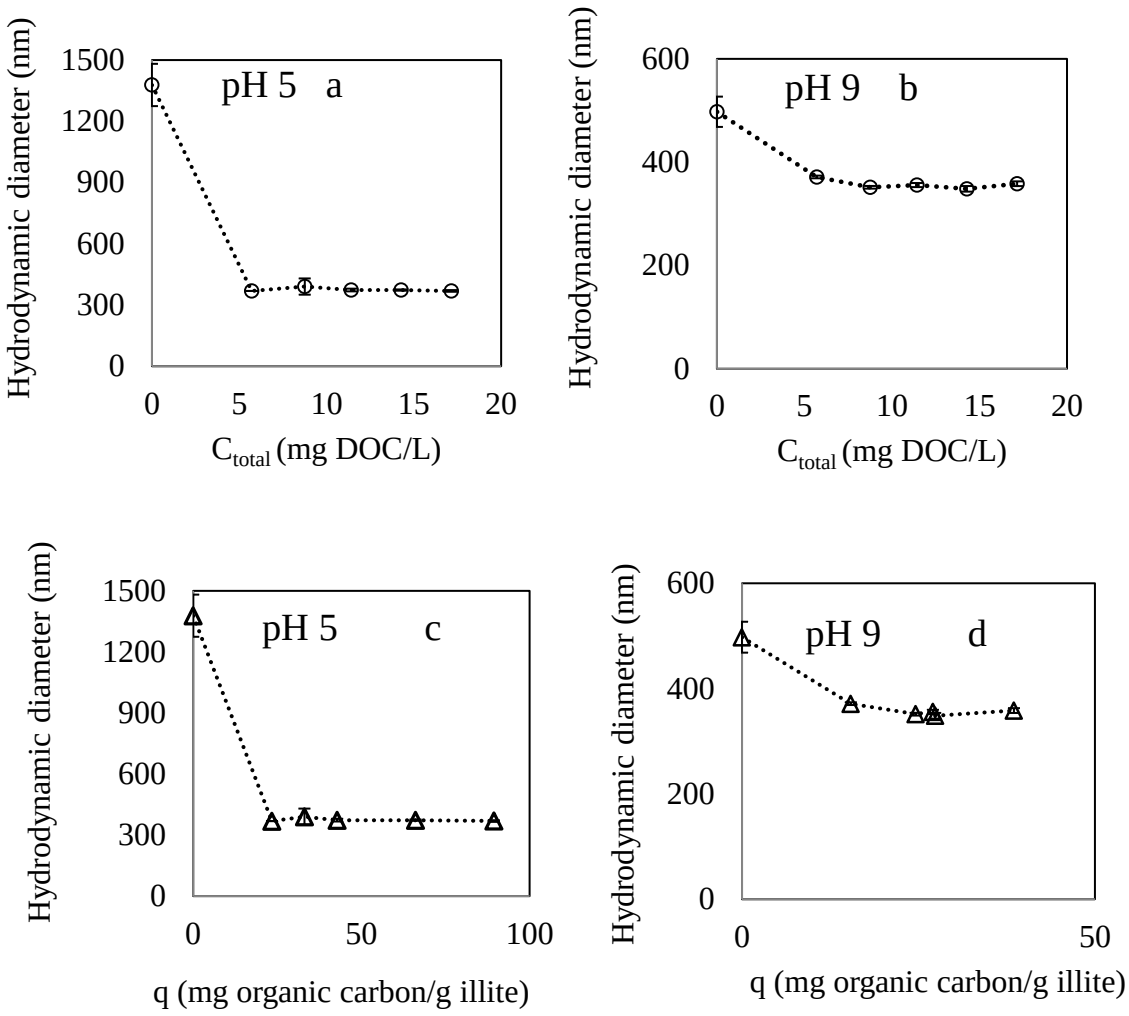

Fig.3.6. HDD of illite at different concentration of HA was measured by a Zetasizer at pH 5 and pH 9. Measured HDD are expressed as mean of triplicate measurements. Trend lines are added to guide visual inspection.Panel (a) and (b) represent HDD of illite as a function of total HA concentration (C_{total}), Panel (c) and (d) represent HDD of illite as a function of adsorbed HA concentration on illite (q). q was calculated using Langmuir adsorption isotherm and mass balance equation (Wu and Cheng, 2016). Data is expressed as mean ± standard deviation of three measurements.

3.1.4Attachment of illite to the quartz sand in the absence HA

In the absence of HA, attachment of illite particles to the clean quartz sand strongly depends on pH. At pH 5, the amount of illite attached was higher than that at pH 9 (Fig. 3.7a). Langmuir adsorption isotherm was used to model the data and found the maximum attachment for illite to pure quartz sand were $5.25x10^{-3}$ mg/g at pH 5 and $5.09x10^{-4}$ mg/g at pH 9 respectively (Table 1).

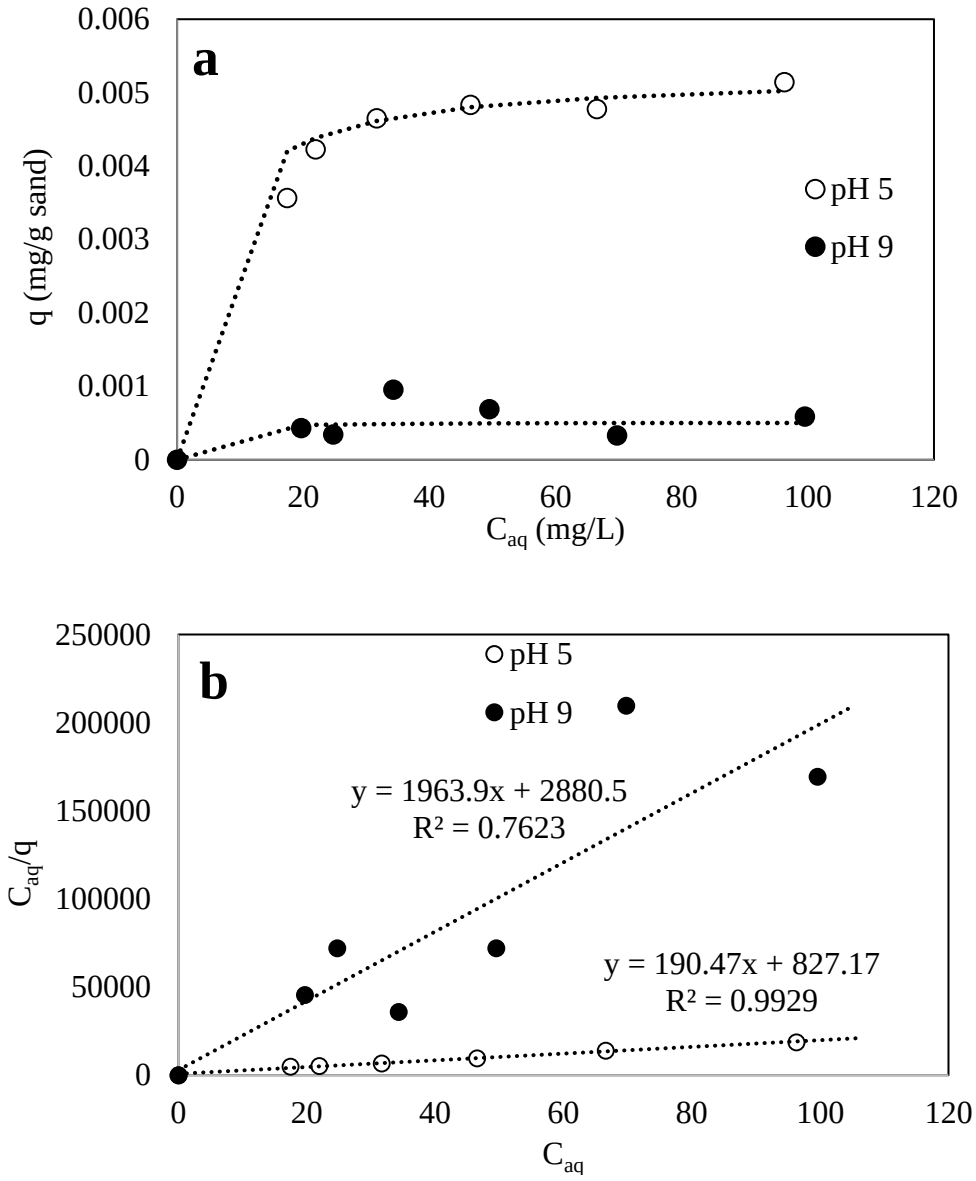

Fig. 3.7. Panel (a) represents attachment behavior of illite to 25 g of clean quartz sand in 35 ml 1 mM NaCl solution at pH 5 and 9. Symbols: experimental measurements; lines: simulated Langmuir adsorption isotherms. q = concentration of illite attached to sand; C_{aq}= concentration of suspended illite. Panel (b) represents Langmuir adsorption isotherm ($q = \frac{q_{max} K C_{aq}}{1+K C_{aq}}$) parameters for illite attachment to quartz sand at pH 5 and pH 9. K and q_{max} were determined from the slope and intercept of a linear plot of C_{aq}/q against C_{aq}. Dotted lines represent the linear regression.

Illite attachment to quartz sand can be explained by DLVO theory. ZP of both illite particles and sand are negative at both pH 5 and pH 9 (Fig. 3.1). Therefore, an energy barrier exists between illite particles and sand at both pH 5 and pH 9 (Table 1). At pH 5, absolute value of ZP of illite particles and sand are less than the absolute value of ZP of illite particles and sand at pH 9. DLVO interaction energy is +290.2 K_BT at pH 5 and +465.3 K_BT at pH 9 (Table 1). But a very limited amount of illite particles were attached to the sand due to hydrophobic interaction, surface complexation and other non-electrostatic mechanisms. Hence, at pH 5 attachment of illite particles is higher than pH 9 and the quantity of illite clay particles adsorbed by the sand is higher (Fig. 3.7).

Table 1. Langmuir adsorption isotherm ($q = \frac{q_{max}KC_{aq}}{1+KC_{aq}}$) parameters for HA absorption to illite, illite absorption to quartz sand, illite absorption to Fe coated sand, HA absorption to quartz sand and HA absorption to Fe coated sand. DLVO interaction energies between illite particles and quartz sand with and without presence of HA, illite particles and Fe coated sand with and without presence of HA. All the experiments were done at both pH 5 and pH 9. K and q_{max}were determined from the slope and intercept of a linear plot of 1/q against C_{aq} (Wu and Cheng, 2016). $R^2$is the coefficient of linear regression.

	pH	q_{max}(mg/g)	K (L/mg)	R^2	$\boldsymbol{\phi_{max}}$(K_BT)
HA to illite	5	83.33	0.24	0.36	not calculated
HA to illite	9	38.00	0.34	0.79	not calculated
Illite to quartz sand	5	$5.25x10^{-3}$	0.23	0.99	+290.2
Illite to quartz sand	9	$5.09x10^{-4}$	0.68	0.76	+465.3
Illite to Fe coated sand	5	0.13	0.19	0.81	+9.4
Illite to Fe coated sand	9	$-2.47x10^{-4}$	-0.06	0.63	+292.4
HA to quartz sand	5	$3.87x10^{-5}$	0.31	0.78	not calculated
HA to quartz sand	9	$-1.39x10^{-6}$	-0.18	0.16	not calculated
HA to Fe coated sand	5	$3.52x10^{-3}$	1.04	0.98	not calculated
HA to Fe coated sand	9	$3.12x10^{-5}$	-0.67	0.96	not calculated

3.1.5 Attachment of illite to the Fe coated sand in the absence of HA

At pH 5, experimental data showed that the maximum adsorption of illite to Fe coated sand was 0.114 mg/g (Fig. 3.8a). Light absorbance of illite free control was 0.004 Au which was negligible. Langmuir adsorption isotherm was used to model the data and found the adsorption capacity of Fe coated sand was q_{max}= 0.13 mg/g at pH 5 (Table 1). At pH 5, illite particles were negatively charged but Fe coating carried positive charge (Fig. 3.1). As a result, illite particles were strongly attracted by the Fe coated sand. Therefore, quantity of illite clay particles adsorbed by the Fe coated sand is almost 80% at pH 5 (Fig. 3.13).

At pH 5, ZP of the illite particles was 29 mV when there was no HA presence in the illite suspension (Fig. 3.9a). ZPs of the illite particles were approximately -55 mV when 5.7 mg DOC/L to 17.1 mg DOC/L of HA were present in the suspension (Fig. 3.9a and Fig. 3.9c). At pH 9, ZP of the illite particles is -46 mV when there is no HA presence (Fig. 3.9b). ZPs of illite particles were around -59 mV when 5.7 mg DOC/L to 17.1 mg DOC/L of HA were present (Fig. 3.9b and Fig. 3.9d). ZP of the illite particles were influenced by the concentration of HA.

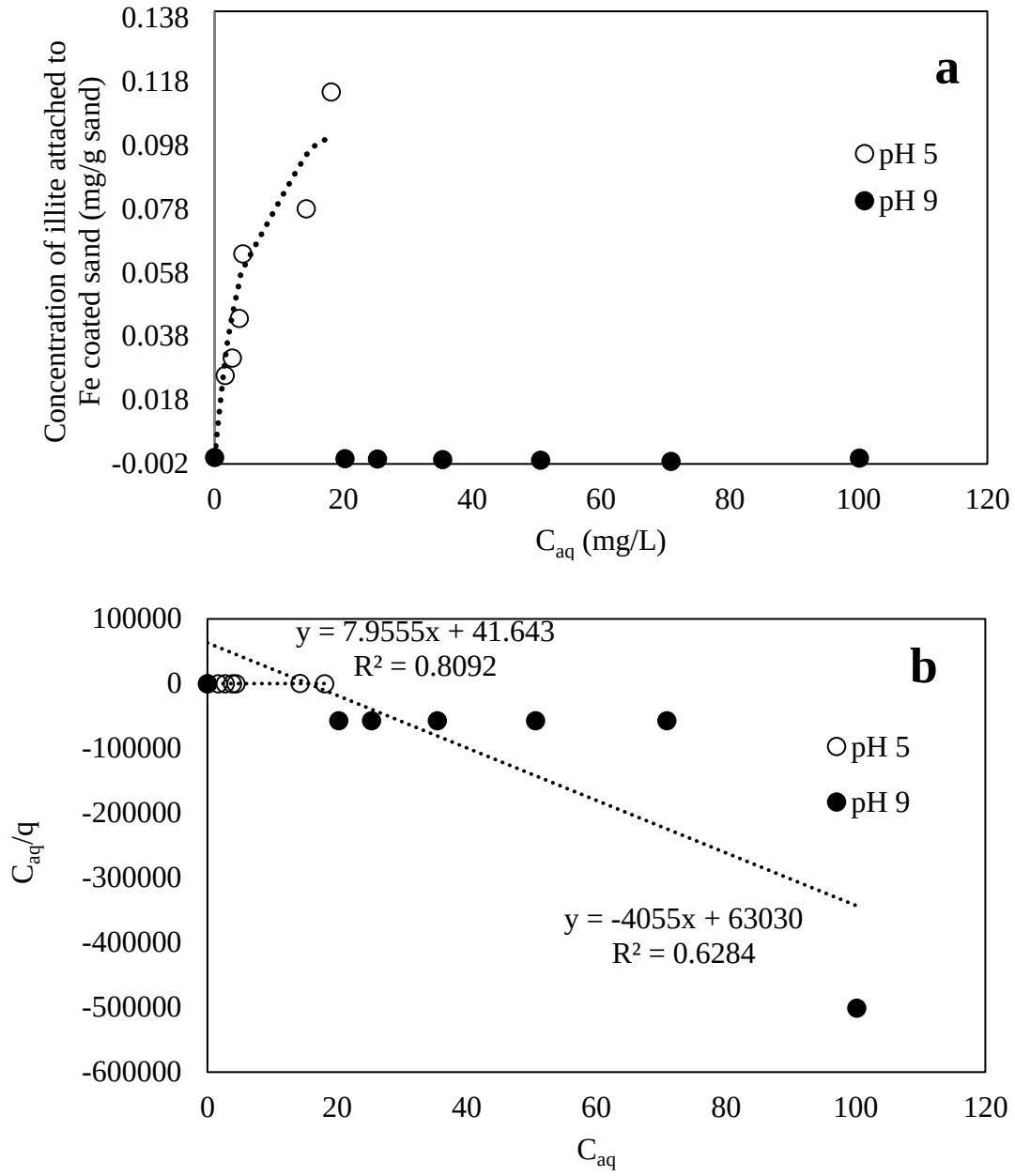

Fig.3.8. Panel (a) represents attachment behavior of illite to 25 g of Fe coated sand in 35 ml 1 mM NaCl solution at pH 5 and 9. Symbols: experimental measurements; lines: simulated Langmuir adsorption isotherms.q= concentration of illite attached to Fe coated sand; C_{aq}= concentration of suspended illite. Panel (b) represents Langmuir adsorption isotherm ($q = \frac{q_{max} K C_{aq}}{1+K C_{aq}}$) parameters for HA attachment to Fe coatedsand at pH 5 and pH 9. K and q_{max} were determined from the slope and intercept of a linear plot of C_{aq}/q against C_{aq}. Dotted lines represent the linear regression.

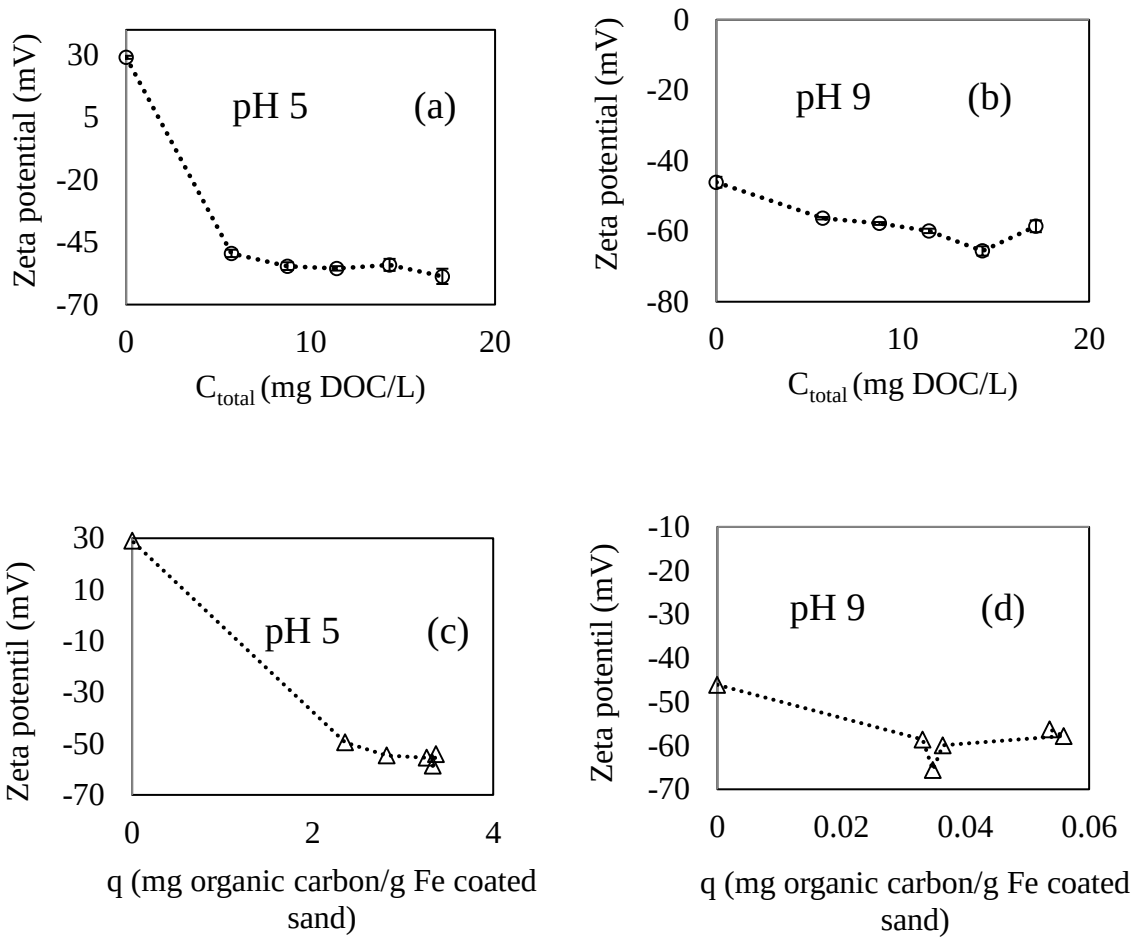

Fig.3.9. ZP of Fe oxyhydroxide (125 mg/L) at different concentration of HA was measured by a Zetasizer. Panel (a) and (b) represents the zeta potential of Fe oxyhydroxide at different concentration of HA. Panel (c) and (d) represent zeta potential of Fe oxyhydroxide as a function of adsorbed HA concentration on Fe oxyhydroxide where dotted lines were added to guide visual inspection. q was calculated using Langmuir adsorption isotherm and mass balance equation (Wu and Cheng, 2016).

At pH 5, ZPs of both illite and pure quartz sand were negative and ZP of the Fe coating was positive (Fig. 3.1). The surface of the Fe coated sand was not chemically homogenous because of incomplete coverage by Fe coating, therefore, a modified DLVO calculation was done to calculate interaction energy between illite and Fe coated sand. The total interaction energy was calculated using a linear equation (described in the section 2.3). DLVO interaction energy profile calculations were done based on the assumption of sand surface covered by Fe coating. Backscatter SEM images of the Fe coated sand (Fig.3.15) and the EDX profile analysis report (Table 2) showed that the quartz sand was coated with Fe oxyhydroxide by 34% and 66% of the sand surface was uncovered. DLVO interaction energy were calculated for both covered and uncovered quartz surface. Calculated DLVO interaction energy between illite and quartz surface was positive where Fe coating surface showed negative. However, the energy profile for illite to Fe coated sand was less positive (ϕ_{max} =+9.5 K_BT) (Fig. 3.10a), attributable to partial coverage of the sand surface by positively charged Fe coating, which increased adsorption of negatively charged illite particles.

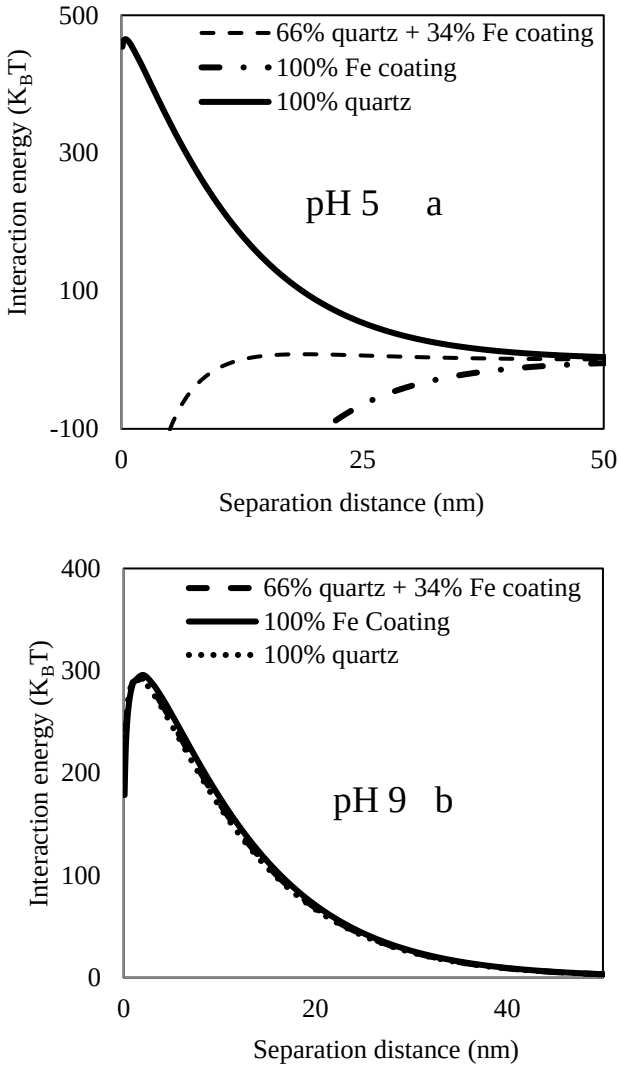

Fig.3.10. DLVO interaction energy profile between illite and Fe Coated sand in 1 mM of NaCl solution in the absence of humic acid (HA) at pH 5 (a) and pH 9 (b).

At pH 9, experimental data shows us that the adsorption of illite particles to Fe coated sand was not detectable (Fig. 3.8a). It was found that the light absorbance of illite free control was 0.008 Au at pH 9 for that reason the final absorbance of the suspension in the equilibrium was higher than the initial absorbance. Langmuir adsorption isotherm was used to model the data and found the maximum attachment for illite to pure quartz sand was -2.47×10^{-4} mg/g (Table 1), which indicated that no adsorption occurred at pH 9.

Illite particles, Fe coating and quartz sand were negatively charged at pH 9 (Fig. 3.1). DLVO interaction energy profile was calculated based on the assumption of sand surface covered by Fe coating. Backscatter SEM images of the Fe coated sand and the EDX profile analysis report showed that the quartz sand was coated with Fe oxyhydroxide by 34% and 66% of the sand surface was uncovered. DLVO interaction energy profiles were calculated for both covered and uncovered surface of the sand and a linear equation (described in the Section 2.3) was used to sum up the total interaction energy between illite particles and Fe coated sand that was positive and $\phi_{max} = +292.4$ K_BT (Fig. 3.10b). This result indicated that a large energy barrier existed between the illite particles and Fe coated sand, suggesting illite particles should not attach to the Fe coated sand at pH 9.

3.1.6 Attachment of HA to quartz sand and Fe coated sand

My experiments showed that there was negligible amount of HA absorbed by the quartz sand at both pH 5 and pH 9 (Fig. 3.11a). Quartz sands were negatively charged at both pH 5 and pH 9 (Fig. 3.1), and HA were also negatively charged at these pH (Fig. 3.1). Therefore, HA was repelled by the quartz sand and there was no HA adsorbed.

Experimental data showed us that the maximum adsorption ($3.64x10^{-5}$ mg/g) occurred when 11.42 mg DOC/L HA present in the suspension. Langmuir adsorption isotherm was used to model the data and found the maximum attachment for HA to pure quartz sand was $3.87x10^{-5}$ mg/g (Table 1).

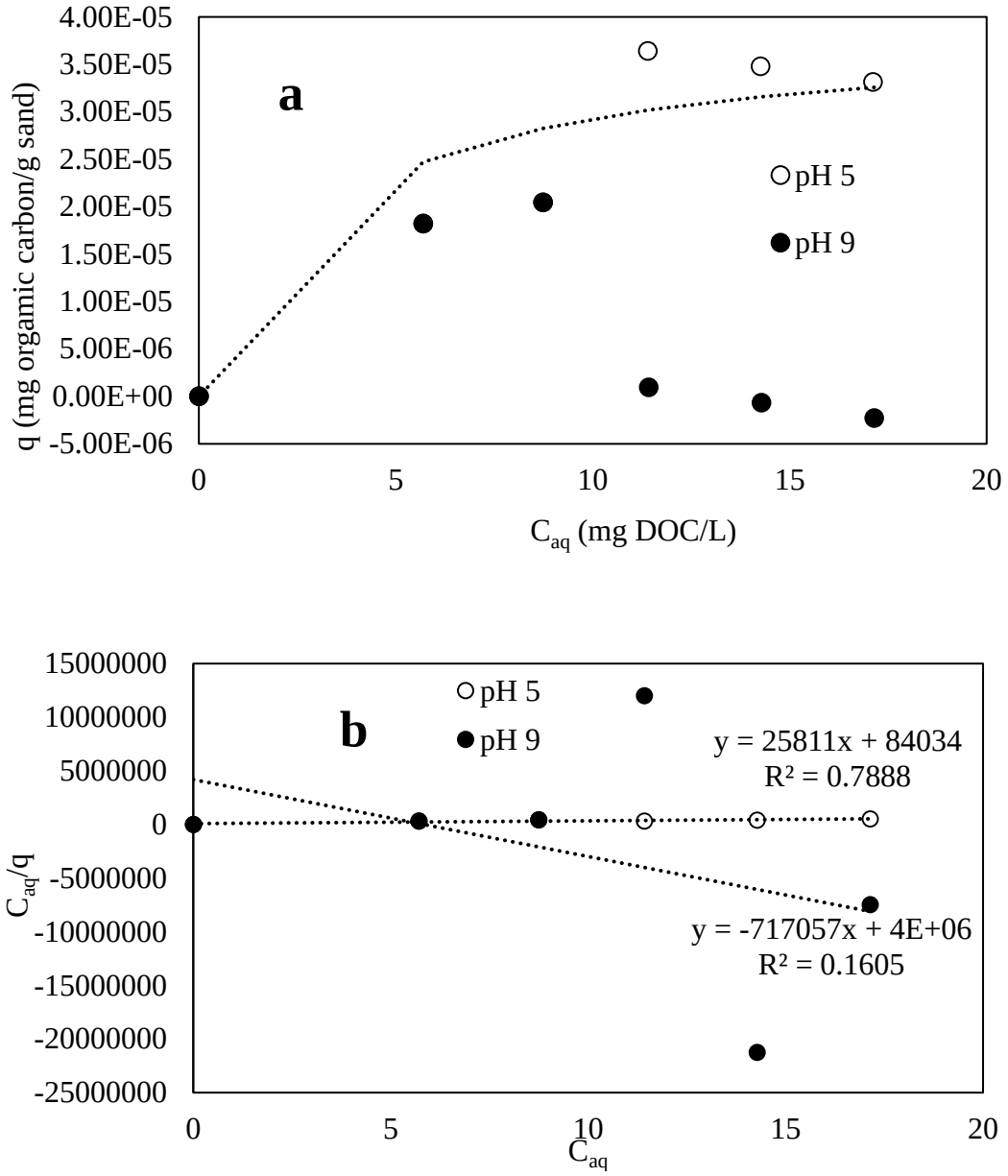

Fig. 3.11. Panel (a) represents adsorption of humic acid (HA) to 25 g of clean quartz sand at both pH 5 and pH 9 in 35 mL of 1 mM NaCl solution. Symbols: experimental measurements; Lines: simulated Langmuir adsorption isotherms. q: adsorbed HA concentration after 3 hours of mixing; C_{aq}: aqueous-phase HA concentration of after 3 hours of mixing. Panel (b) represents Langmuir adsorption isotherm ($q = \frac{q_{max} K C_{aq}}{1+K C_{aq}}$) parameters for HA attachment to quartz sand at pH 5 and pH 9. K andq_{max} were determined from the slope and intercept of a linear plot of C_{aq}/q against C_{aq}. Dotted lines represent the linear regression. A very small quantity of HA was adsorbed by the clean quartz sand. Therefore, the results of the calculations was fluctuated for a very small difference. As result, a poor linear regression was found at pH 9. Therefore, there could be large and uncertainities in the calculated q_{max} and the K.

Conversely, experimental data showed that, at pH 5 maximum adsorption ($3.36x10^{-3}$ mg/g) occurred when 14.28 mg DOC/L HA present in the suspension (Fig. 3.12). Langmuir adsorption isotherm was used to model the data and found the maximum attachment for HA to Fe coated sand was $3.52x10^{-3}$ mg/g (Table 1). At pH 9, maximum adsorption ($3.64x10^{-5}$ mg/g) occurred when 11.42 mg DOC/L HA present in the suspension (Fig. 3.12). Langmuir adsorption isotherm was used to model the data and found the maximum attachment for HA to Fe coated sand was $3.12x10^{-5}$ mg/g (Table 1).

At pH 5, ZP of Fe coating is positive, quartz sand and HA are negative (Fig. 3.1). The surface of the Fe coated sand is not chemically homogenous because of incomplete coverage by Fe coating. Therefore, partial coverage of the sand surface by positively charged Fe coating increased adsorption of negatively charged HA. At pH 9, Fe coating and the quartz sand surface was negatively charged, HA was negatively charged as well. Therefore, a negligible amount of HA was adsorbed by the Fe coated sand. Although other mechanisms may also influence HA adsorption, electrostatic force between HA and sorbent surface is sufficient to explain the observed results, indicating that electrostatic forces play a major role in the adsorption of HA to illite, quartz sand and Fe coated sand.

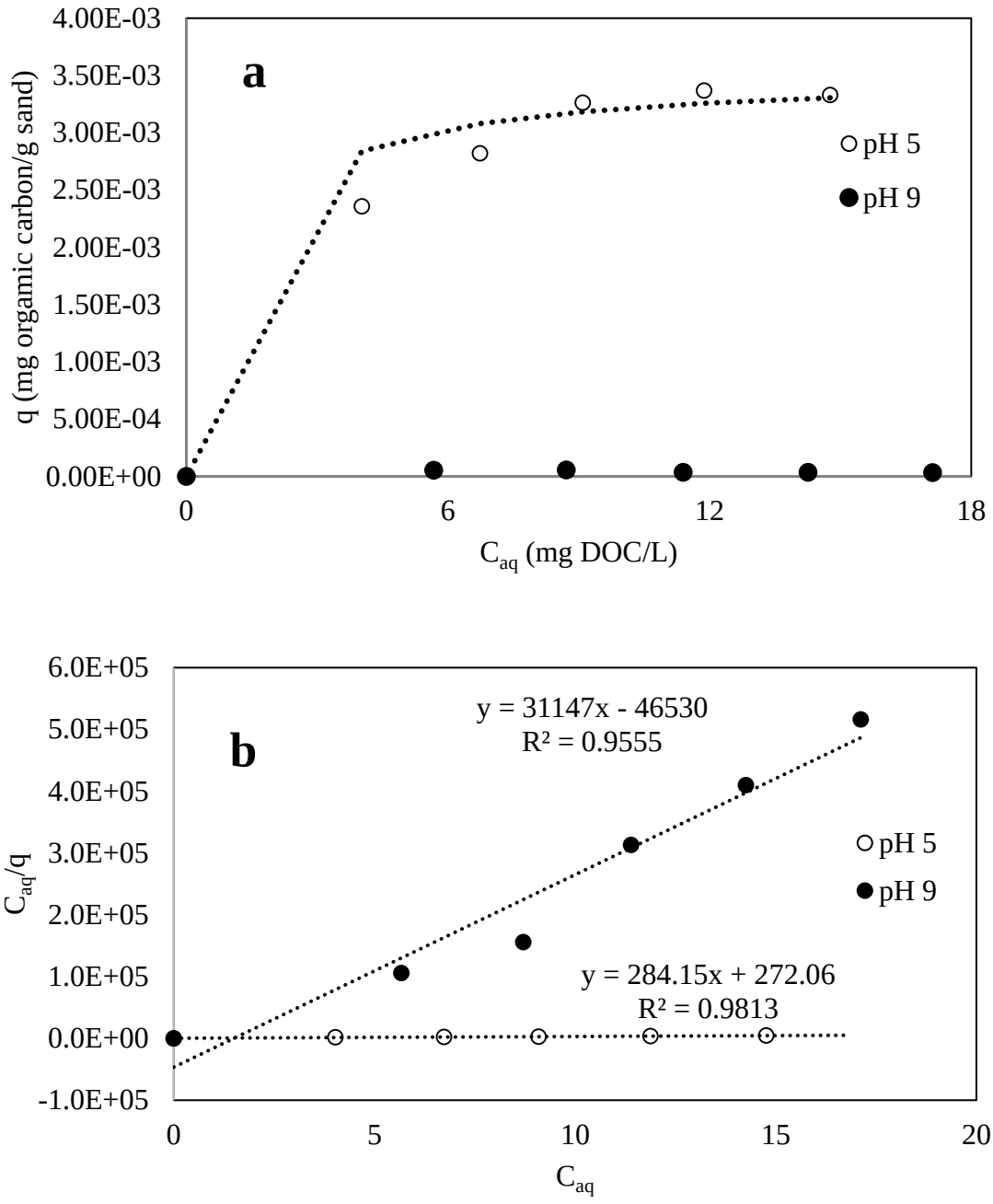

Fig.3.12. Panel (a) represents adsorption of humic acid (HA) to 25 g of Fe coated sand at both pH 5 and pH 9 in 35 mL of 1 mM NaCl solution. Symbols: experimental measurements; Lines: simulated Langmuir adsorption isotherms. q: adsorbed HA concentration after 3 hours of mixing; C_{aq}: aqueous-phase HA concentration of after 3 hours of mixing. Panel (b) represents Langmuir adsorption isotherm ($q = \frac{q_{max} K C_{aq}}{1+K C_{aq}}$) parameters for HA attachment to Fe coated sand at pH 5 and pH 9. K and q_{max} were determined from the slope and intercept of a linear plot of C_{aq}/q against C_{aq}. Dotted lines represent the linear regression.

3.1.7 HA influence on illite attachment to quartz sand and Fe coated sand

Experimental data showed that little to no illite particles were adsorbed to the quartz sand at pH 5 or pH 9 either in the absence of presence of HA (Fig. 3.13a).While more than 80% of illite particles were attached to the Fe coated sand at pH 5 in the absence of HA, the presence of HA at pH 5 substantially decreased the percentage of illite attached to the Fe coated sand to less than 10% (Fig. 3.13b). At pH 9, less than 1 percent of illite particles were attached to the Fe coated sand either in the absence or presence of HA.

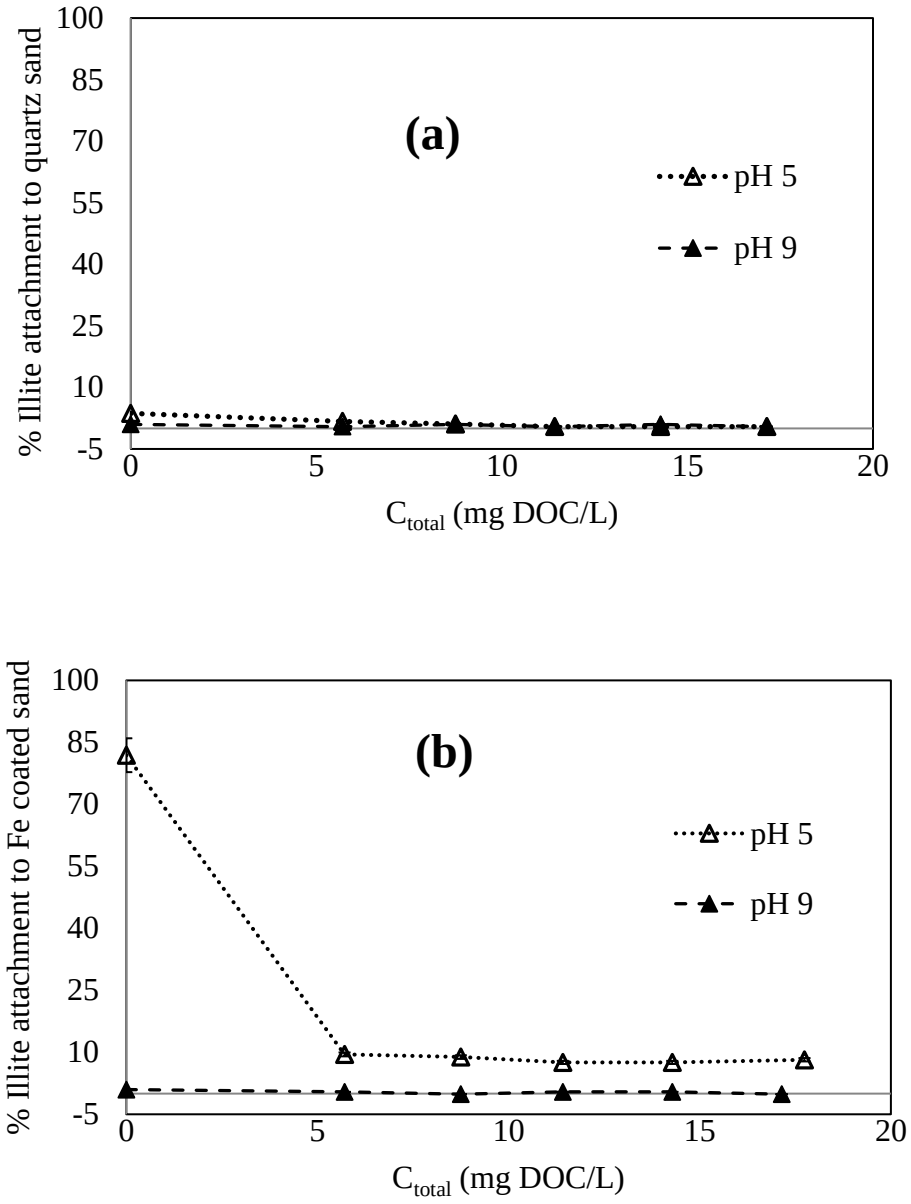

Fig. 3.13. Attachment of illite (100 mg/L) particles to quartz sand and Fe coated sand. Figure represents the percentage of illite particles to 25 g of quartz sand and 25 g of Fe coated sand with five different concentration of HA at pH 5 and pH 9. Dotted lines represent the trend lines added to guide visual inspection. Error bars represent analytical errors.

HA, illite particles, and quartz sand surface were all negatively charged at both pH 5 and pH 9 (Fig. 3.1). The calculated DLVO energy profile showed strong repulsion between the illite particle and the quartz sand at both pH for different concentrations of HA (Fig. 3.14). At pH 5, the energy barriers between the quartz sand and illite particle ranged from +240.9 K_BT to +465.3 K_BT (Fig. 3.14a). At pH 9, the DLVO energy barriers between the quartz sand illite particle were even higher, ranging from +290.2 K_BT to +580.2 K_BT (Fig. 3.18b). The high energy barriers explained the experimentally observed low illite attachment to the quartz sand.

Wu and Cheng (2016) conducted a study of $nTiO_2$ attachment to quartz sand and they showed that at pH 5, 100% $nTiO_2$ were attached to quartz sand in the absence of HA, and the attachment of $nTiO_2$was practically zero in the presence of HA. Freake (2016) studied the effects of phosphate on the attachment of $nTiO_2$ and illite colloids to quartz sand and showed that at pH 5 (i) attachment of illite to quartz sand was very low both in the absence and presence of phosphate, and (ii) >95% of $nTiO_2$ were adsorbed by the quartz in the absence of phosphate, and $nTiO_2$ adsorption decreased with increasing phosphate concentration and became practically zero at phosphate concentrations >4 mg/L. At pH 5, $nTiO_2$ was positively charged in the absence of HA or phosphate, but quartz sand and illite were negatively charged. Therefore, in the absence of HA or phosphate, positively charged $nTiO_2$ particles were adsorbed by the negatively charged quartz sand. In the presence of HA or phosphate, $nTiO_2$ particles adsorbed HA or phosphate and became negatively charged.As a result, thenegativelycharged $nTiO_2$ were repelled by the negatively charged quartz sand, resulting in low $nTiO_2$ attachment. Those previous studies showed that $nTiO_2$ attachment is mainly controlled by the ZP of $nTiO_2$

and the collector surface, and HA and phosphate influence $nTiO_2$ attachment by adsorbing to $nTiO_2$ and changing the ZP of $nTiO_2$. Conversely, adsorption of HA or phosphate to illite was low and did not change the ZP of illite, and therefore illite attachment to quartz sand was low either in the absence or presence of HA and phosphate.

At pH 9, Wu and Cheng (2016) showed that no $nTiO_2$ were attached to quartz sand either in the presence and absence of HA. Freake (2016) also showed that attachment of illite and $nTiO_2$ colloidal particles were low both in the absence and presence of phosphate. All the above results are similar to my experimental results, which illustrated that at pH 9, attachment of illite particles was low (<1%) both in the presence and absence of HA. At pH 9, $nTiO_2$, illite, quartz sand, HA, phosphate all were negatively charged, and the presence of HA or phosphate did not influence the ZP of $nTiO_2$ and illite. Therefore, HA and phosphate did not change the extent of $nTiO_2$ and illite attachment to the quartz sand.

The high illite attachment to the Fe coated sand at pH 5 (Fig. 3.13b) in the absence of HA was due to illite attachment to the Fe coating on the sand. From the SEM backscatter image analysis (Fig. 3.15) it was found that on average 34% of the quartz sand surface area were covered by the Fe coating (Table 2). At pH 5, in the absence of HA, the negatively charged illite particles were repelled by the like-charged quartz surface. However, the positive Fe coating (Fig. 3.1) on the sand attracted the illite particles, and the overall result was high illite attachment to the sand. At pH 5, when HA was added to the illite-Fe coated sand systems, ZP of the illite particles were still negative (Fig. 3.5) and ZP of the quartz surface remained negative (i.e., unchanged) due to very low HA adsorption to quartz sand (Fig. 3.11). However, due to the strong adsorption of

HA to the Fe coating (Fig. 3.12), ZP of the Fe coating changed from positively to negative (Fig. 3.9). As a result, the negatively charged illite particles were repelled by the like-charged quartz surface, as well as the Fe coating, causing low illite attachment (Fig. 3.13b). The percentage of illite attached, although low (~8%), was still substantial, which cannot be explained only by the electrostatic forces. Wu and Cheng (2016) showed that a small fraction of $nTiO_2$ colloidal particles attached to the quartz sand and Fe coated sand under unfavorable conditions due to the surface roughness of the sand and Fe coating. It is likely that the small fraction of illite particles attached to the sand observed in my experiments was also due to the surface roughness of the sand and Fe coating.

Wu and Cheng (2016) observed that in the absence of HA, 100% of $nTiO_2$ particles were attached to Fe coated sand at pH 5, and $nTiO_2$ particle attachment decreased to ~5% with increasing HA concentration, similar to what my experimental results with illite, i.e., >80% of illite were attached to the Fe coated sand in the absence of HA, but very low percentage (~8%) of illite attached in the presence of HA. At pH 5, in the absence of HA, $nTiO_2$ and Fe coating were positively charged, but illite and quartz sand surface were negatively charged. As a result, positively charged $nTiO_2$ particles were adsorbed by the negatively charged quartz surface, and negatively charged illite particles were adsorbed by the positively charged Fe coating surface. Therefore, attachment of both $nTiO_2$ and illite particles to Fe coated sand were high in the absence of HA. In the presence of HA, due to HA adsorption to $nTiO_2$ and Fe coating, both $nTiO_2$ and Fe coating became negative. As a result, the negatively-charged $nTiO_2$ and illite were repelled by the like-charged Fe coating (and the quartz), resulting in low$nTiO_2$ and illite attachment.

At pH 5, in the presence of HA, due to the repulsive electrostatic forces between $nTiO_2$/illite and Fe coated sand, no $nTiO_2$/illite particles are expected to attach to the sand. However, both Wu and Cheng (2016) and my results showed a small fraction of colloidal particles attached. This is likely caused by surface roughness of the Fe coating. Backscatter SEM images of Fe coated sand showed significant depressions and roughness on Fe coated surface (Fig. 3.15). Microscale even nanoscale surface roughness may favor particle retention (Benderskyand Davis, 2011). Sharp asperities on sand surfaces may facilitate colloid deposition (Shen et al., 2011), resulting low attachment of both TiO_2 and illite particles to the Fe coated sand.

Wu and Cheng (2016) found that at pH 9 attachment of $nTiO_2$ to Fe coated sand was low, both in the absence and presence of HA. My experiments with illite showed that attachment of illite to Fe coated sand was also low both in the absence and presence of HA. At pH 9, $nTiO_2$, illite particles, Fe coated surface, quartz surface and HA all were negatively charged, and no HA were adsorbed by $nTiO_2$ and Fe coated surface.Therefore, $nTiO_2$ and illite particles were repelled by the negatively-charged Fe coated sand, resulting in low attachment of $nTiO_2$ and illite particles.

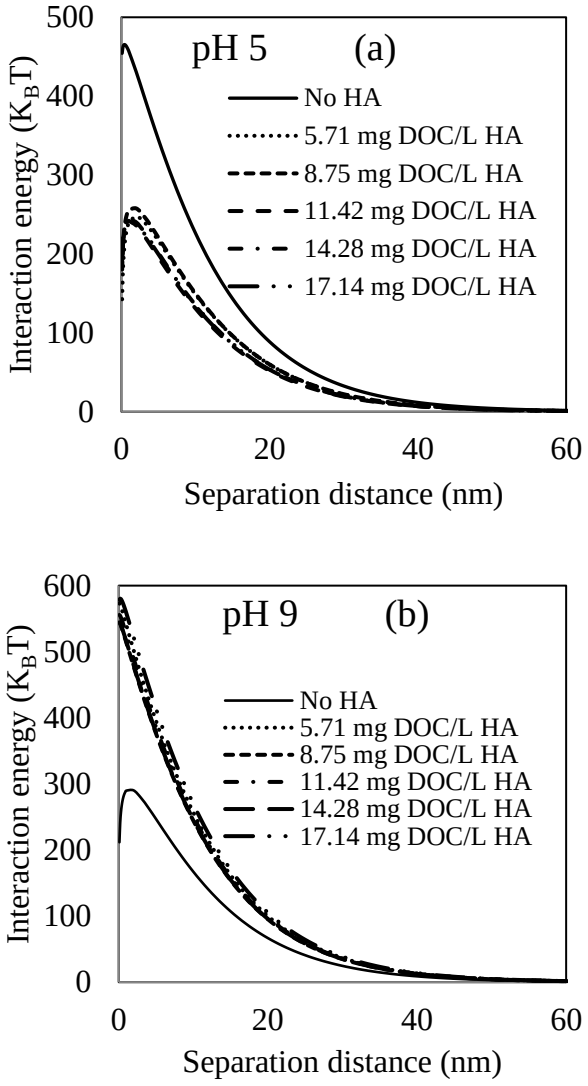

Fig. 3.14. DLVO interaction energy profiles for illite to quartz sand at pH 5 (a) and pH 9 (b).

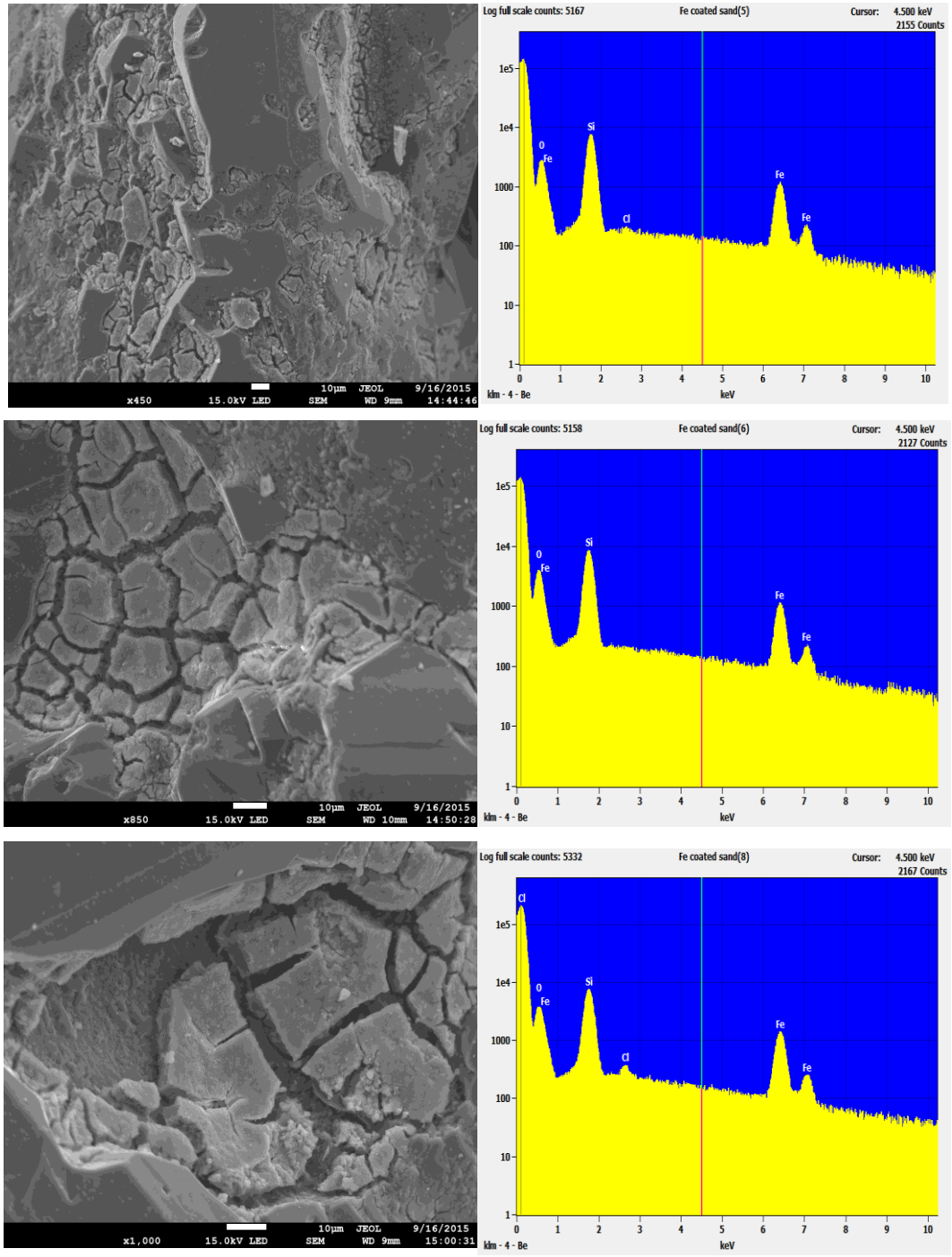

Fig. 3.15. Backscatter SEM image of Fe coated sand (left) and the EDX profile analysis (right) obtained for the surface shown in the image.

Table 2.EDX profile analysis report of Backscatter SEM image of Fe coated sand

Quantitative Results for: Fe coated sand sample #1

ElementLine	NetCounts	Weight %	Atom%
O K	36484	24.30	42.08
Si K	162371	41.29	40.74
Si L	0	---	---
Cl K	1053	0.38	0.30
Cl L	0	---	---
Fe K	29089	34.03	16.88
Fe L	0	---	---
Total		100.00	100.00

Quantitative Results for: Fe coated sand sample #2

ElementLine	NetCounts	Weight %	Atom%
O K	52909	30.05	48.86
Si K	181250	40.31	37.34
Si L	0	---	---
Fe K	28507	29.63	13.80
Fe L	0	---	---
Total		100.00	100.00

Quantitative Results for: Fe coated sand sample #3

ElementLine	NetCounts	Weight %	Atom%
O K	50017	26.66	46.07
Si K	160325	35.52	34.97
Si L	0	---	---
Cl K	2659	0.80	0.63
Cl L	0	---	---
Fe K	37341	37.02	18.33
Fe L	0	---	---
Total		100.00	100.00

3.2 Effect of pH, surfactant (xanthan gum), and grain size of the porous media on the transport of $nTiO_2$ in water saturated sand column

3.2.1 Zeta potential and hydrodynamic diameter

At pH 5, zeta potential (ZP) of $nTiO_2$ was positive, and ZPs of xanthan gum, $nTiO_2$ with suspended xanthan gum, fine sand and coarse sand were negative (Fig. 3.16). At pH 9, ZPs of $nTiO_2$, xanthan gum, $nTiO_2$ with suspended xanthan gum, fine sand, coarse sand all of them were negative (Fig. 3.16).At pH 5, hydrodynamic diameter (HDD) of $nTiO_2$ and xanthan gum were found smaller compare to pH 9 (Fig. 3.16).

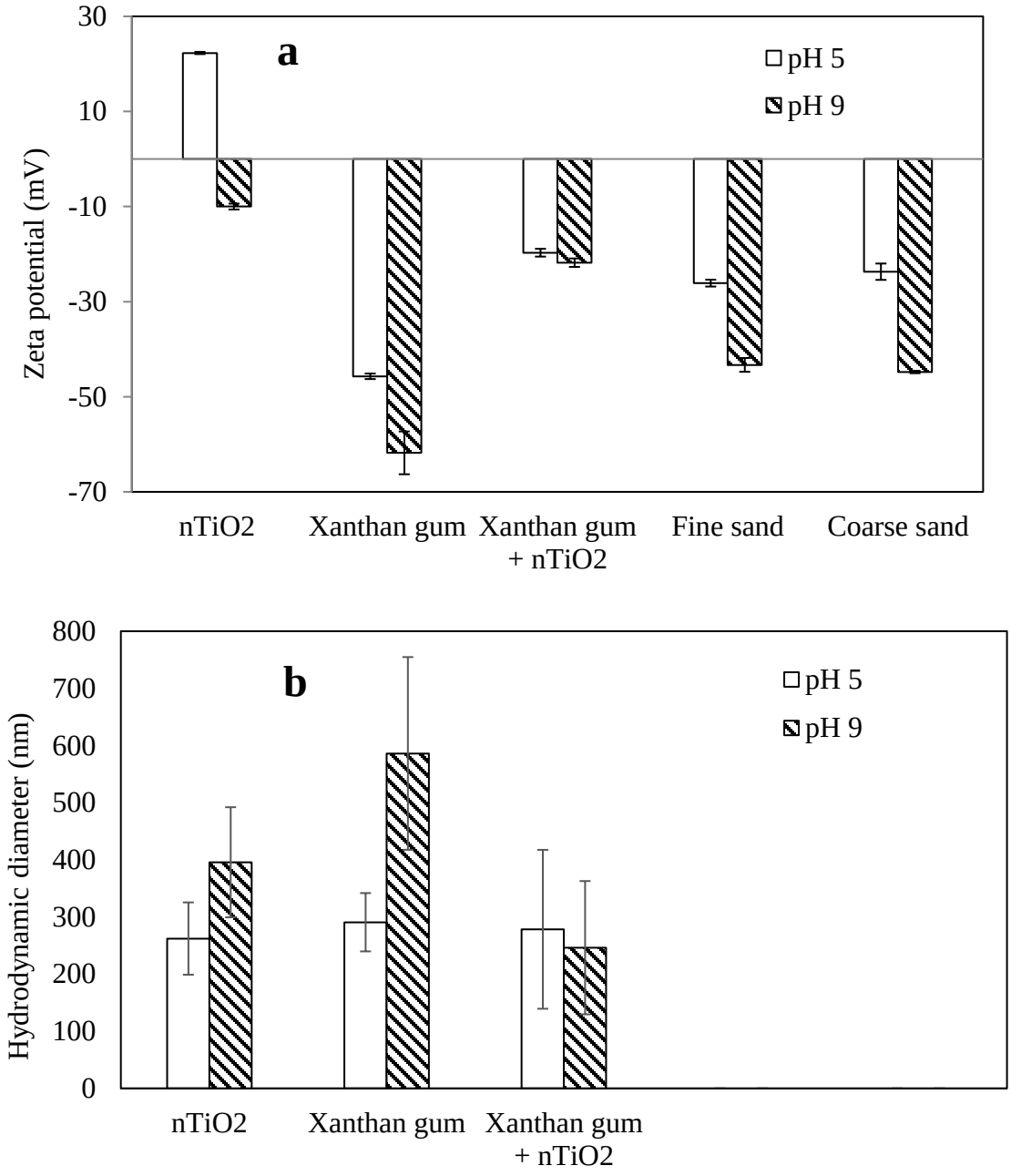

Fig. 3.16. Zeta potential of $nTiO_2$, xanthan gum, suspended $nTiO_2$ with xanthan gum, coarse sand and fine sand measured both at pH 5 and 9 (a). Hydrodynamic diameter of $nTiO_2$, xanthan gum and suspended $nTiO_2$ with xanthan gum measured both at pH 5 and 9 (b). For all the measurements, 20 mg/L of $nTiO_2$ and 10 mg/L of xanthan gum were used. 0.1 mM of NaCl was used as background solution. Hydrodynamic diameter was intensity weighted. Data are expressed as mean ± standard deviation of multiple measurements.

3.2.2 Stability test

Light absorbance of particle suspensions was used as an indicator of suspension stability. While constant light absorbance shows that the suspension is stable, decrease in light absorbance indicates unstable suspension caused by particle aggregation and/or sedimentation. My results showed that at pH 5, light absorbance of $nTiO_2$suspensions was stable at low ionic strength (1 and 2 mM), but not stable at higher ionic strength (10, 50, and 100 mM) (Fig. 3.17a). At pH 9, light absorbance of $nTiO_2$ was not stable at high ionic strength (50 and 100 mM) (Fig. 3.17b). Fig. 3.18 represents the effects of xanthan gum. At pH 5, without xanthan gum, light absorbance of $nTiO_2$ was not stable at high ionic strength (100 mM), yet light absorbance of $nTiO_2$ suspension only slightly decreased in the presence of xanthan gum.

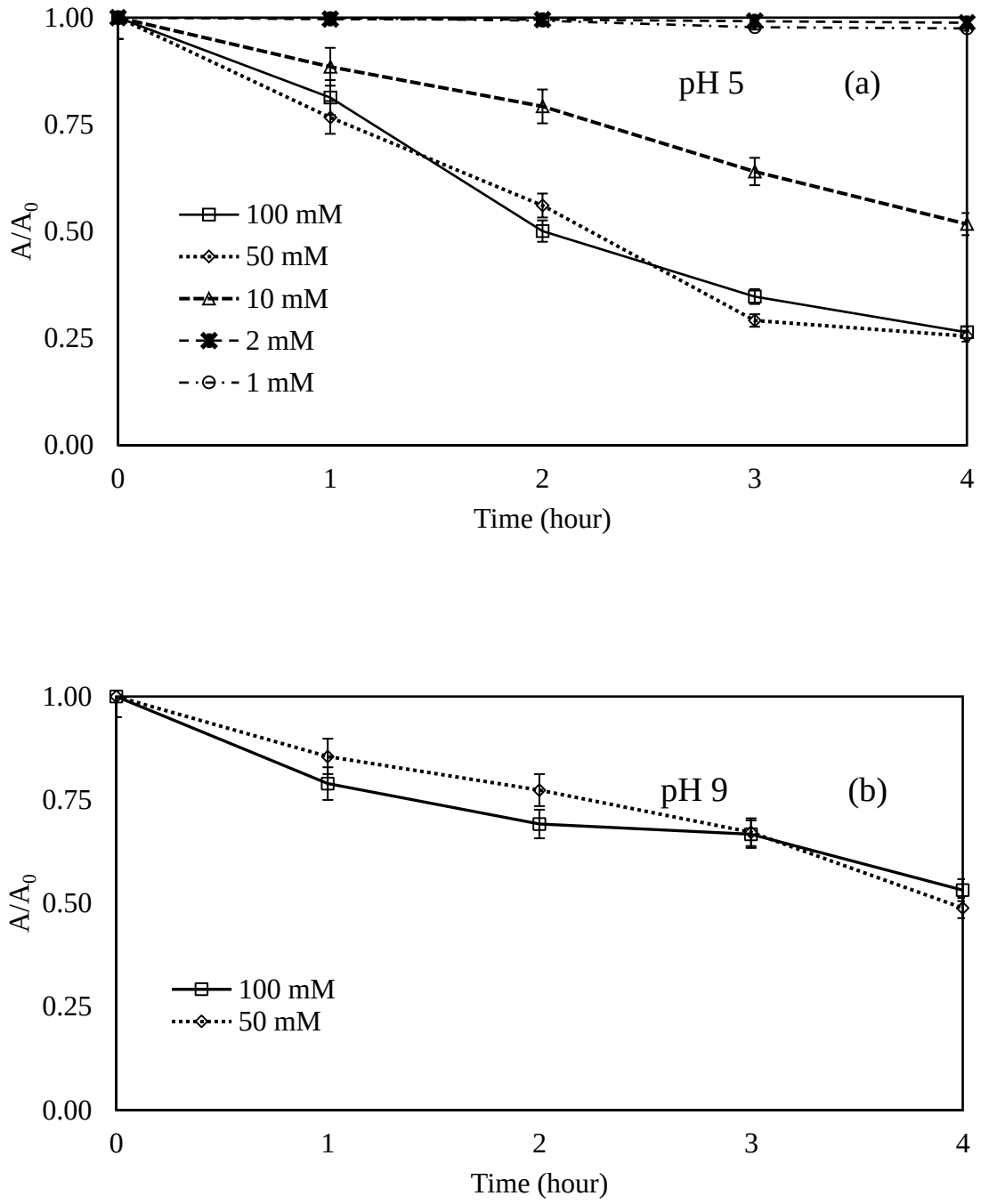

Fig. 3.17. Panel (a) represents, at pH 5, $nTiO_2$ suspension was stable in lower ionic strength (≤ 2 mM) and $nTiO_2$ becomes unstable in higher ionic strength. Panel (b) represents, at pH 9 $nTiO_2$ was unstable in high ionic strength. For all the measurements, 20 mg/L of $nTiO_2$ was used. Error bars represent analytical errors.

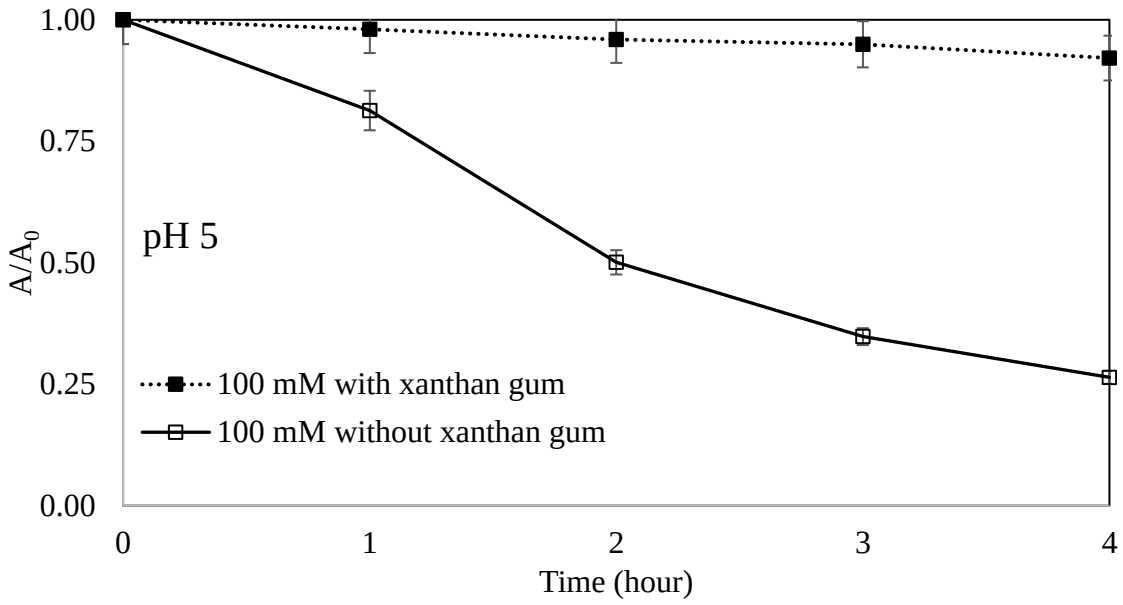

Fig. 3.18. At pH = 5, $nTiO_2$ suspension was stable at high ionic strength (IS) (100 mM) with the presence of surfactant (xanthan gum), but not stable without xanthan gum. For all the measurements, 20 mg/L of $nTiO_2$ and 10 mg/L of xanthan gum were used. 100 mM of NaCl was used as background solution. Error bars represent analytical errors.

Stability of $nTiO_2$ suspension depends on the repulsive forces against van der waals attractive forces, which derived from the electrostatic double layer repulsion and the steric repulsion forces, generated from the surface charge of the particle (Hirtzel and Rajagopalan, 1985). Electrostatic and steric repulsion forces suppress aggregation and attachment of particles to grain surfaces (Kretzschmarand Sticher, 1997). At low ionic strength electrostatic and steric repulsion forces were high, resulting stable $nTiO_2$ suspension. On the other hand, at high ionic strength, electrostatic and steric repulsion forces were low, resulting unstable $nTiO_2$ suspension. Compère et al (2001) also showed that aggregation and deposition increases when ionic strength increases.

Surfactants can contribute to the steric repulsion forces and inhibited the aggregation of $nTiO_2$ (Godinez and Darnault, 2011). In my experiments, xanthan gum served as a surfactant that could contribute to the electrostatic and/or steric repulsion forces and inhibited the aggregation of $nTiO_2$ suspension.

3.2.3 Column experiments

3.2.3.1 pH effect

The affects of pH on titanium dioxide transport through coarse sand (0.600 – 0.710 mm) column sand fine sand (0.250 - 0.355 mm) columns are shown in Fig. 3.19 (open symbols). The concentration of titanium dioxide found in the effluent is not detectable at pH 5 in both coarse and fine grained sand columns. On the other hand, the concentration of titanium dioxide found in the effluent is almost 95% at pH 9 in both coarse and fine grained sand columns.

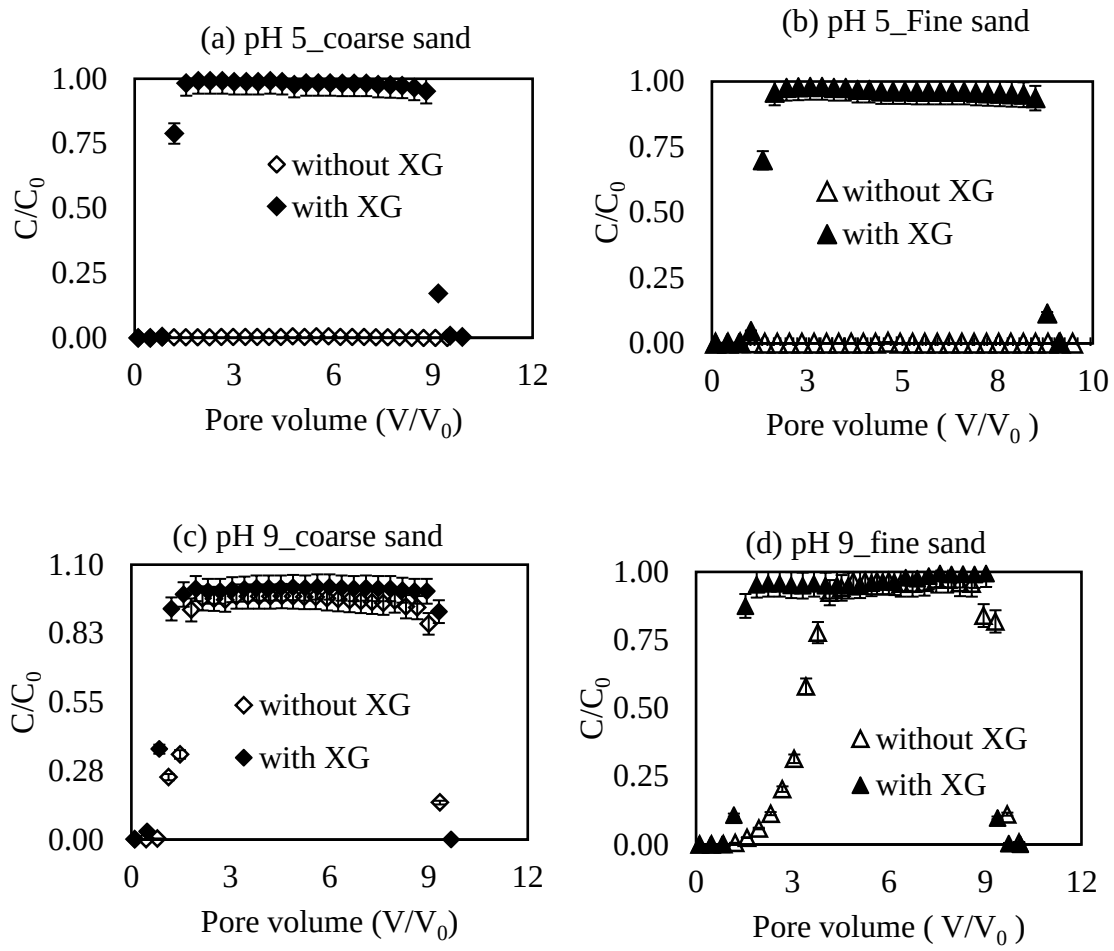

Fig. 3.19. At pH 5 and with XG (xanthan gum), concentration of titanium dioxide in the effluent is 100%; on the other hand, it is not detectable without xanthan gum both in coarse and fine sand (Panel 3.19a and 3.19b). At pH 9 and without xanthan gum concentration of $nTiO_2$ in the effluent increased gradually and with xanthan gum it increased sharply both in coarse and fine sand (Panel 3.19c and 3.19d). For all the measurements, 20 mg/L of $nTiO_2$ was used. For the experiments with surfactant, 10 mg/L of xanthan gum was used. 0.1 mM of NaCl was used as background solution. Error bars represent analytical errors.

At pH 5, zeta potential of $nTiO_2$ and quartz sand were found positive and negative respectively (Fig.3.16). For this reason, the retention of titanium dioxide nano-particles on sand was high, which prevents $nTiO_2$ transport through the column. On the other hand, at pH 9, zeta potential of titanium dioxide and quartz sand were found negative (Fig.3.16). Therefore, titanium dioxide and sand repelled each other and the retention of $nTiO_2$ on sand surface was zero, resulting in full breakthrough of $nTiO_2$.

To further understand the interactions between $nTiO_2$ and the porous media, interaction energy profiles between $nTiO_2$ and the sand was calculated using the DLVO theory. The ZP and HDD used for the calculations are given in Fig.3.16. At pH 5, $nTiO_2$ is positively charged and quartz sand is negatively charged (Fig. 3.16), and the calculated DLVO interaction energy between $nTiO_2$ and the coarse sand and between $nTiO_2$ and fine sand were negative, which means no energy barriers exist that prevent $nTiO_2$ attachment to the sand (Fig. 3.20a, b). At pH 9, $nTiO_2$, coarse sand, and fine sand are all negatively charged, and the calculated interaction energy profiles showed high energy barriers (ϕ_{max}= +42 K_BT) between $nTiO_2$ and coarse sand, and between $nTiO_2$ and fine sand (Fig. 3.20c, d). This indicated that the adhesion of $nTiO_2$ to sand was unfavorable and therefore the transport of $nTiO_2$ through the sand columns at pH 9 were predictable to behigh.

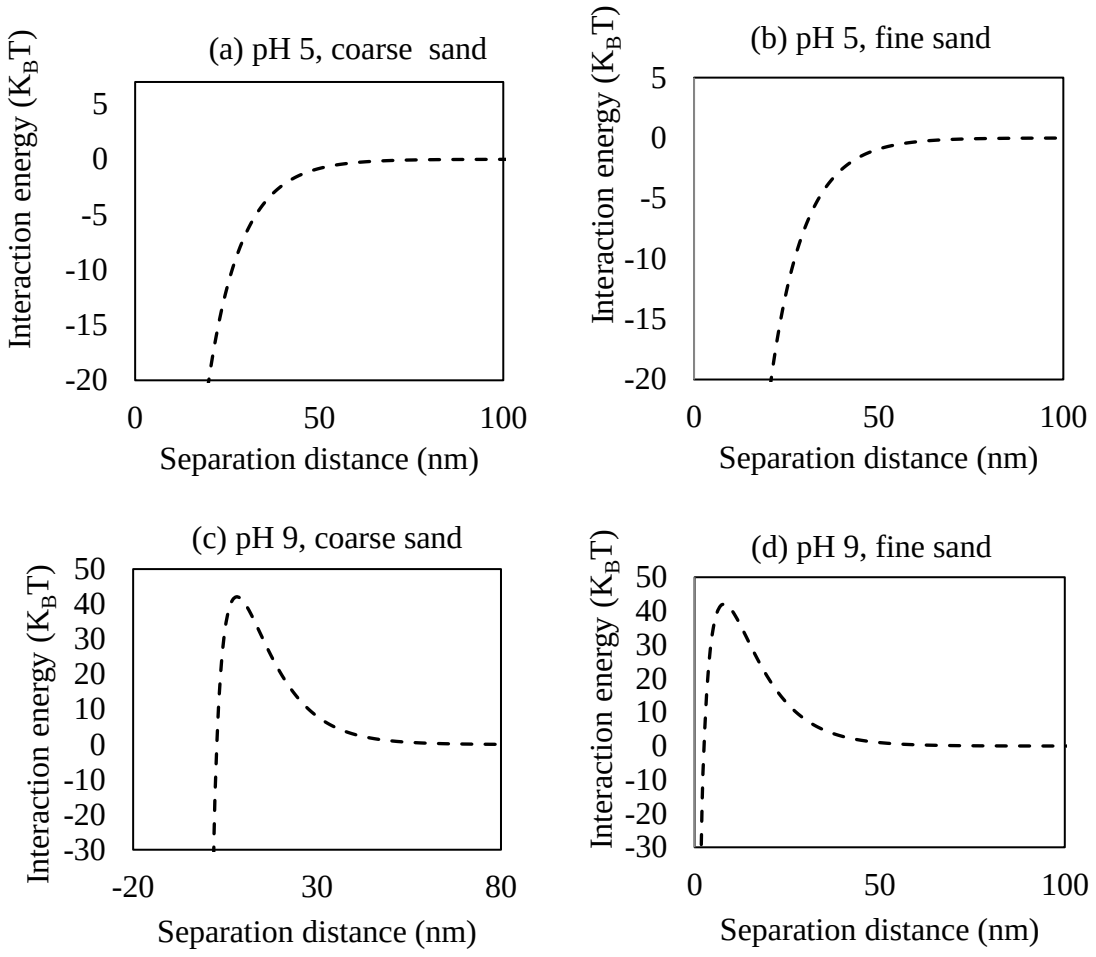

Fig. 3.20. $nTiO_2$ - sand grain interaction energy profiles in the absence of xanthan gum calculated using DLVO theory.

3.2.3.2 Surfactant (xanthan gum) effect

At pH 5, without the presence of the surfactant, effluent concentration of $nTiO_2$ was not detected in both coarse and fine sand column experiments (Fig. 3.19a, b). Conversely, effluent concentration of $nTiO_2$ approached 100% when 10 mg/L surfactant (xanthan gum) was present in the suspension (Fig. 3.19a, b). At pH 9, the concentration of $nTiO_2$ in the effluent was high even in the absence of xanthan gum, and the presence of xanthan gum in the suspension slightly increased effluent $nTiO_2$ concentration (Fig. 3.19c, d). Godinez and Darnault (2011) showed that xanthan gum in the titanium dioxide nanoparticle suspension reduced the attachment of titanium dioxide nanoparticles and increased their transport, consistent with my experimental results.

When 10 mg/L xanthan gum was present in the suspension, ZP of $nTiO_2$ became negative at pH 5 (Fig.3.16), but the ZP of the sand were unchanged (i.e., still negative). The calculated interaction energy between TiO_2 and the sand showed high energy barriers, i.e., ϕ_{max}= +88.4 K_BT for the coarse sand (Fig. 3.21a) and ϕ_{max}=+82.8 K_BT for the fine sand (Fig. 3.21b). This indicated that the adhesion of $nTiO_2$ to sand was unfavorable and therefore the transport of titanium dioxide nanoparticles through the sand column should be high. Similarly, at pH 9, with the presence of 10 mg/L xanthan gum, the interaction energy profiles for TiO_2 for both coarse sand and fine sand showed high energy barriers (i.e.,ϕ_{max} are 116 K_BT for both coarse and fine sand (Fig. 3.21c, d), indicating the existence of high energy barriers that prevent $nTiO_2$ attachment to the sand.

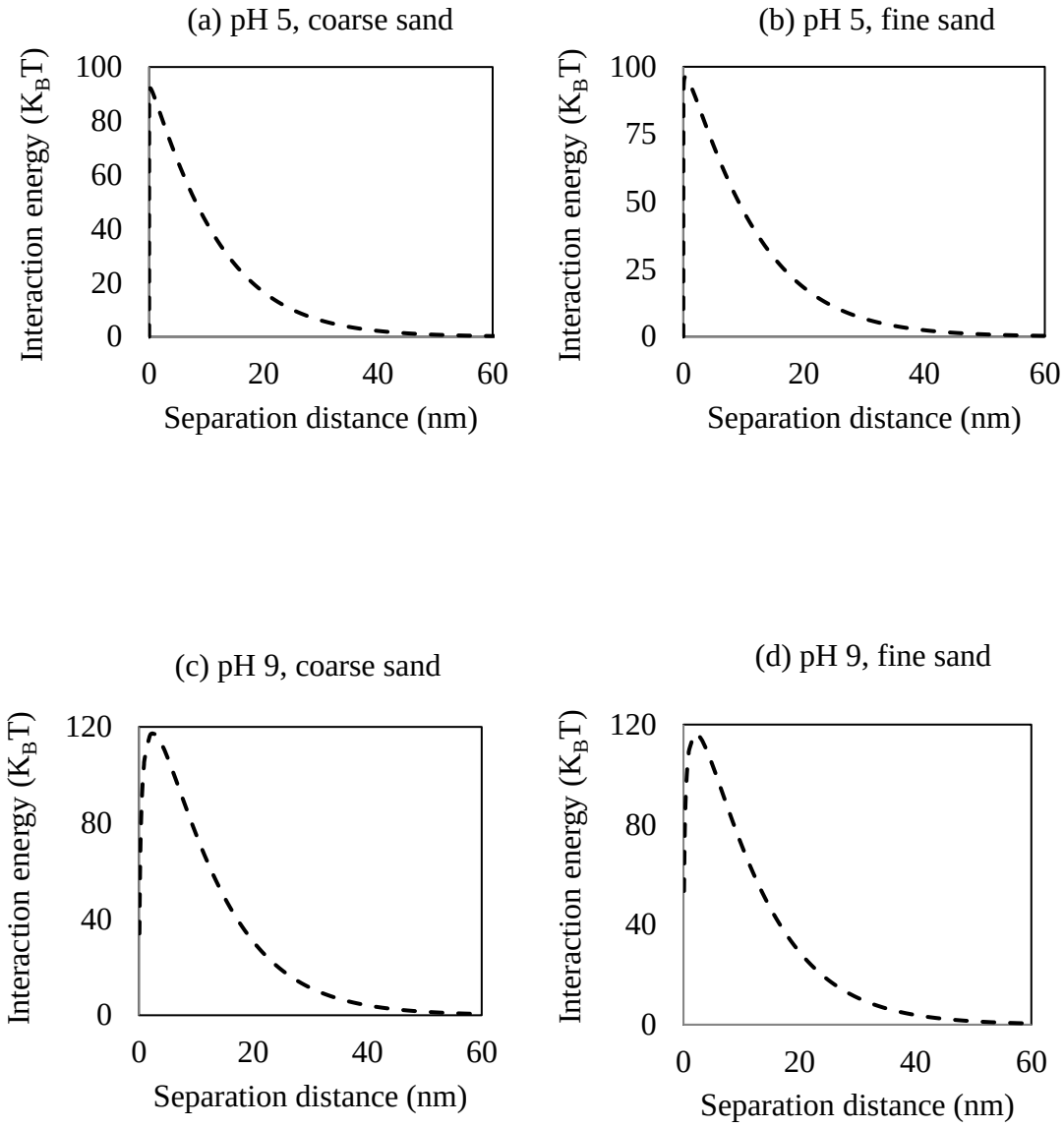

Fig. 3.21. $nTiO_2$ - sand grain interaction energy profiles in the presence of xanthan gum calculated using DLVO theory.

3.2.3.3 Grain size effect

At pH5, $nTiO_2$ breakthrough curves were not influenced by the grain size of the media, i.e., for both the coarse sand and the fine sand columns, $nTiO_2$ effluent concentration was not detected in the absence of xanthan gum, and was 100% in the presence of xanthan gum (Fig. 3.19a, b). At pH 9, in the presence of xanthan gum, $nTiO_2$ breakthrough was almost 100% and was not influenced by the grain size of the media (Fig. 3.19c, d). In the above experiments, due to the strong DLVO interactions between TiO_2 and the sand, $nTiO_2$ was either totally attracted to the sand, resulting in zero transport, or completely repelled by the sand, resulting in 100% transport. Therefore, the effects of grain size on $nTiO_2$ transport were not observed.

At pH 9, in the absence of xanthan gum, however, the breakthrough curve of $nTiO_2$ for the coarse sand column and the fine sand column were different (the open diamonds in Fig. 3.19c versus the open triangles in Figure 3.19d). The effluent concentration for the fine sand column gradually increased and reached its maximum at 4.5 pore volume, while for the coarse sand column the effluent concentration sharply increased and reached its maximum at 2.0pore volume.

Fig. 3.20c and 3.20d show that in the absence of xanthan gum, a high energy barrier exist between $nTiO_2$ and the sand. A careful comparison indicates that the DLVO interaction energy profiles for the coarse and fine sand are almost identical. Therefore, the differences in $nTiO_2$ transport in the coarse and fine sand columns are likely caused by mechanisms other than DLVO forces. Some researchers argued that smaller grain size may result in low particle transport due to straining effects. The effects of straining need to be considered when d_p/d_g (d_p is particle diameter, d_g is grain diameter) exceeds 0.008

(Xu et al., 2006). For my column experiments, however, d_p= 0.29 µm at pH 9 in the absence of xanthan gum (Fig. 3.16), so the average d_p/d_g = 0.00095 for the fine sand (d_g= 0.250-0.355 mm), and the average d_p/d_g= 0.000442 for the coarse sand (d_g = 0.600-0.710 mm), both of which were less than 0.008. Therefore, the lower transport in the fine sand columns cannot be explained by straining effects, and further investigations are needed to clarify the reasons.

Chapter 4: Conclusions

Nanoparticles and mineral colloids, which may occur naturally or be unintentionally or intentionally produced, have important functions in soil and groundwater. Colloidal illite particles ($nTiO_2$) is one of the most abundant clay colloids in groundwater. Titanium dioxide nanoparticles, one of the most common engineered nano-materials, which are toxic to human cells and aquatic organisms, may also enter groundwater. In order to understand the fate and distribution of sub-micron sized small particles such as titanium dioxide nanoparticles and illite colloids in the environment, it is important to understand the factors that influence the stability, attachment, and transport of $nTiO_2$ and illite particles in the vadose zone and groundwater.

In this study, experiments were performed to determine the effects of HA on the stability of illite colloidal particles in water and on illite colloid attachment to pure quartz sand and Fe coated sand. The effects of surfactant (xanthan gum) and grain size of the porous media on the transport of $nTiO_2$ in water-saturated quartz sand columns were also studied. Experimental results showed that illite colloids were stable at both pH 5 and pH 9 in 1 mM NaCl background solutions either in the absence of HA, or with a HA concentration of 0.625−20 mg DOC/L. The attachment of illite colloids to quartz sand was practically undetectable at both pH 5 and 9 and not influenced by HA concentrations. The attachment of illite colloids to Fe coated sand depended on pH and HA concentration. In the absence of HA, high attachment (~85%) occurred at pH 5, and low attachment (almost zero) occurred at pH 9. At pH 5, illite attachment decreased with increasing HA concentration. At pH 9, illite attachment remained very low in spite of increasing HA concentration. The influence of HA on illite attachment to sand is due to

HA adsorption to illite and Fe coating, which changed the surface potential of illite and Fe coating. The interaction energies between illite colloids and quartz sand, and between illite colloids and Fe coated sand calculated based on DLVO theory for different pH and HA concentrations were in agreement with my experimental results, indicating that electrostatic forces played a major role in controlling illite attachment.

Stability tests showed that ionic strength had a big impact on the stability of $nTiO_2$ in water. $nTiO_2$ in water was stable in water at low ionic strength of 1 and 2 mM, but unstable at high ionic strengths above 10 mM. The presence of xanthan gum substantially increased the stability of $nTiO_2$ at high ionic strength. Column experiments in this study elucidated the effects of xanthan gum, pH, and grain size of the porous media on the transport of $nTiO_2$ in water saturated media. Xanthan gum markedly reduced the retention of titanium dioxide nanoparticles on the sand surface and increased the transport through the sand column. My results also indicated that the transport of $nTiO_2$ in quartz sand was low at pH 5 and high at pH 9. Measurements on the zeta potential of the quartz sand and $nTiO_2$ showed that the low transport at pH 5 was caused by the strong attraction of the positively-charged $nTiO_2$ by negatively-charged quartz sand, and the high transport at pH 9 was due to strong repulsive forces between the negatively-charged $nTiO_2$ and like-charged quartz sand. The presence of surfactant (xanthan gum) substantially increased $nTiO_2$ transport, especially at pH 5. In the presence of xanthan gum, the high transport of $nTiO_2$ was caused by xanthan gum adsorption to $nTiO_2$, which changed the zeta potential of $nTiO_2$ from positive to negative at pH 5, and therefore changed the forces between the $nTiO_2$ and the quartz sand from attraction to repulsion. It was also showed that at pH 9 in the absence of xanthan gum, transport of $nTiO_2$ was higher in coarse-grained quartz sand

columns compared tothat in fine-grained quartz sand columns. Neither DLVO theory, nor straining effects seemed to account for the observed grain size effects. Further investigations are needed to elucidate the mechanisms.

Notwithstanding the experiments in my research were performed on small scale circumferences, the aforementioned outcomes demonstrated that the transport of $nTiO_2$ and mineral colloids like illite is very much sensitive to pH and adsorbing species like humic acid and xanthan gum.

References

Battin, T. J., Kammer, F. V. D., Weilhartner, A., Ottofuelling, S., and Hofmann, T. (2009). Nanostructured TiO2: transport behavior and effects on aquatic microbial communities under environmental conditions. *Environmental Science and Technology*, *43*(21), 8098–8104. http://doi.org/10.1021/es9017046

Bayat, A. E., Junin, R., Mohsin, R., Hokmabadi, M., and Shamshirband, S. (2015). Influence of clay particles on Al2O3 and TiO2 nanoparticles transport and retention through limestone porous media: measurements and mechanisms. *Journal of Nanoparticle Research*, *17*(5), 219. http://doi.org/10.1007/s11051-015-3031-4

Bendersky, M., and Davis, J. M. (2011a). DLVO interaction of colloidal particles with topographically and chemically heterogeneous surfaces. *Journal of Colloid and Interface Science*, *353*(1), 87–97. http://doi.org/10.1016/j.jcis.2010.09.058

Bendersky, M., and Davis, J. M. (2011b). DLVO interaction of colloidal particles with topographically and chemically heterogeneous surfaces. *Journal of Colloid and Interface Science*, *353*(1), 87–97. http://doi.org/10.1016/j.jcis.2010.09.058

Bradford, S. A., and Torkzaban, S. (2013). Colloid interaction energies for physically and chemically heterogeneous porous media. *Langmuir*, *29*(11), 3668–3676. http://doi.org/10.1021/la400229f

Brar, S. K., Verma, M., Tyagi, R. D., and Surampalli, R. Y. (2010). Engineered nanoparticles in wastewater and wastewater sludge - Evidence and impacts. *Waste Management*, *30*(3), 504–520. http://doi.org/10.1016/j.wasman.2009.10.012

Brunet, L., Lyon, D. Y., Hotze, E. M., Alvarez, P. J. J., and Wiesner, M. R. (2009). Comparative photoactivity and antibacterial properties of C60 fullerenes and titanium dioxide nanoparticles. *Environmental Science and Technology*, *43*(12), 4355–4360. http://doi.org/10.1021/es803093t

Cai, L., Tong, M., Wang, X., and Kim, H. (2014). Influence of clay particles on the transport and retention of titanium dioxide nanoparticles in quartz sand. *Environmental Science and Technology*, *48*(13), 7323–7332. http://doi.org/10.1021/es5019652

Chen, G., Liu, J., Tawfiq, K., Yang, K., and Banks, C. (2009). Colloid Retention in Unsaturated Porous Media as Impacted by Colloid Size. *Particulate Science and Technology*, *27*(1), 35–49. http://doi.org/10.1080/02726350802611754

Chen, L., Sabatini, D. A., and Kibbey, T. C. G. (2008). Role of the air-water interface in the retention of TiO2 nanoparticles in porous media during primary drainage. *Environmental Science and Technology*, *42*(6), 1916–1921. http://doi.org/10.1021/es071410r

Clogston, J. D., and Patri, A. K. (2011). Zeta Potential Measurement. In E. S. McNeil (Ed.), *Characterization of Nanoparticles Intended for Drug Delivery* (pp. 63–70). Totowa, NJ: Humana Press. http://doi.org/10.1007/978-1-60327-198-1_6

Comba, S., and Sethi, R. (2009). Stabilization of highly concentrated suspensions of iron nanoparticles using shear-thinning gels of xanthan gum. *Water Research*, *43*(15), 3717–3726. http://doi.org/10.1016/j.watres.2009.05.046

Compère, F., Porel, G., and Delay, F. (2001). Transport and retention of clay particles in saturated porous media. Influence of ionic strength and pore velocity. *Journal of Contaminant Hydrology*, *49*(1-2), 1–21. http://doi.org/10.1016/S0169-7722(00)00184-4

Cox, H. A. (2012). *Transport Mechanisms of Titanium dioxide Nanoparticles in porous media (A Dissertation Submitted to the Faculty of the soil , water and environmental science department In Partial Fulfillment of the Requirements For the Degree of Doctor of Philosophy)*. The University of Arizona.

Crittenden, J. C., Howe, K. J., Hand, D. W., Tchobanoglous, G., and Trussell, R. R. (2012). *Principles of Water Treatment*. John Wiley and Sons, Incorporated.

Dalla Vecchia, E., Luna, M., and Sethi, R. (2009). Transport in porous media of highly concentrated iron micro- and nanoparticles in the presence of xanthan gum. *Environmental Science and Technology*, *43*(23), 8942–8947. http://doi.org/10.1021/es901897d

Dunphy Guzman, K. A, Finnegan, M. P., and Banfield, J. F. (2006). Influence of surface potential on aggregation and transport of itiania nanoparticles. *Environmental Science and Technology*, *40* (24), 7688–7693.

Elimelech, M., Gregory, J., Jia, X., Williams, R. A., Gregory, J., Jia, X., … Elimelech, M. (1995). *Particle Deposition and Aggregation*. *Particle Deposition and Aggregation*. Elsevier. http://doi.org/10.1016/B978-075067024-1/50000-5

Fang, J., Shan, X. Q., Wen, B., Lin, J. M., and Owens, G. (2009). Stability of titania

nanoparticles in soil suspensions and transport in saturated homogeneous soil columns. *Environmental Pollution*, *157*(4), 1101–1109. http://doi.org/10.1016/j.envpol.2008.11.006

Faure, B., Salazar-Alvarez, G., and Bergström, L. (2011). Hamaker constants of iron oxide nanoparticles. SI. *Langmuir : The ACS Journal of Surfaces and Colloids*, 1–4. http://doi.org/10.1021/la201387d

Freake, B., (2016). *EFFECTS OF PHOSPHATE ON THE ATTACHMENT OF TITANIUM DIOXIDE NANOPARTICLES (nTiO 2) AND ILLITE COLLOIDS TO QUARTZ SAND By A thesis submitted to the Department of Earth Sciences in partial fulfillment of the requirements for the degree ofBSc*. Memorial University of Newfoundland.

Gaiser, C., and Fellmuth, B. (2011). Low-temperature determination of the Boltzmann constant by dielectric-constant gas thermometry. *Metrologia*, *49*(1), L4–L7. http://doi.org/10.1088/0026-1394/49/1/L02

García-Ochoa, F., Santos, V. E., Casas, J. A., and Gómez, E. (2000). Xanthan gum: Production, recovery, and properties. *Biotechnology Advances*, *18*(7), 549–579. http://doi.org/10.1016/S0734-9750(00)00050-1

Godinez, I. G., and Darnault, C. J. G. (2011). Aggregation and transport of nano-TiO2 in saturated porous media: Effects of pH, surfactants and flow velocity. *Water Research*, *45*(2), 839–851. http://doi.org/10.1016/j.watres.2010.09.013

Gottschalk, F., and Nowack, B. (2011). The release of engineered nanomaterials to the

environment. *Journal of Environmental Monitoring : JEM*, *13*, 1145–1155. http://doi.org/10.1039/c0em00547a

Grassian, V. H., O'Shaughnessy, P. T., Adamcakova-Dodd, A., Pettibone, J. M., and Thorne, P. S. (2007). Inhalation exposure study of Titanium dioxide nanoparticles with a primary particle size of 2 to 5 nm. *Environmental Health Perspectives*, *115*(3), 397–402. http://doi.org/10.1289/ehp.9469

Guo, H., Wang, Y., Shpeizer, G. M., and Yan, S. (2003). Natural occurrence of arsenic in shallow groundwater, Shanyin, Datong Basin, China. *Journal of Environmental Science and Health. Part A, Toxic/hazardous Substances and Environmental Engineering*, *38*(11), 2565–2580. http://doi.org/10.1081/ESE-120024447

Gurr, J. R., Wang, A. S. S., Chen, C. H., and Jan, K. Y. (2005). Ultrafine titanium dioxide particles in the absence of photoactivation can induce oxidative damage to human bronchial epithelial cells. *Toxicology*, *213*(1-2), 66–73. http://doi.org/10.1016/j.tox.2005.05.007

H.Van Olphena and J.J. Fripiat. (1979). SOURCE CLAY PHYSICAL/CHEMICAL DATA. In H.Van Olphena and J.J. Fripiat (Ed.), *Data Handbook for Clay Minerals and OtherNon-metallic Minerals*. Aurora,CO 80046-0130 USA: Pergamon Press. Retrieved from https://www.agry.purdue.edu/cjohnston/sourceclays/chem.htm

Hamaker, H. C. (1937). The London—van der Waals attraction between spherical particles. *Physica*, *4*(10), 1058–1072. http://doi.org/10.1016/S0031-8914(37)80203-7

He, Y. T., Wan, J., and Tokunaga, T. (2008). Kinetic stability of hematite nanoparticles: The effect of particle sizes. *Journal of Nanoparticle Research*, *10*, 321–332. http://doi.org/10.1007/s11051-007-9255-1

Hiemenz, P. C., and Rajagopalan, R. (1997). *Principles of Colloid and Surface Chemistry* (3rd ed.). New York: Marcel Dekker Inc.

Hirtzel, C. S., and Rajagopalan, R. (1985). *Colloidal phenomena: Advanced topics*. Noyes Pubns.

Hogg, R., Healy, T. W., and Fuerstenau, D. W. (1966). Mutual coagulation of colloidal dispersions. *Transactions of the Faraday Society*, *62*(615), 1638. http://doi.org/10.1039/tf9666201638

Hund-Rinke, K., and Simon, M. (2006). Ecotoxic effect of photocatalytic active nanoparticles (TiO2) on algae and daphnids. *Environmental Science and Pollution Research International*, *13*(4), 225–232. http://doi.org/10.1065/espr2006.06.311

Israelachvili, J. N. (2011). Intermolecular and surface forces. *Academic Press.*, 3152–3158. http://doi.org/10.1002/elps.201000212

J Gregory. (1981). Approximate expressions for retarded van der waals interaction. *Journal of Colloid and Interface Science*, *83*(1), 138–145.

Joseph N. Ryan, P. M. G. (1994). Effects of Ionic Strength and Flow Rate on Colloid Release Relating Kinetics to Intersurface Potential Energy. *Journal of Colloid and Interface Science*, *164*(1), 21–34.

Jovanović, B., Anastasova, L., Rowe, E. W., Zhang, Y., Clapp, A. R., and Palić, D.

(2011). Effects of nanosized titanium dioxide on innate immune system of fathead minnow (Pimephales promelas Rafinesque, 1820). *Ecotoxicology and Environmental Safety*, *74*, 675–683. http://doi.org/10.1016/j.ecoenv.2010.10.017

Kasel, D., Bradford, S. a., Šimůnek, J., Heggen, M., Vereecken, H., and Klumpp, E. (2013). Transport and retention of multi-walled carbon nanotubes in saturated porous media: Effects of input concentration and grain size. *Water Research*, *47*, 933–944. http://doi.org/10.1016/j.watres.2012.11.019

Kiser, M. a., Westerhoff, P., Benn, T., Wang, Y., Pérez-Rivera, J., and Hristovski, K. (2009). Titanium Nanomaterial Removal and Release from Wastewater Treatment Plants. *Environmental Science and Technology*, *43*(17), 6757–6763. http://doi.org/10.1021/es901102n

Kretzschmar, R., and Sticher, H. (1997). Transport of Humic-Coated Iron Oxide Colloids in a Sandy Soil: Influence of Ca2+ and Trace Metals. *Environmental Science and Technology*, *31*(12), 3497–3504. http://doi.org/10.1021/es970244s

Kubicki, J. D., Itoh, M. J., Schroeter, L. M., and Apitz, S. E. (1997). Bonding mechanisms of salicylic acid adsorbed onto illite clay: An ATR- FTIR and molecular orbital study. *Environmental Science and Technology*, *31*(4), 1151–1156. http://doi.org/10.1021/es960663+

Langford, J. I., and Louër, D. (1999). Powder diffraction. *Reports on Progress in Physics*, *59*, 131–234. http://doi.org/10.1088/0034-4885/59/2/002

Liang, Y., Bradford, S. a., Simunek, J., Vereecken, H., and Klumpp, E. (2013).

Sensitivity of the transport and retention of stabilized silver nanoparticles to physicochemical factors. *Water Research*, *47*(7), 2572–2582. http://doi.org/10.1016/j.watres.2013.02.025

Malmberg, C. G., and Maryott, a. a. (1956). Dielectric constant of water from 0 to 100 C. *Journal of Research of the National Bureau of Standards*, *56*(1), 1. http://doi.org/10.6028/jres.056.001

Mattison, N. T., Carroll, D. M. O., Rowe, R. K., and Petersen, E. J. (2011). Impact of Porous Media Grain Size on the Transport of Multi-walled Carbon Nanotubes, 9765–9775.

Mehra, O. P., and Jackson, M. L. (1958). Iron Oxide Removal from Soils and Clays by a Dithionite-Citrate System Buffered with Sodium Bicarbonate. *Clays and Clay Minerals*, *7*(1), 317–327. http://doi.org/10.1346/CCMN.1958.0070122

Mills, A. L., Herman, J. S., Hornberger, G. M., Dejesús, H., and Dejesust, T. H. (1994). Effect of Solution Ionic Strength and Iron Coatings on Mineral Grains on the Sorption of Bacterial Cells to Quartz Sand Effect of Solution Ionic Strength and Iron Coatings on Mineral Grains on the Sorption of Bacterial Cells to Quartz Sand, *60*(9), 3300–3306.

Mohr, P. J., Taylor, B. N., and Newell, D. B. (2012). CODATA recommended values of the fundamental physical constants: 2010. *Reviews of Modern Physics*, *84*(4), 1527–1605. http://doi.org/10.1103/RevModPhys.84.1527

Novich, B. E., and Ring, T. A. (1985). Photon correlation spectroscopy of a coagulating

suspension of illite platelets. *Journal of the Chemical Society, Faraday Transactions 1*, *81*(6), 1455. http://doi.org/10.1039/f19858101455

Pal, T., Mukherjee, P. K., Sengupta, S., Bhattacharyya, A. K., and Shome, S. (2002). Arsenic Pollution in Groundwater of West Bengal, India - An Insight into the Problem by Subsurface Sediment Analysis. *Gondwana Research*, *5*(2), 501–512. http://doi.org/10.1016/S1342-937X(05)70738-3

Petosa, A. R., Jaisi, D. P., Quevedo, I. R., Elimelech, M., and Tufenkji, N. (2010). Aggregation and deposition of engineered nanomaterials in aquatic environments: Role of physicochemical interactions. *Environmental Science and Technology*, *44*(17), 6532–6549. http://doi.org/10.1021/es100598h

Polubesova, T., and Nir, S. (1999). Modeling of organic and inorganic cation sorption by illite. *Clays and Clay Minerals*, *47*(3), 366–374. http://doi.org/10.1346/CCMN.1999.0470313

Saiers, J. E., and Hornberger, G. M. (1999). The influence of ionic strength on the facilitated transport of cesium by kaolinite colloids. *Water Resources Research*, *35*(6), 1713–1727. http://doi.org/10.1029/1999WR900055

Scheidegger, A., Borkovec, M., and Sticher, H. (1993). Coating of silica sand with goethite: preparation and analytical identification. *Geoderma*, *58*(1-2), 43–65. http://doi.org/10.1016/0016-7061(93)90084-X

Sharma, V. K. (2009). Aggregation and toxicity of titanium dioxide nanoparticles in aquatic environment--a review. *Journal of Environmental Science and Health. Part*

A, Toxic/hazardous Substances and Environmental Engineering, *44*(September 2014), 1485–1495. http://doi.org/10.1080/10934520903263231

Shen, C. Y., Li, B. G., Wang, C., Huang, Y. F., and Jin, Y. (2011). Surface Roughness Effect on Deposition of Nano- and Micro-Sized Colloids in Saturated Columns at Different Solution Ionic Strengths. *Vadose Zone Journal*, *10*(3), 1071–1081. http://doi.org/Doi 10.2136/Vzj2011.0011

Wang, Q., Cheng, T., and Wu, Y. (2014). Influence of mineral colloids and humic substances on uranium(VI) transport in water-saturated geologic porous media. *Journal of Contaminant Hydrology*, *170*, 76–85. http://doi.org/10.1016/j.jconhyd.2014.10.007

Wang, Y., Gao, B., Morales, V. L., Tian, Y., Wu, L., Gao, J., … Yang, L. (2012). Transport of titanium dioxide nanoparticles in saturated porous media under various solution chemistry conditions. *Journal of Nanoparticle Research, 14*. http://doi.org/10.1007/s11051-012-1095-y

Warheit, D. B., Sayes, C. M., Reed, K. L., and Swain, K. a. (2008). Health effects related to nanoparticle exposures: Environmental, health and safety considerations for assessing hazards and risks. *Pharmacology and Therapeutics*, *120*(1), 35–42. http://doi.org/10.1016/j.pharmthera.2008.07.001

Weir, A., Westerhoff, P., Fabricius, L., and von Goetz, N. (2012). Titanium Dioxide Nanoparticles in Food and Personal Care Products. *Environ. Sci. Technol.*, *46*(4), 2242–2250. http://doi.org/10.1021/es204168d.

Wiesner, M. R., Lowry, G. V., Alvarez, P., Dionysiou, D., and Biswas, P. (2006). Assessing the risks of manufactured nanomaterials. *Environmental Science and Technology*, *40*(14), 4336–4345. http://doi.org/10.1021/es062726m

Wu, Y. (2016). *Stability of nTiO 2 particles and their attachment to sand : Effects of humic acid at different pH*. Memorial University of Newfoundland.

Wu, Y., and Cheng, T. (2016). Stability of nTiO 2 particles and their attachment to sand : Effects of humic acid at different pH. *Science of the Total Environment*, *541*, 579–589.

Xu, S., Gao, B., and Saiers, J. E. (2006). Straining of colloidal particles in saturated porous media. *Water Resources Research*, *42*(December), 1–10. http://doi.org/10.1029/2006WR004948

Zhang, L., Yu, X., Zhang, H., Chen, E., and Dong, T. (2013). Impact of environmental conditions on the sorption behavior of 60Co(II) on illite. *Journal of Radioanalytical and Nuclear Chemistry*, *295*(2), 1473–1485. http://doi.org/10.1007/s10967-012-1934-4

Appendices

Appendix 1: Calibration curve for illite and HA at pH 5 and pH 9

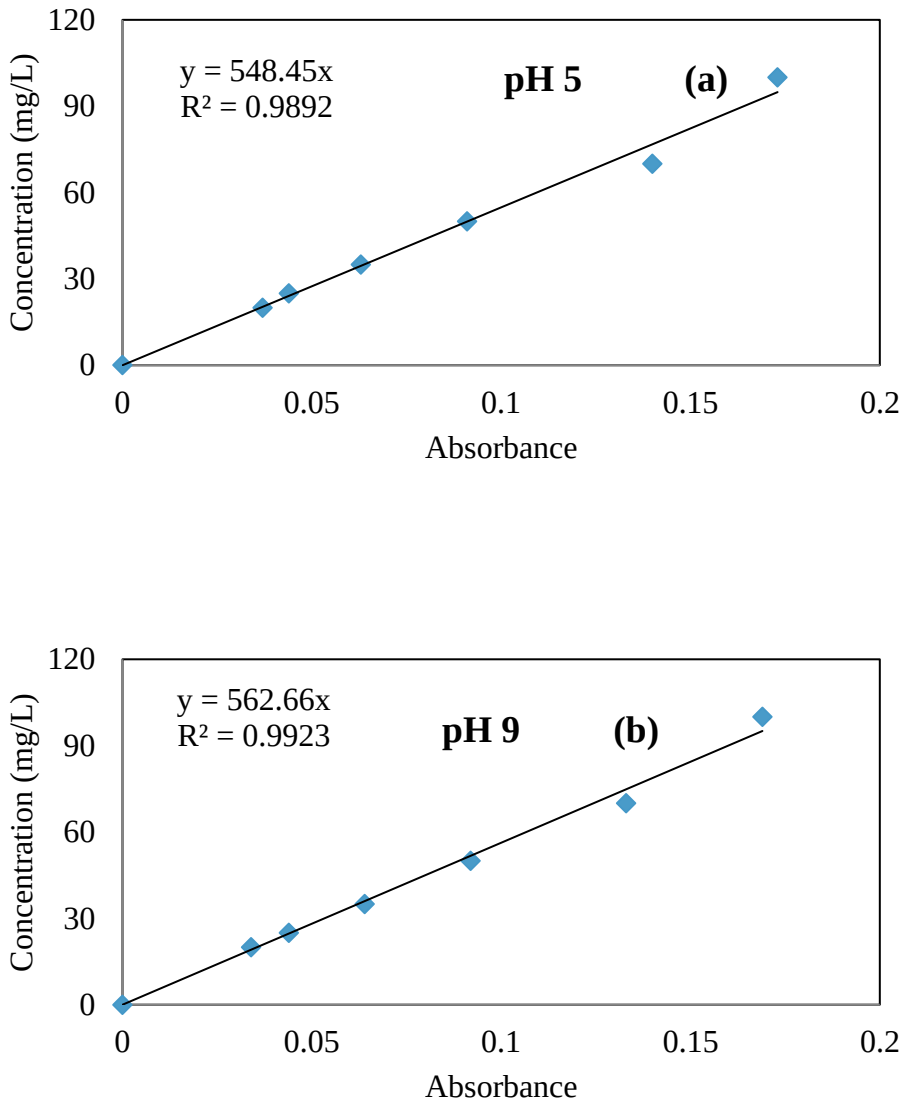

Fig. A1. Calibration curves of illite at pH 5 (a) and pH 9 (b). Absorbance of the illite samples of different concentration was measured using a spectrophotometer at 368 nm of wavelength.

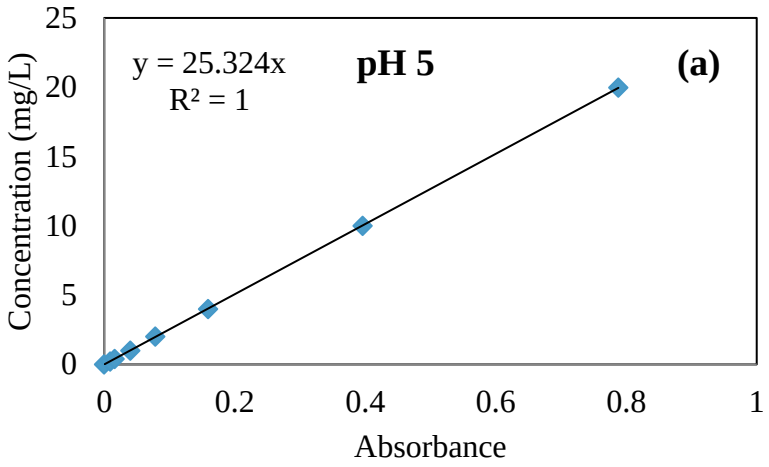

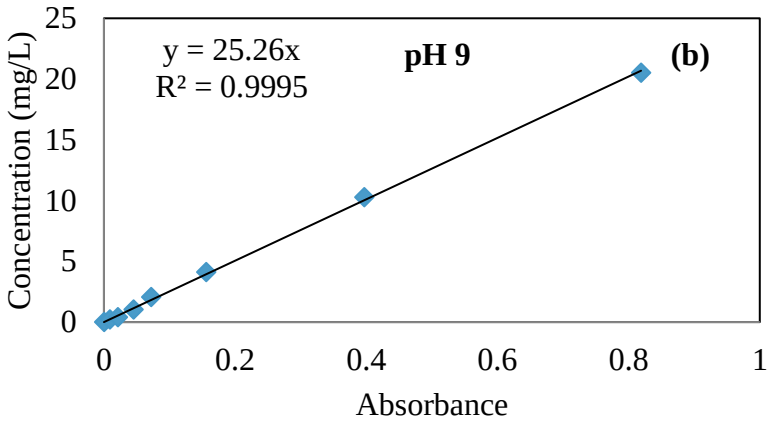

Fig.A2. Calibration curves of humic acid (HA) at pH 5 (a) and pH 9 (b). A spectrophotometer was used to measure the light absorbance of HA solution at a wavelength of 368 nm.

Appendix 2: Hamaker constant calculation for different chemical condition

In order to calculate the DLVO theory, we need to calculate the Hamaker constant of the associate material. We can determine the unknown Hamaker constant of Illite and Fe coated sand collector according to the method described by Hiemenz and Rajagopalan, 1997. When there are two dissimilar materials we can determine the Hamaker constant by the following equation

$$A_{12} = \frac{2A_{11}A_{22}}{A_{11} + A_{22}} (8)$$

When these two dissimilar materials are in the presence of another different media, then this equation can be written as

$$A_{132} = A_{12} + A_{33} - A_{13} - A_{23} (9)$$

So, we can calculate our Hamaker constant according to the following equation, where we used our materials (Illite, Fe coated sand and pure Quartz sand).

For Illite, Water and Fe coated sand,

$$A_{Illite-Water-FeOx} = A_{Illite-FeOx} + A_{Water-Water} - A_{Illite-Water} - A_{FeOx-water} \quad (10)$$

For, Illite, Water and Pure Quartz sand,

$$A_{Illite-Water-Sand} = A_{Illite-Sand} + A_{Water-Water} - A_{Illite-Water} - A_{Sand-Water} \quad (11)$$

Appendix 3: Calibration curve of titanium dioxide nanoparticle

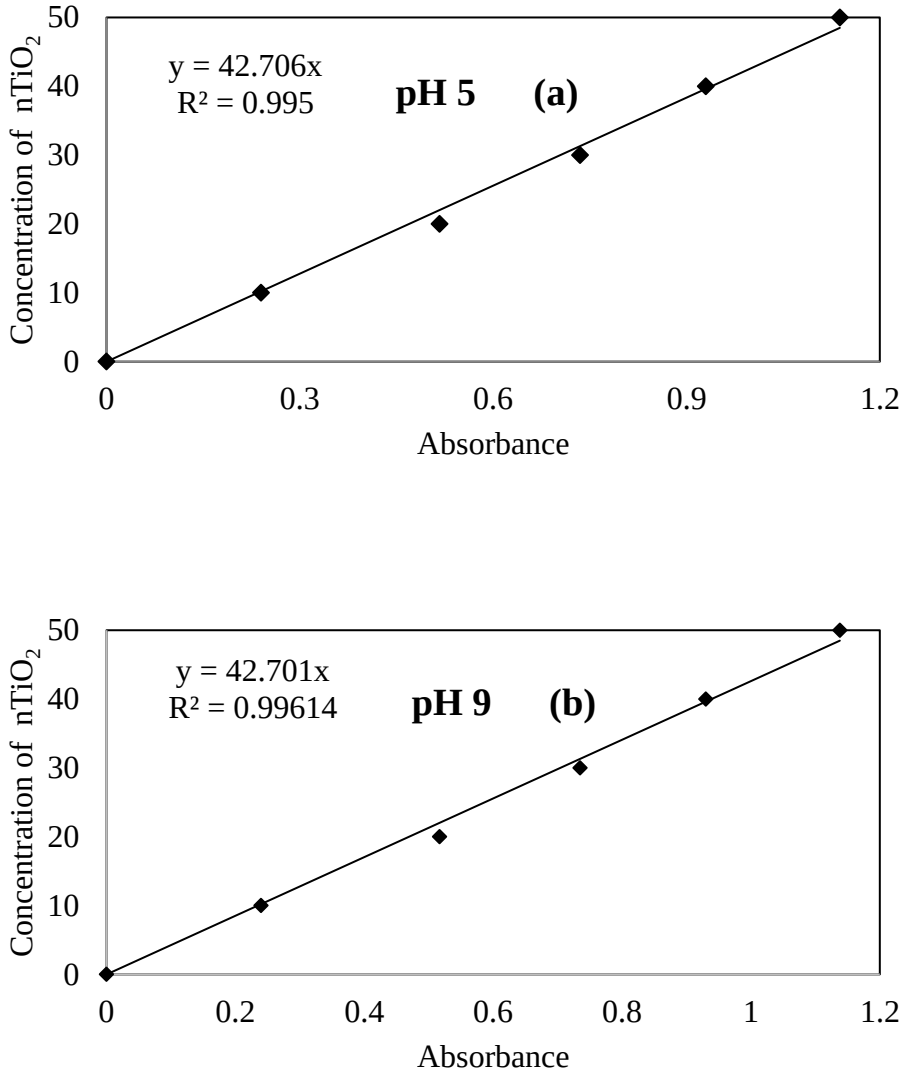

Fig. A3. Calibration curve of titanium dioxide nanoparticle at pH 5 (a) and pH 9 (b). 0.1 mM of NaCl was used as background solution.Absorbance of the titanium dioxide nanoparticle suspensions of different concentration were measured using a spectrophotometer at 368 nm of wavelength.

Appendix 4: Parameter, nomenclature and the values used in the $nTiO_2$-$nTiO_2$, $nTiO_2$-Sand and ($nTiO_2$+XG)- (Sand+XG) DLVO interaction energy calculations.

Table A1. Parameter and nomenclature of the DLVO equations

A_{123}	Hamaker constant
h	Separation distance
r_1	Particle radius
λ	Characteristic wavelength
ε	Dielectric constant of water
ε_0	Permittivity of free space
Ψ_1	Zeta potential of nanoparticle
Ψ_2	Zeta potential of sand
k	Debye length
K_B	Boltzman constant
T	Absolute temperature

Table A2. Parameter and values used in the calculation of the $nTiO_2$-$nTiO_2$, $nTiO_2$-Sand and ($nTiO_2$+XG)- (Sand+XG) interaction energy profiles.

Parameter (Unit)	Value	Reference
$A_{121\ (TiO2\text{-}Water\text{-}TiO2)}$ (J)	0.35×10^{-20}	(Petosa, Jaisi, Quevedo, Elimelech, and Tufenkji, 2010)
$A_{123\ (TiO2\text{-}Water\text{-}Sand)}$ (J)	1.4×10^{-20}	(Petosa et al., 2010)
λ (m)	10^{-7}	(J Gregory, 1981)
r_1 (pH 5) (nm)	131.1	This study
r_1 (pH 9) (nm)	197.85	This study
ε	80	(Malmberg and Maryott, 1956)
ε_0 (F/m)	$8.854\ 187\ 817 \times 10^{-12}$	(Mohr et al., 2012)
Ψ_1 (TiO_2) (pH 5) (mV)	+22.3	This study
Ψ_1 (TiO_2) (pH 9) (mV)	-10.0	This study
Ψ_1 (TiO_2+XG) (pH 5) (mV)	-19.7	This study
Ψ_1 (TiO_2+XG) (pH 9) (mV)	-21.8	This study
Ψ_2 (Fine sand) (pH 5) (mV)	-26.1	This study

Ψ_2 (Fine sand) (pH 9) (mV)	-43.3	This study
Ψ_2 (Coarse sand) (pH 5) (mV)	-23.7	This study
Ψ_2 (Coarse sand) (pH 9) (mV)	-44.8	This study
Ψ_2 (Fine sand+XG) (pH 5) (mV)	-24.5	This study
Ψ_2 (Fine sand+XG) (pH 9) (mV)	-43.8	This study
Ψ_2 (Coarse sand+XG) (pH 5) (mV)	-28.9	This study
Ψ_2 (Coarse sand+XG) (pH 9) (mV)	-45.8	This study
k (m)	1.04	This study
K_B (J K^{-1})	1.380 655 × 10−23	(Gaiser and Fellmuth, 2011)
T (K)	298	This study

Appendix 5: Zeta potential report (Graph) both at pH 5 and pH 9

Illite

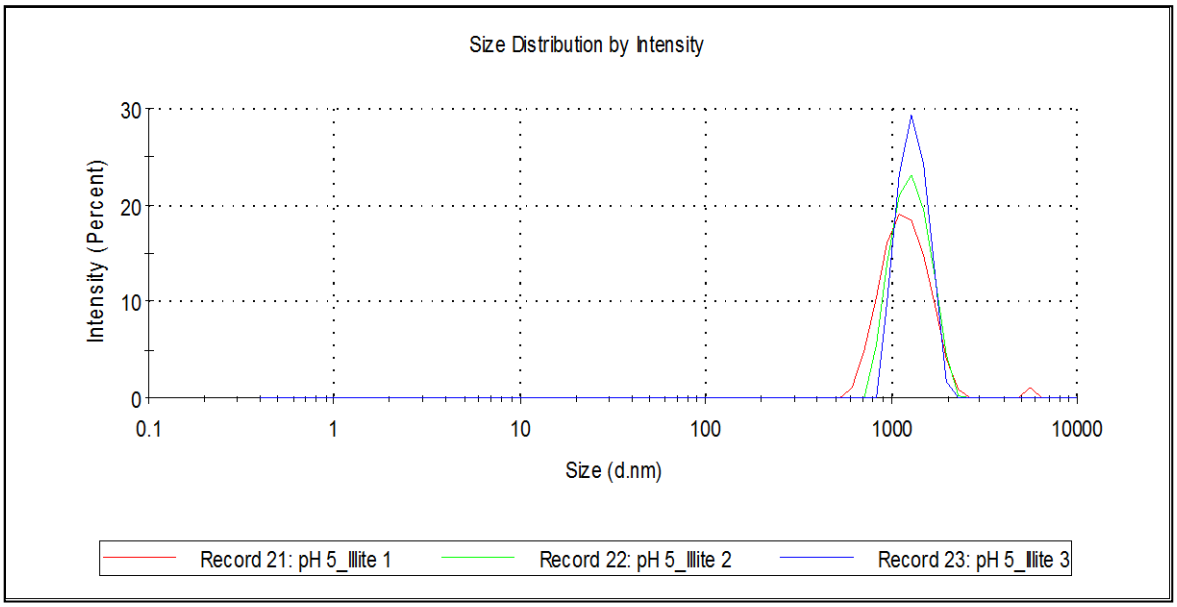

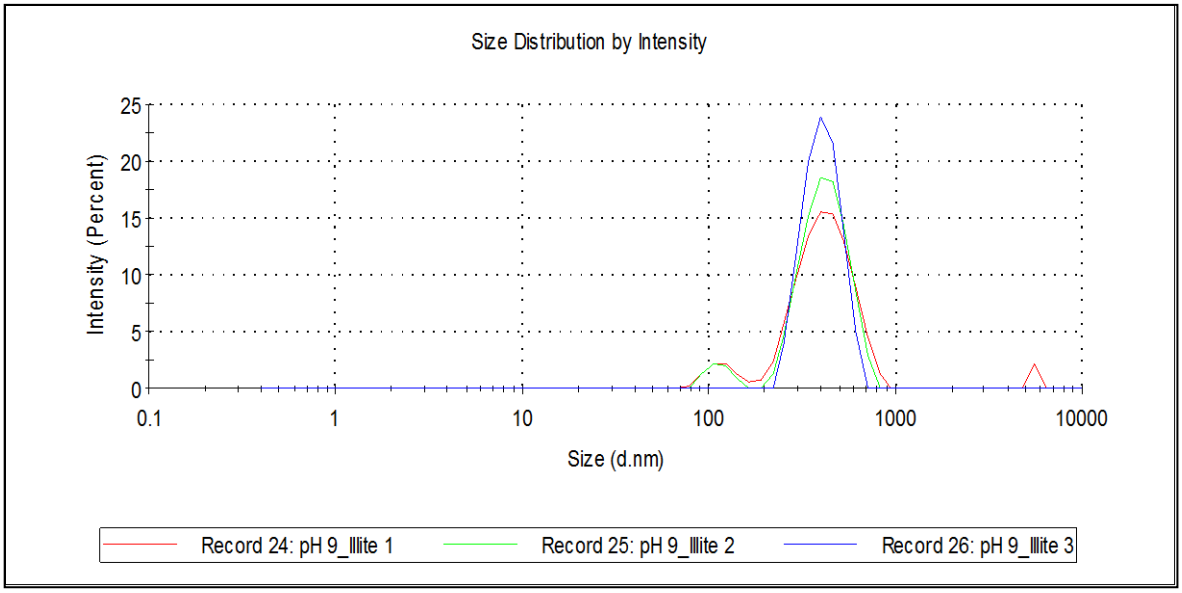

Humic acid

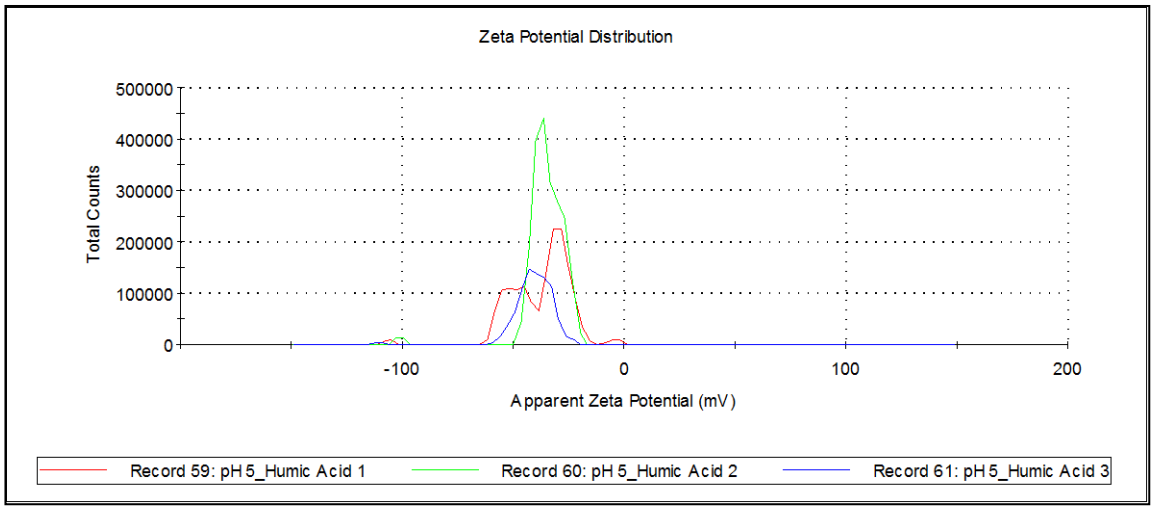
Zeta Potential Distribution
Total Counts
500000
400000
300000
200000
100000
0
-100
0
100
200
Apparent Zeta Potential (mV)
Record 59: pH 5_Humic Acid 1
Record 60: pH 5_Humic Acid 2
Record 61: pH 5_Humic Acid 3

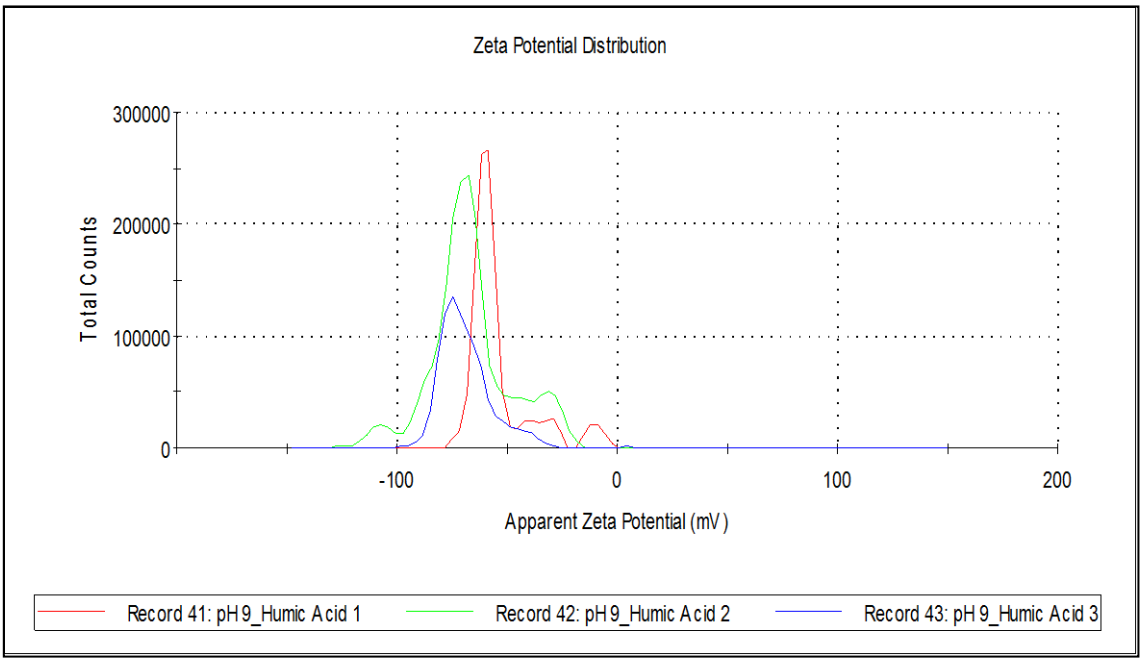
Zeta Potential Distribution
Total Counts
300000
200000
100000
0
-100
0
100
200
Apparent Zeta Potential (mV)
Record 41: pH 9_Humic Acid 1
Record 42: pH 9_Humic Acid 2
Record 43: pH 9_Humic Acid 3

Illite + humic acid

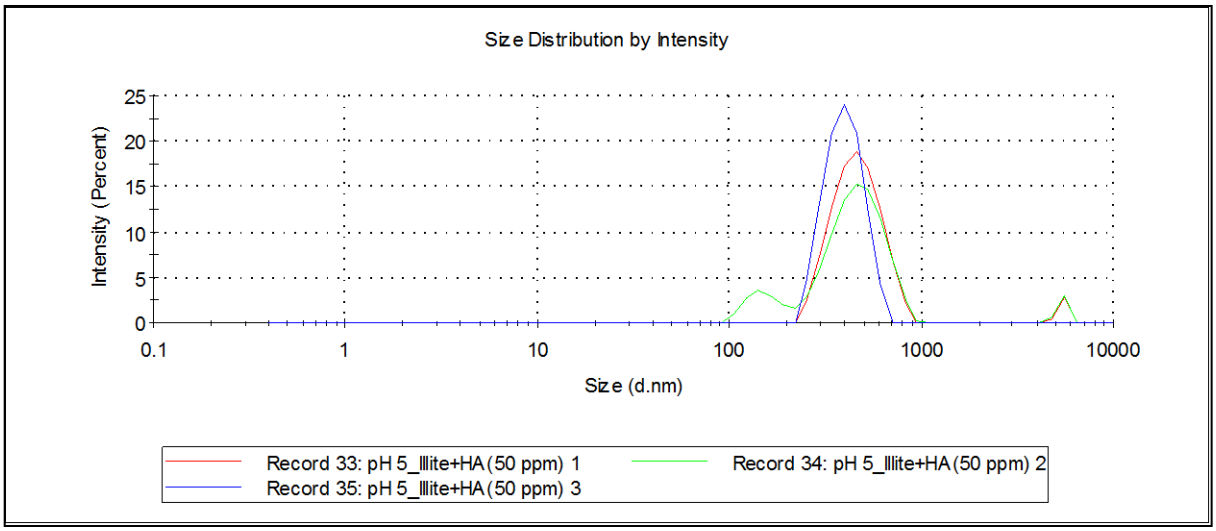

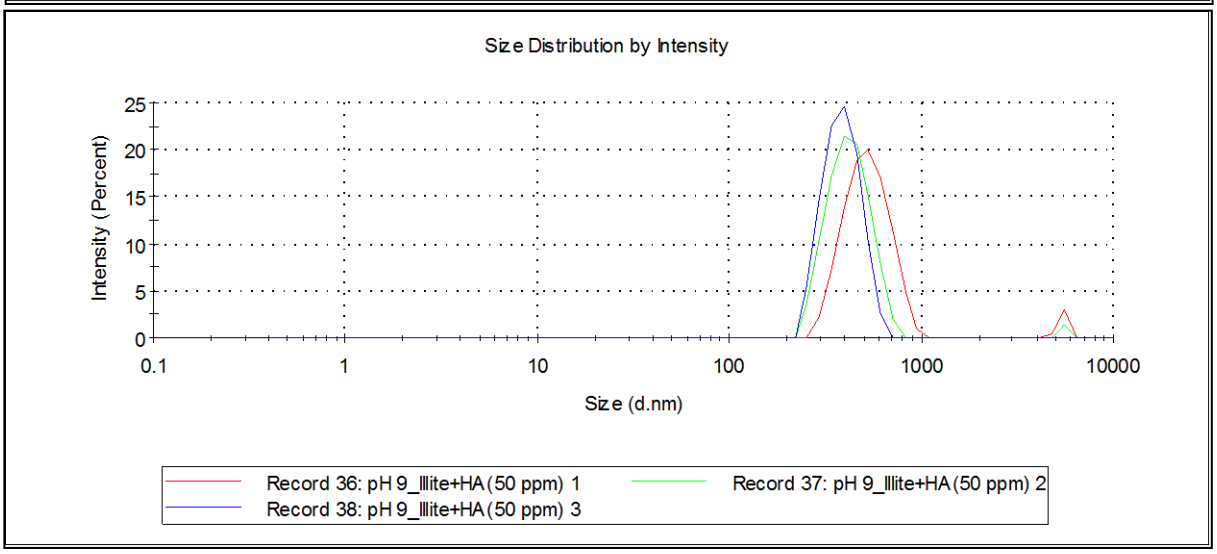

Fe Coating

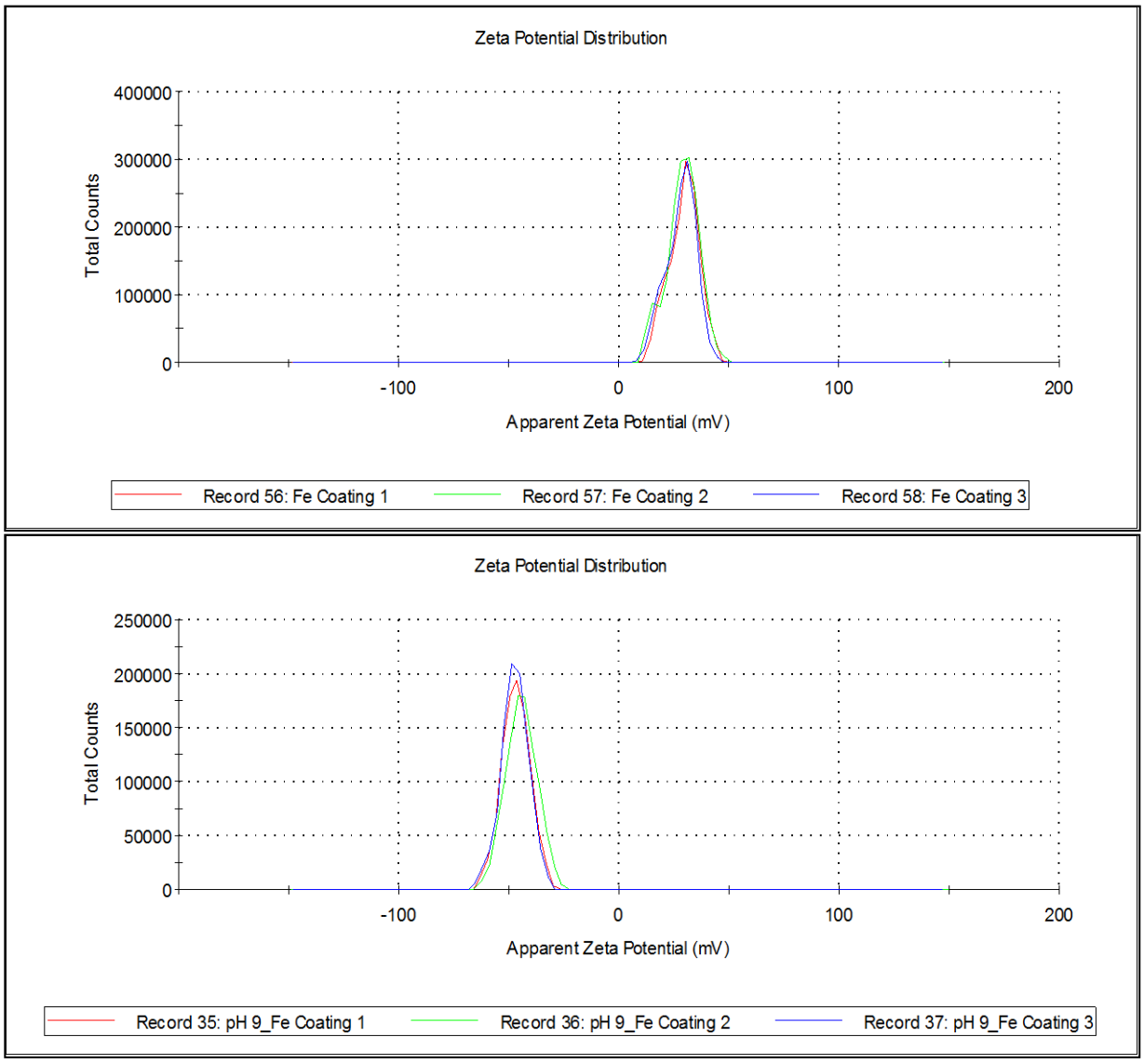
Zeta Potential Distribution
Total Counts
400000
300000
200000
100000
0
-100
0
100
200
Apparent Zeta Potential (mV)
Record 56: Fe Coating 1
Record 57: Fe Coating 2
Record 58: Fe Coating 3

Zeta Potential Distribution
Total Counts
250000
200000
150000
100000
50000
0
-100
0
100
200
Apparent Zeta Potential (mV)
Record 35: pH 9_Fe Coating 1
Record 36: pH 9_Fe Coating 2
Record 37: pH 9_Fe Coating 3

Fine Sand

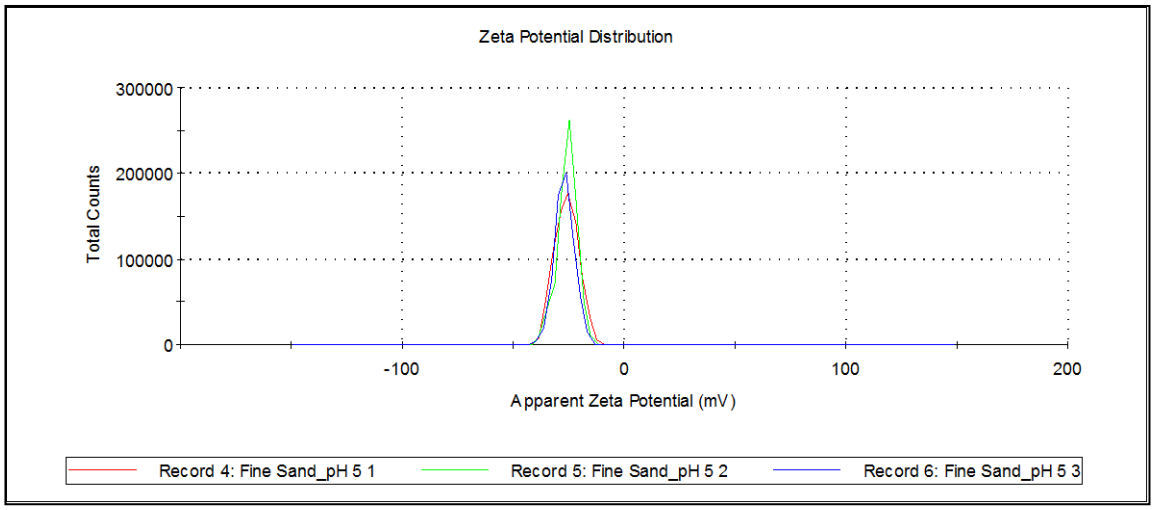
Zeta Potential Distribution
300000
200000
100000
0
Total Counts
-100
0
100
200
Apparent Zeta Potential (mV)
Record 4: Fine Sand_pH 5 1
Record 5: Fine Sand_pH 5 2
Record 6: Fine Sand_pH 5 3

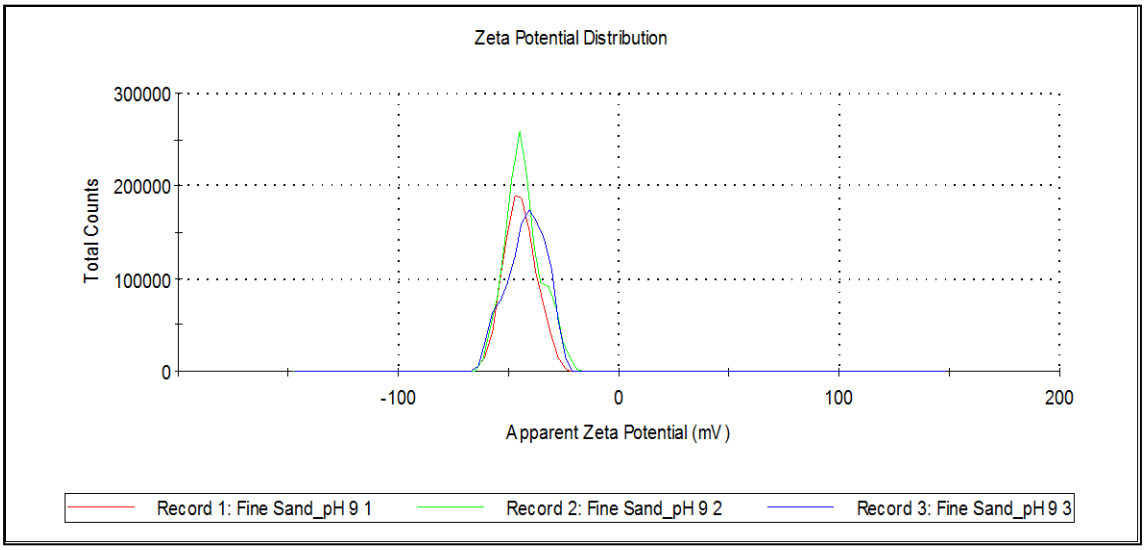
Zeta Potential Distribution
300000
200000
100000
0
Total Counts
-100
0
100
200
Apparent Zeta Potential (mV)
Record 1: Fine Sand_pH 9 1
Record 2: Fine Sand_pH 9 2
Record 3: Fine Sand_pH 9 3

Coarse sand

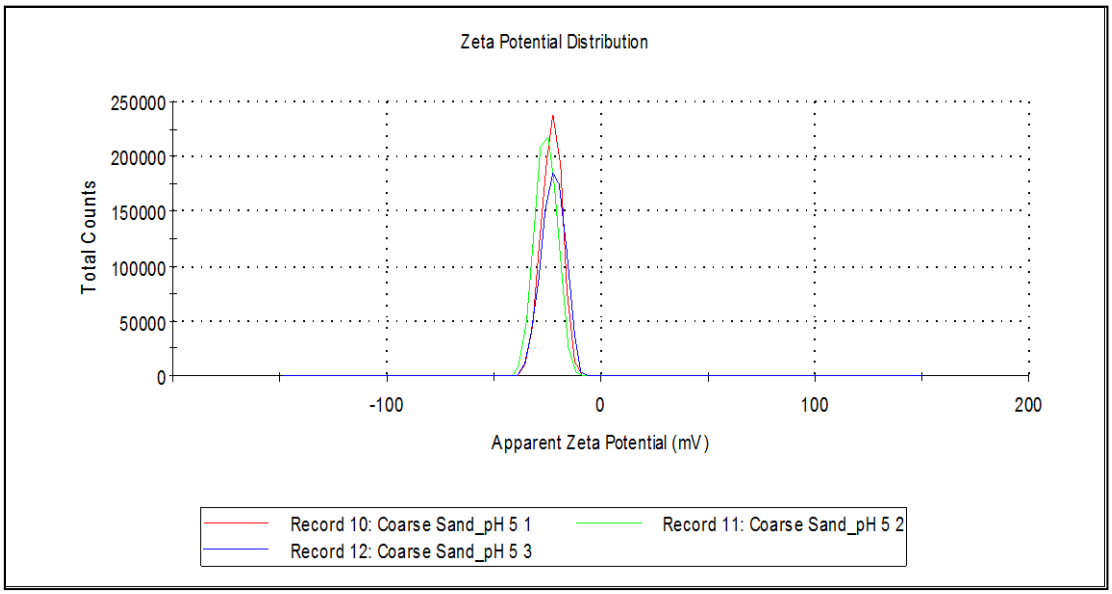
Zeta Potential Distribution
Total Counts
250000
200000
150000
100000
50000
0
-100
0
100
200
Apparent Zeta Potential (mV)
Record 10: Coarse Sand_pH 5 1
Record 11: Coarse Sand_pH 5 2
Record 12: Coarse Sand_pH 5 3

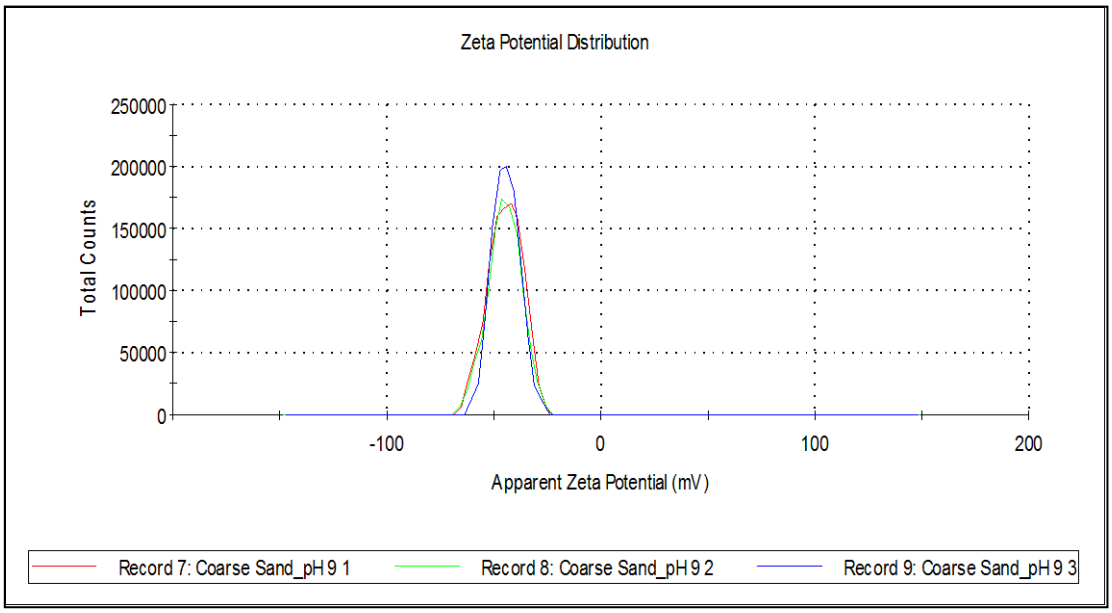
Zeta Potential Distribution
Total Counts
250000
200000
150000
100000
50000
0
-100
0
100
200
Apparent Zeta Potential (mV)
Record 7: Coarse Sand_pH 9 1
Record 8: Coarse Sand_pH 9 2
Record 9: Coarse Sand_pH 9 3

Titanium dioxide nanoparticle

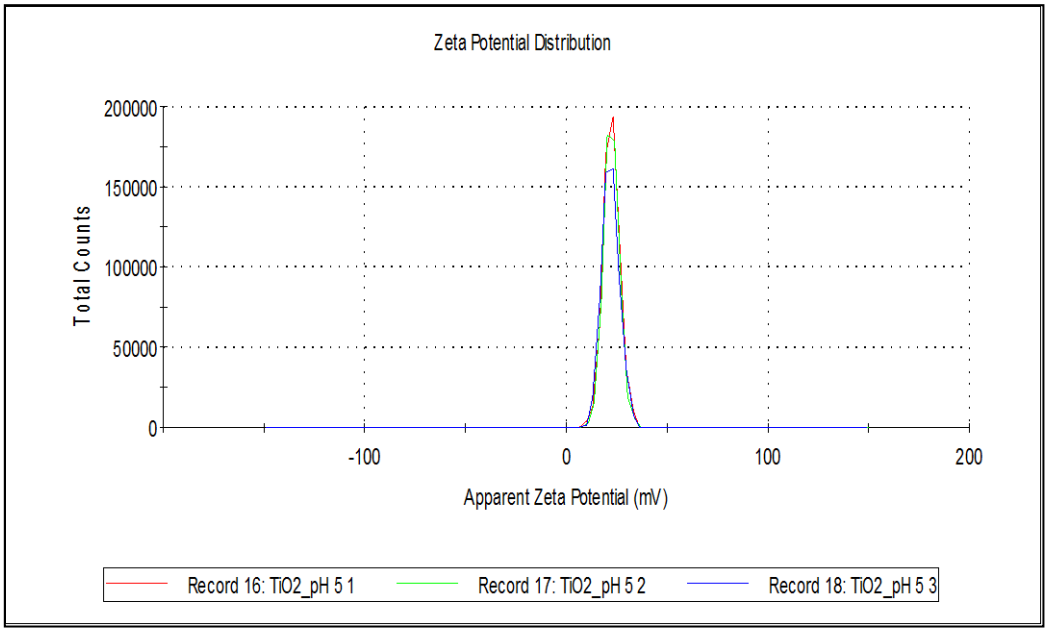

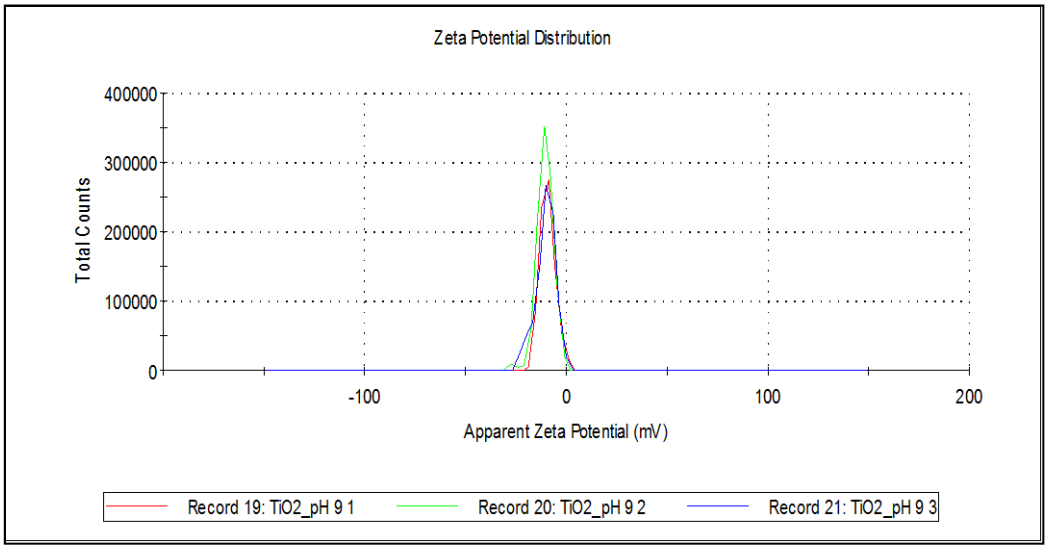

Xanthan gum

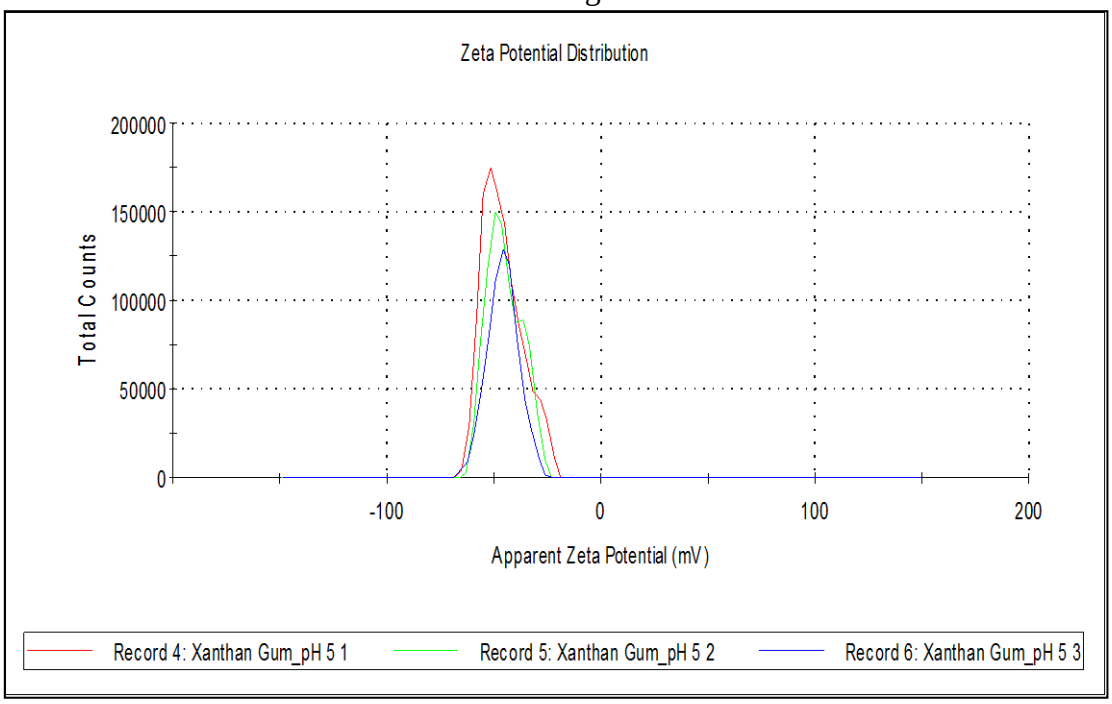
Zeta Potential Distribution
200000
150000
100000
50000
0
Total Counts
-100
0
100
200
Apparent Zeta Potential (mV)
Record 4: Xanthan Gum_pH 5 1
Record 5: Xanthan Gum_pH 5 2
Record 6: Xanthan Gum_pH 5 3

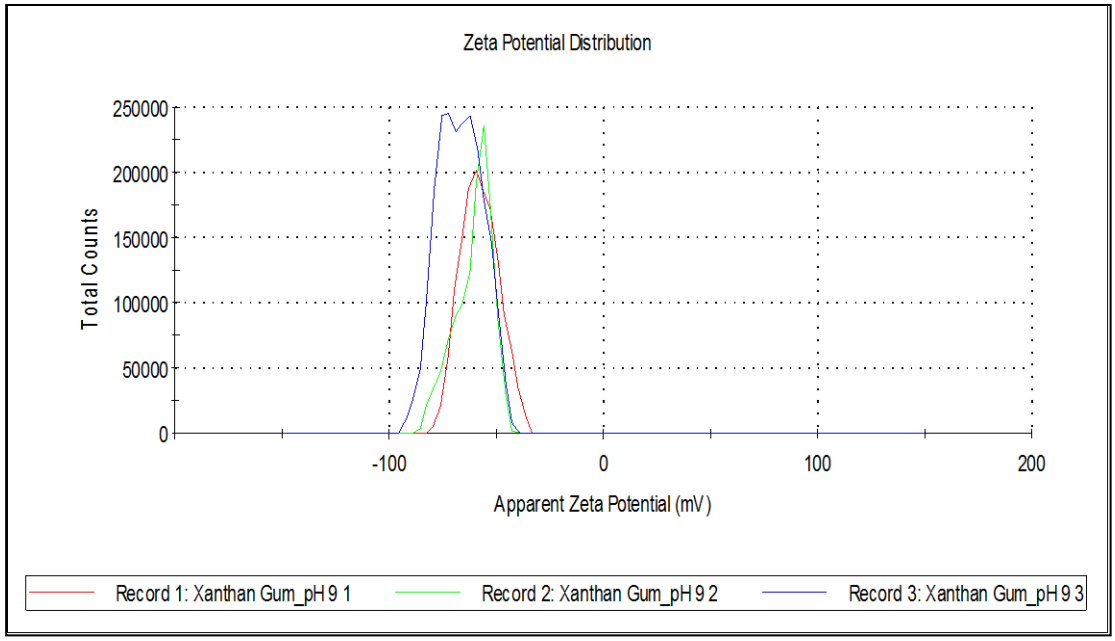
Zeta Potential Distribution
250000
200000
150000
100000
50000
0
Total Counts
-100
0
100
200
Apparent Zeta Potential (mV)
Record 1: Xanthan Gum_pH 9 1
Record 2: Xanthan Gum_pH 9 2
Record 3: Xanthan Gum_pH 9 3

$nTiO_2$ + Xanthan gum

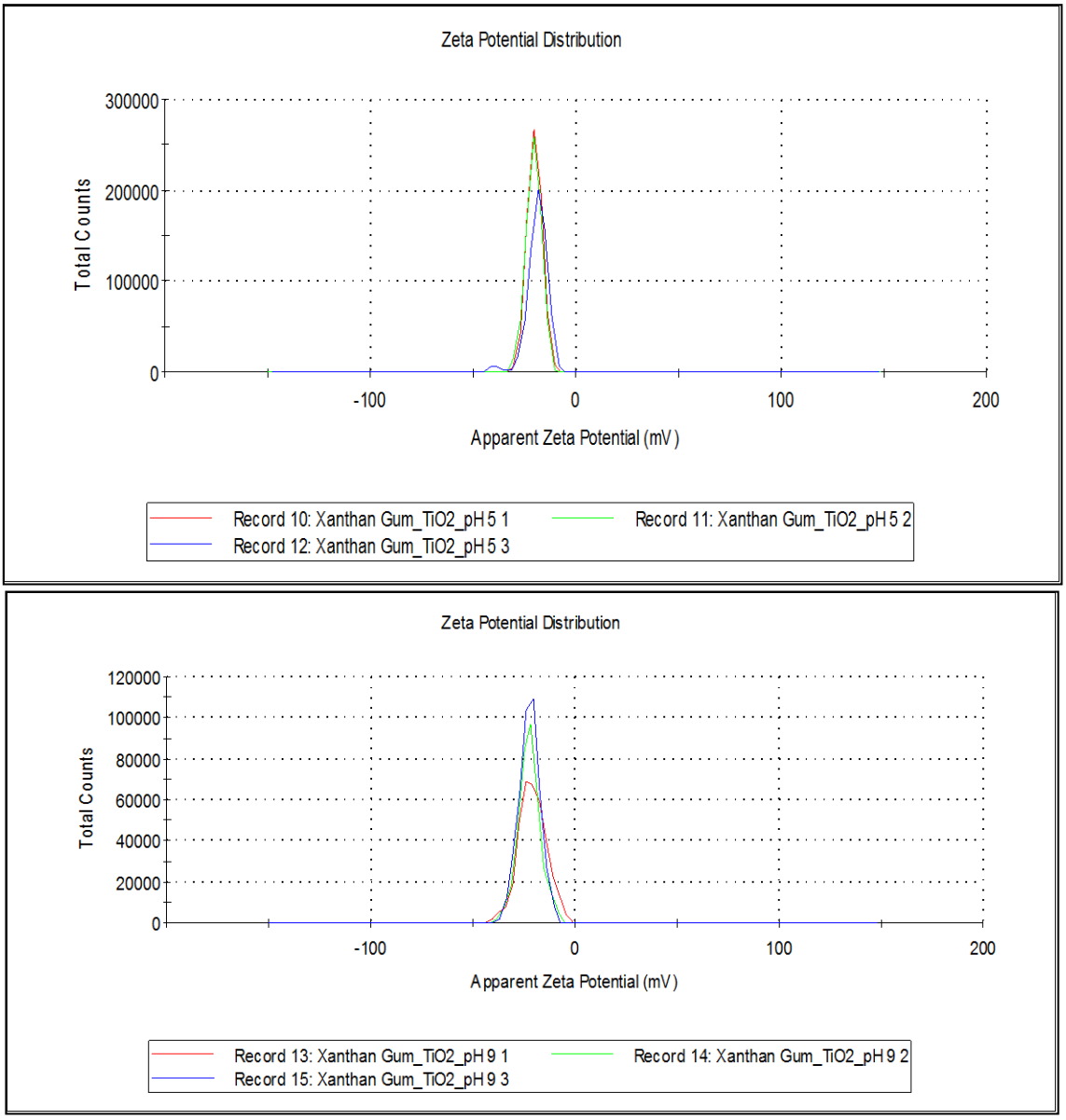

Fig. A4. Zeta potential reports (Graphs) measured using Zetasizer Nano S (Malvern Instrument Inc.).

Appendix 6: Tables of DLVO interaction energies calculations parameters and results

Table A3: Experimentally measured zeta potential and HDD of Illite with different concentration of HA. Zeta potential of Fe coating measured experimentally with different concentration of HA. DLVO interaction energy parameters (Φmax: energy barrier) for illite and Fe coated sand at different concentration of HA. Aqueous phase HA concentration at equilibrium (C_{eq}) and adsorbed HA concentration on illite (q_{Illite}) were calculated based on Langmuir adsorption isotherm and mass balance of HA equation.

	HDD (nm) of Illite	**ZP of illite**	**ZP of Fe coating**	**C_{Total}**	**$q_{Illite(Sand)}$**	**$Q_{HA(Fe\ coated\ sand)}$**	**$q_{HA(Sand)}$**	Φmax	Separation distance
pH	**nm**	**mV**	**mV**	**mg DOC/L**	**mg/kg sand**	**mg OC/kg sand**	**mg DOC/L**	KBT	nm
5	1378	-19.4	29	0	81.898	0	0	+27.6	13
5	368.7	-41.5	-49.5	5.71	9.490	2.357	0.018	+333.5	1.0
5	390.3	-46.7	-54.6	8.75	8.843	2.820	0.020	+400.7	0.8
5	373.4	-42.1	-55.5	11.42	7.550	3.262	0.036	+357.09	0.7
5	373.2	-43.7	-54.1	14.28	7.550	3.366	0.034	+364.4	0.7
5	368.9	-43.9	-58.7	17.14	8.197	3.329	0.033	+371.9	0.8
9	497.6	-24.6	-46.1	0	0.982	0	0	+292.4	2.0
9	371.4	-48.9	-56.3	5.71	0.419	0.053	0.018	+629.6	0.1
9	351.4	-49.2	-57.8	8.75	0	0.055	0.020	+602.7	0.1
9	355.7	-49.9	-59.9	11.42	0.419	0.036	0	+623.05	0.1
9	348.4	-49.9	-65.6	14.28	0.419	0.034	0	+619.4	0.2
9	358.3	-53.4	-58.6	17.14	0	0.033	0	+661.8	0.1

Table A4: Experimentally measured zeta potential and HDD of Illite with different concentration of HA. Zeta potential of Fe coating measured experimentally. Adsorbed HA concentration on illite ($q_{HA(Illite)}$),adsorbed HA to Fe coated sand$q_{HA(Fe\ coated\ sand)}$were calculated based on Langmuir adsorption isotherm and mass balance of HA equation.

	HDD (illite)	**ZP (illite)**	**ZP (Fe coating)**	**C_{Total}**	**$q_{HA(illite)}$**	**$q_{HA(Fe\ coated\ sand)}$**
pH	**nm**	**mV**	**mV**	**mg DOC/L**	**mg OC/kg illite**	**mg OC/ kg Fe coated sand**
5	1378	-19.4	29	0	0	0
5	368.7	-41.5	-49.5	5.71	0.281	2.357
5	390.3	-46.7	-54.6	8.75	0.396	2.820
5	373.4	-42.1	-55.5	11.42	0.513	3.262
5	373.2	-43.7	-54.1	14.28	0.792	3.366
5	368.9	-43.9	-58.7	17.14	1.072	3.329
9	497.6	-24.6	-46.1	0	0	0
9	371.4	-48.9	-58.6	5.71	0.185	0.033
9	351.4	-49.2	-65.6	8.75	0.295	0.034
9	355.7	-49.9	-59.9	11.42	0.324	0.036
9	348.4	-49.9	-57.8	14.28	0.328	0.055
9	358.3	-53.4	-56.3	17.14	0.462	0.053

Table A5: Zeta potential and HDD were measured using ZetaSizer. Illite to sand interaction energy parameters Φmax = energy barrier. Illite concentration=C_{total}, Aqueous phase illite concentration at the equilibrium=C_{aq} and q_{max}= maximum attachment of illite to sand were calculated using Langmuir adsorption isotherm equation (Appendix 3).

pH	**IS**	**HA (DOC/L)**	**C_{total} (mg/L)**	**C_{eq} (mg/L)**	**q_{max}(mg/kg)**	**ZP of Illite (mV)**	**ZP of Sand**	**HDD of Illite (nm)**	**HDD of Sand (mm)**	**Φmax (KBT)**	**Separation distance (nm)**
5	0.001	0	100	96	5.1401	-19.4	-26.1	1378	0.3025	+290.16	2
9	0.001	0	35	34	0.95329	-24.6	-43.3	4497.6	0.3025	+465.33	0.4
5	0.001	10	NA	NA	NA	-31.6	-26.1	524.4	0.3025	+305.72	0.2
9	0.001	10	NA	NA	NA	-38.6	-43.3	597.5	0.3025	+729.32	0.1

Table A6: Zeta potential and HDD were measured using Zetasizer. TiO_2 to sand interaction energy parameters Φ_{max} = energy barrier.

pH	IS	XG (DOC/L)	ZP of TiO_2	ZP of XG	ZP of sand	Φ_{max}(KBT)	Separation distance (nm)
5	0.001	0	+22.3	-	-26.1	NE	NE
9	0.001	0	-10	-	-43.3	42.04	8
5	0.001	10	+22.3	-45.7	-26.1	96.34	0.4
9	0.001	10	-10	-61.8	-43.3	116.29	2
5	0.001	0	+22.3	-	-23.7	N E	NE
9	0.001	0	-10	-	-44.8	42.07	8
5	0.001	10	+22.3	-45.7	-23.7	88.41	0.7
9	0.001	10	-10	-61.8	-44.8	116.75	2

*NE=Not exist